Prospects of Nanoscience with Nanocrystals

Maksym V. Kovalenko,[*,†,‡] Liberato Manna,[§,⊥] Andreu Cabot,[∥,¶] Zeger Hens,[#,△] Dmitri V. Talapin,[▲,▽] Cherie R. Kagan,[▼,⊗] Victor I. Klimov,[⬡] Andrey L. Rogach,[●] Peter Reiss,[∞] Delia J. Milliron,[&] Philippe Guyot-Sionnnest,[▲] Gerasimos Konstantatos,[⊕] Wolfgang J. Parak,[□,★] Taeghwan Hyeon,[■,○] Brian A. Korgel,[&,●] Christopher B. Murray,[⊗] and Wolfgang Heiss[*,$,@,♦]

[†]Institute of Inorganic Chemistry, Department of Chemistry and Applied Biosciences, ETH Zürich, CH-8093 Zürich, Switzerland, [‡]Laboratory for Thin Films and Photovoltaics, EMPA Swiss Federal Laboratories for Materials Science and Technology, CH-8600 Dübendorf, Switzerland, [§]Nanochemistry Department, Italian Institute of Technology, Genoa, Italy, [⊥]Kavli Institute of NanoScience, Delft University of Technology, 2628 CJ Delft, The Netherlands, [∥]Catalonia Energy Research Institute, Sant Adria del Besos 08930, Spain, [¶]Institució Catalana de Recerca i Estudis Avançats, ICREA, Barcelona 08010, Spain, [#]Physics and Chemistry of Nanostructures and [△]Center for Nano- and Biophotonics, Ghent University, Ghent, Belgium, [▲]Department of Chemistry and James Franck Institute, University of Chicago, Chicago, Illinois 60637, United States, [▽]Center for Nanoscale Materials, Argonne National Lab, Argonne, Illinois 60439, United States, [▼]Department of Electrical and Systems Engineering and [⊗]Department of Materials Science and Engineering and Department of Chemistry, University of Pennsylvania, Philadelphia, Pennsylvania 19104, United States, [⬡]Chemistry Division, Los Alamos National Laboratory, Los Alamos, New Mexico 87545, United States, [●]Department of Physics and Materials Science and Centre for Functional Photonics, City University of Hong Kong, Kowloon, Hong Kong, [∞]Laboratoire d'Electronique Moléculaire, Organique et Hybride, UMR 5819 SPrAM (CEA-INAC, CNRS, Univ. Grenoble Alpes, 38054 Grenoble, France, [&]McKetta Department of Chemical Engineering, The University of Texas at Austin, Austin, Texas 78712 United States, [□]Philipps Universität Marburg, Marburg, Germany, [★]CIC Biomagune, San Sebastian, Spain, [■]Center for Nanoparticle Research, Institute for Basic Science, Seoul 151-742, Korea, [○]School of Chemical and Biological Engineering, Seoul National University, Seoul 151-742, Korea, [⊕]ICFO, The Institute of Photonic Sciences, 08860 Castelldefels, Spain, [●]Texas Materials Institute, Center for Nano- and Molecular Science and Technology, The University of Texas at Austin, Austin, Texas 78712, United States, [$]Institute of Semiconductor and Solid State Physics, Johannes Kepler University Linz, 4040 Linz, Austria, [@]Materials for Electronics and Energy Technology (i-MEET), Friedrich-Alexander-Universität Erlangen-Nürnberg, 91058 Erlangen, Germany, and [♦]Energie Campus Nürnberg, 90429 Nürnberg, Germany

ABSTRACT **Colloidal nanocrystals (NCs, *i.e.*, crystalline nanoparticles) have become an important class of materials with great potential for applications ranging from medicine to electronic and optoelectronic devices. Today's strong research focus on NCs has been prompted by the tremendous progress in their synthesis. Impressively narrow size distributions of just a few percent, rational shape-engineering, compositional modulation, electronic doping, and tailored surface chemistries are now feasible for a broad range of inorganic compounds. The performance of inorganic NC-based photovoltaic and light-emitting devices has become competitive to other state-of-the-art materials. Semiconductor NCs hold unique promise for near- and mid-infrared technologies, where very few semiconductor materials are available. On a purely fundamental side, new insights into NC growth, chemical transformations, and self-organization can be gained from rapidly progressing *in situ* characterization and direct imaging techniques. New phenomena are constantly being discovered in the photophysics of NCs and in the electronic properties of NC solids. In this Nano Focus, we review the state of the art in research on colloidal NCs focusing on the most recent works published in the last 2 years.**

Thermodynamically stable colloidal solutions of nanosized inorganic materials are well-described in colloidal chemistry textbooks as "sols" and have been known in a modern scientific context since the 19th century, with ruby-colored gold sols produced by Michael Faraday as one notable example.[1] The birth of modern nanoscience with nanocrystals (NCs) is, however, attributed to a much later period: beginning in the early 1980s and extending to the present. Early photochemistry studies on tailored colloidal CdS and TiO_2 arose from the oil crisis in the late 1970s, and semiconductor NCs with enhanced surface chemistry were considered highly important for efficient harvesting of solar energy by means of photoelectrochemistry (A. Nozik, L. Brus, A. Henglein, and their co-workers).[2−9] Semiconductor NCs were termed quantum dots (QDs) after the discovery and explanation of quantum size effects in the optical spectra of CuCl NCs embedded into glass and alkali-halide matrices (A. Ekimov, A. Onushchenko, A. Efros, T. Itoh, and co-workers)[10−12] and in aqueous solutions of colloidal CdS NCs (L. Brus and co-workers).[6−8] Since the mid-1990s, colloidal QDs have become a masterpiece of NC research and one of the most accomplished building blocks of modern nanoscience due to the emergence of surfactant-assisted

* Address correspondence to mvkovalenko@ethz.ch, wolfgang.heiss@fau.de.

Received for review October 31, 2014

Published online January 22, 2015
10.1021/nn506223h

precision synthesis that provides narrow size distributions, highly uniform morphologies, well-controlled surface chemistry, and enhanced optical properties such as bright, spectrally tunable, and stable photoluminescence.[13−15] Since then, colloidal NCs are among the most modular and versatile nanoscale materials, due to both their unprecedented compositional and morphological tunability and their "free" (unsupported) colloidal state that allows their positioning onto various surfaces or integration into various matrices. These characteristics are hardly simultaneously achievable with any *physical* nanostructuring method, whether it is a top-down (*e.g.*, electron beam lithography) or a bottom-up (*e.g.*, molecular beam epitaxy) procedure. Beginning in the 2000s and until now, a multitude of metals, metal oxides, and semiconductors have been developed in the form of isotropic and anisotropic NCs.

This Nano Focus article is structured into five main sections. First, we review the most recent trends in the synthesis of NCs, then we describe NC surface chemistry, self-assembled long-range-ordered NC superlattices, and novel applications of NCs, and finally, we discuss our vision for the future of this field.

SYNTHESIS OF COLLOIDAL NANOCRYSTALS

The accessible complexity of NCs is rapidly expanding, in terms of both compositional variety and shape engineering.[16−18] Much present-day research focuses on solving challenging problems in the synthesis of novel NCs and nanoparticles (NPs) such as the synthesis of highly covalent group IV elements (Si, Ge),[19−22] III−V compounds (GaAs, InAs, InSb, *etc.*),[23−26] multicomponent chalcogenides, carbon nanostructures, or even organic compounds in the form of highly uniform NCs. Several recent examples are illustrated below. Continuing efforts are underway to engineer NC composition and morphology by means of galvanic replacement,[27,28] ion-exchange reactions,[29−32] or through the nanoscale Kirkendall effect.[33,34] Even "classical" QD materials such as core−shell CdSe/CdS NCs have recently been further perfected to yield above 90% luminescence quantum yields with narrowed emission lines and high photostability.[35,36] Equally important are efforts toward the development and use of *in situ* characterization methods to obtain insights into the nucleation and growth of NCs or to monitor structural and compositional transformations in NCs directly in the electron microscope, as briefly reviewed below.

The accessible complexity of NCs is rapidly expanding, in terms of both compositional variety and shape engineering.

Colloidal Silicon Nanostructures. The field of nanomaterials chemistry aims to develop synthetic routes to produce macroscopic quantities of stable NCs with controlled and tunable size and shape. This is accomplished by employing reaction chemistry that yields the desired nanomaterial in the presence of capping ligands that bind to the NC surface and stabilize the material. This usually requires capping ligands with surface bonding that is at least partially reversible to enable NC growth up to a desired size. Considerable progress has been made recently in the development of chemical routes to silicon (Si) nanomaterials, including Si NCs, nanorods, and nanowires (Figure 1).

Silicon is one of the most commercially important semiconductors and one of the most interesting to study at the nanoscale because it has an indirect band gap that makes it a poor light emitter as a bulk material but one that can emit light relatively efficiently as a nanostructure due to quantum confinement. Yet, Si has been one of the least studied colloidal NC materials because of the various challenges facing its synthesis, until recently. These challenges include the identification of suitable reaction pathways to generate Si atoms in a colloidal system, the tendency of Si to form stable amorphous structures and thus require relatively high temperatures for crystallization, its propensity to oxidize, and capping ligand chemistry that is significantly different from that of the well-studied metals and metal chalcogenides.

One of the first relatively successful synthetic routes to Si NCs was developed by Brus and co-workers in the early 1990s, which employed an aerosol system that enabled high synthesis temperatures—much higher than those available in high boiling solvents.[37] These NCs were made by pyrolysis of silane and were captured in stabilizing solvents like ethylene glycol. In this early work, the Si NC surfaces were intentionally oxidized to create an inorganic passivating shell. This approach worked well, but the tunability of the optical properties was relatively limited and the oxide shell created traps at the Si interface that limited the light emission from the NCs. To overcome these limitations, several different colloidal approaches have been explored, including metathesis reactions,[38] silane reduction,[39] and thermal decomposition of silanes in high-temperature supercritical fluids;[40] however, none of these colloidal routes has provided a general, high-yield synthesis of Si NCs with widely tunable size and optical properties. Again, one of the challenges facing colloidal syntheses is the relatively low temperatures in these reaction systems. To date, two of the most successful methods for producing Si NCs with tunable size and optical properties are still aerosol methods. Swihart's group has developed a method using laser

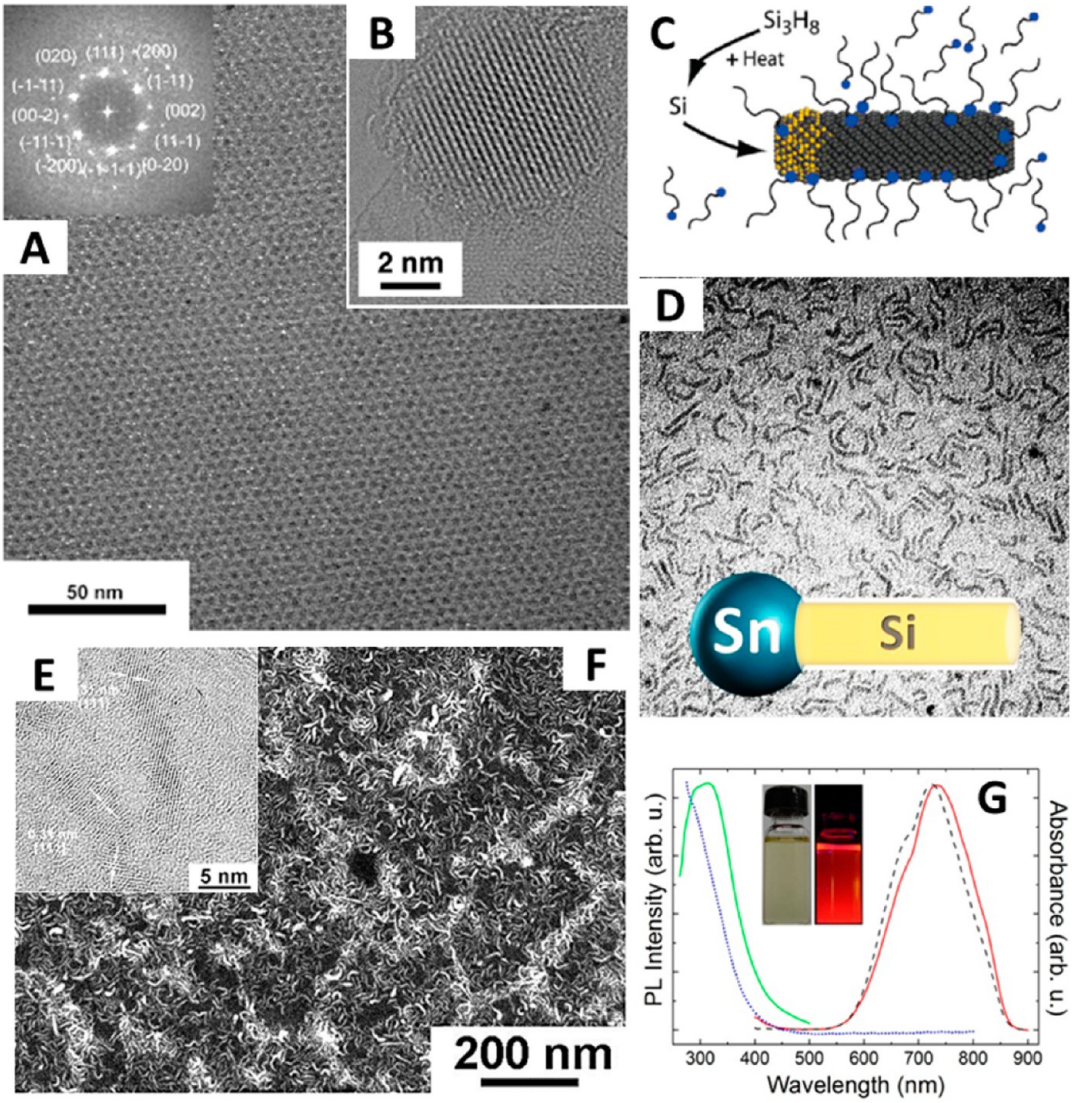

Figure 1. (A) Silicon nanocrystal superlattice (Inset: Fast Fourier transform of the image). Reprinted with permission from ref 19. Copyright 2013 Wiley Interscience. (B) Transmission electron microscopy (TEM) image of an octadecene-capped Si NC. Reprinted from ref 50. Copyright 2012 American Chemical Society. (C) Schematic of the ligand-assisted solution–liquid–solid (SLS) synthesis of Si nanorods. Reprinted from ref 51. Copyright 2009 American Chemical Society. (D) TEM image of a field of Si nanorods made with Sn seeds. (E) TEM image of two Si nanorods showing their crystal structure. (F) High-angle annular dark-field (HAADF) scanning transmission electron microscopy (STEM) image of a field of Si nanorods. (G) Room temperature optical properties of fluorescent Si nanorods. (D–G) Reprinted from ref 20. Copyright 2013 American Chemical Society.

pyrolysis of silanes to produce large quantities of NCs, but in the >30 nm diameter size range. These are far too large to exhibit quantum confinement, but they can be captured and etched to smaller sizes and then passivated with alkenes by hydrosilylation.[41,42] To obtain much smaller NCs in the aerosol phase, Kortshagen developed a nonthermal plasma approach to generate Si NCs in the quantum size regime that are captured in a solvent for subsequent hydrosilylation.[43,44] Both methods work well but face limitations, especially in producing NCs in the smaller range of sizes (~2 nm in diameter, for instance). For example, high photoluminescence quantum yields of up to 60% can be achieved using plasma-based synthesis but only for NCs in the larger size range (above 4 nm in diameter), and the photoluminescence quantum yield drops significantly for smaller sizes. Ultimately, a direct arrested precipitation of Si NCs in a solvent-based medium is desired to produce a wider range of sizes with well-passivated NC surfaces, but such a method has thus far continued to elude the field.

An approach that is close to a colloidal synthesis of Si NCs was developed by the Veinot group, which uses a high-temperature thermal decomposition of a $SiO_{1.5}$ precursor, hydrogen silsequioxane (HSQ), to create Si NCs embedded in an oxide host.[45] The NC diameter is widely tunable, from as small as ~1.5 nm to more than 10 nm in diameter, depending on the temperature used to decompose HSQ. The Si NCs can then be liberated

from the silica host by etching and then by passivating with a capping ligand layer by hydrosilylation with alkenes. This approach has been used to produce Si NCs with size-tunable photoluminescence with relatively high quantum yields across a wide range of wavelengths.[46] Ligand-stabilized Si NCs with near-infrared photoluminescence (PL) quantum yields of over 40% have been produced using this route.[47] This synthetic approach can also provide ligand-stabilized Si NCs with extremely narrow size distributions and has enabled the first examples of colloidal Si NC superlattices (Figure 1A,B).[19] The strong covalent Si−C bonding between the Si core and the alkyl capping ligands provides a new class of extremely thermally stable ligand-capped NCs, with decomposition temperatures that are more than 150 °C higher than those of dodecanethiol-capped gold NCs, for example.[48]

These Si NCs obtained from HSQ decomposition also serve as an effective model system to create a better understanding of the surface reactivity and capping ligand chemistry of Si, which is needed if a direct arrested precipitation method is ever to be developed. After the host matrix is etched, Si NCs are obtained with a H-terminated surface, which can then be used as a platform for carrying out controlled surface passivation reactions. Although there is extensive understanding of surface modification chemistry of Si surfaces, NCs have exhibited some surprisingly new reaction chemistry due to their highly curved surfaces. For example, room temperature hydrosilylation has been demonstrated on small (<4 nm diameter) Si NCs activated by either an ester or an acid functional group.[49]

These reactions do not happen on extended bulk Si surfaces. Colloidal Si NCs made *via* the HSQ decomposition route have also recently been used as models to dock chromophores, such as pyrene derivatives, to study energy transfer and enhanced Si light absorption and PL brightness of Si NCs.[47] The highly controlled H-terminated surfaces of the Si NCs of widely tunable size provide effective models for deeper understanding of capping ligand chemistry on Si NC surfaces.

Although ligand-capped Si NCs cannot yet be made effectively with widely tunable size and high yields by colloidal arrested precipitation routes, Si nanorods and nanowires with these properties can be created (Figure 1C−G). In these reactions, metal seeds are added to promote the crystallization of Si at relatively low temperatures. For example, Si nanowires can be grown using Au NCs as crystallization seeds and catalysts in supercritical toluene at ∼490 °C using diphenylsilane as a reactant[52] or at lower temperature in a high boiling solvent like octacosane, using more reactive trisilane.[53] This approach, based on the vapor−liquid−solid mechanism described by Wagner and Ellis in 1964, can be effectively employed in solution-phase reactions (known as solution−liquid−solid (SLS) growth), as demonstrated by Buhro for Group III−V semiconductors in 1995.[54,55] When capping ligands (dodecylamine) were added to SLS reactions with trisilane reactant, much shorter and narrower diameter Si nanorods could be obtained from colloidal reactions in high boiling solvents, such as squalane, at ∼400 °C using either Au[51] or lower-melting Sn.[20] Nanorods with diameters less than 4 nm can be obtained, which is small enough for quantum confinement. Using this approach, Si nanorods have now been produced with relatively bright photoluminesce (with quantum yields >5%). This was enabled by the use of Sn as a seed metal, followed by a controlled surface etch to remove the Sn seeds and a native oxide layer and then a hydrosilylation passivation of the nanorods.[20] Au-seeded Si nanorods were found to be dark, even after etching away the Au seeds,[56] due to Au contamination of the Si nanorod core. The Si nanorod synthesis has been further simplified to a single-step reaction in which a Sn reactant is combined with trisilane in a reaction mixture before hot injection into the reaction solvent.[21] Trisilane serves as a reducing agent to form the Sn seed particles that promote nanorod growth *in situ* in the reaction. Perhaps this approach might yield a direct arrested precipitation of Si NCs, essentially *via* the addition of a crystallization catalyst to enable high yields of crystalline particles at relatively low synthesis temperatures.

Apart from light emission, Si nanomaterials are being explored for other applications. One particularly promising application for solution-grown Si nanowires is to use them as electrode materials in lithium ion batteries (LIBs) as replacements for the graphite anode. Silicon spontaneously lithiates at room temperature and has 10 times the lithium charge storage capacity of graphite. Silicon, however, also expands by almost 300% in volume when it is fully lithiated, and thus nanostructures are required to tolerate this expansion and provide stable and reliable battery performance. One challenge with Si is that it is electrically insulating, and in reasonably thick Si electrodes in LIBs, poor electrical conductivity becomes a major limitation.[57] By manipulating the Si nanowire chemistry, this problem can be overcome either by creating a thin carbon skin on the Si nanowires that serves as a conductive pathway for charge transport[57,58] or by incorporating large amounts of Sn (up to 10%) in Si nanowires,[59] which is well above the solubility limit of Sn in Si. These Si-based nanomaterials have exhibited relatively high charge storage capacities (∼1000 mA h g^{-1}) at high charging rates of 1C. We will provide further discussion on the use of colloidal nanomaterials in rechargeable batteries later in this Nano Focus.

Multinary (Ternary, Quaternary, *etc.*) Non-Heavy-Metal Chalcogenides. Colloidal NCs with increasingly large numbers of elements and nanoheterostructures with gradually higher levels of sophistication are being

produced with extraordinary size, shape, and composition control by colloidal synthesis routes. This evolution toward more complex NCs responds to the growing demand not only for optimized optoelectronic characteristics, but also for earth-abundant and nontoxic chemical compositions. One example of this evolution is the gradual move from binary II–VI NCs to ternary I–III–VI_2 and quaternary I_2–II–IV–VI_4 metal chalcogenides.[60−73] This evolution has paralleled a trend seen in photovoltaics, where the focus is now placed on absorber materials made of less toxic and more abundant elements. When two divalent cations in II–VI compounds are replaced by one group I and one group III cations, Cd- and Pb-free materials with a direct band gap matching the solar spectrum for photovoltaic applications can be produced (*e.g.*, $CuInS_2$, CIS, and $CuIn_{1-x}Ga_xSe_2$, CIGS, known as chalcopyrites). Further replacing the group III element (*e.g.*, In) with more abundant group II and group IV elements (*e.g.*, Zn, Sn) enables another highly appealing class of optoelectronic materials to be obtained (*e.g.*, Cu_2ZnSnS_4, $Cu_2ZnSnSe_4$, CZTS, known as kesterites).

This evolution toward more complex NCs responds to the growing demand not only for optimized optoelectronic characteristics but also for earth-abundant and nontoxic chemical compositions.

Analogous to solid-state syntheses based on complex phase diagrams, the syntheses of multinary NCs often requires finding narrow parameter spaces for balancing chemical composition and morphology. Nevertheless, highly homogeneous I–III–VI_2 and I_2–II–IV–VI_4 NCs, with excellent size, shape, and compositional control, have been produced by several simple and relatively low temperature protocols (Figure 2).[68,74−78] Some syntheses were based on the sequential increase in the number of elements within the NCs, by initially forming binary nuclei that dissolve or fuse together to form multinary NCs or serve as seeds for the growth of the multinary compound by cation exchange or ionic diffusion.[68,76,77,79] As a recent example, binary copper chalcogenide NCs were subjected to partial cation exchange to replace a portion of copper ions with guest cations Zn^{2+} and/or Sn^{4+}.[80] Often, these mechanisms limit the minimum achievable NC size, as relatively long reaction times are required to reach the target composition. Therefore, to obtain small quantum-confined NCs with controlled composition, the reactivities of all cation precursors need to be finely balanced to form nuclei that already contain all desired elements.[81,82]

Besides size and shape uniformity and overall chemical composition,[68,75−77,83−90] compositional and phase homogeneities within the NC are key parameters for tuning optical characteristics of multinary NCs. One challenge in this direction is that secondary phases often may remain unnoticed as they possess nearly the same crystal structure and lattice parameters as the multinary compound and thus are not discernible by X-ray diffraction. Resonant Raman spectroscopy may provide a solution in this respect. Besides the detection of secondary phases by ensemble-averaging techniques mentioned above, particle-to-particle composition dispersion, in principle, requires single-particle analyses. In this regard, while some reports point to possible broad particle-to-particle composition distributions, others demonstrate compositionally uniform ensembles with dispersions decreasing with the reaction temperature.[80,91,92]

Besides CIS, CIGS, and CZTS, tetrahedrally bonded ternary and quaternary chalcogenide phases can be formed by more than 30 elements.[68,70,71,77,78,91,93−95] Within these compounds, several polymorphs are possible,[96,97] ranging from cation-disordered zinc blende and wurtzite phases to cation-organized chalcopyrite, CuAu-like and orthorhombic wurtzite–chalcopyrite and wurtzite–CuAu-like ternary phases,[63,69,73,75,85,98−103] and kesterite, stannite, wurtzite–kesterite, and wurtzite–stannite quaternary phases.[76,90,101,104,105] The favored crystal phase depends first on the cation's nature; for example, Cu_2ZnSnS_4 tends to crystallize in the kesterite phase and $Cu_2CdSnSe_4$ in the stannite lattice. In Cu_2ZnSnS_4, the Cu–Zn layer appears to be disordered, whereas the Cu–Sn layer is ordered.[106] The organization (site occupancy) of the cations in different phases can also be kinetically controlled by a proper selection of precursors, surfactants, and synthesis conditions. X-ray or electron diffraction studies can easily differentiate between cubic and hexagonal stacking. However, it is not straightforward to determine the atomic site occupancy experimentally. Better control of the cationic order within the structure will require not only a better understanding of the nucleation and growth mechanisms[73,100] but also more accurate insight from the characterization methods. This will increasingly require moving from conventional X-ray diffraction (XRD) and high-resolution transmission electron microscopy (HRTEM) to neutron diffraction[107] and aberration-corrected electron microscopy with analytical mapping on the atomic scale (electron energy loss spectroscopy, energy-dispersive X-ray spectroscopy).[76] Besides being challenging from the characterization point of view, tunable site occupancies of cations in multinary NCs offer exciting opportunities for controlling optical and electronic properties while maintaining compositions of

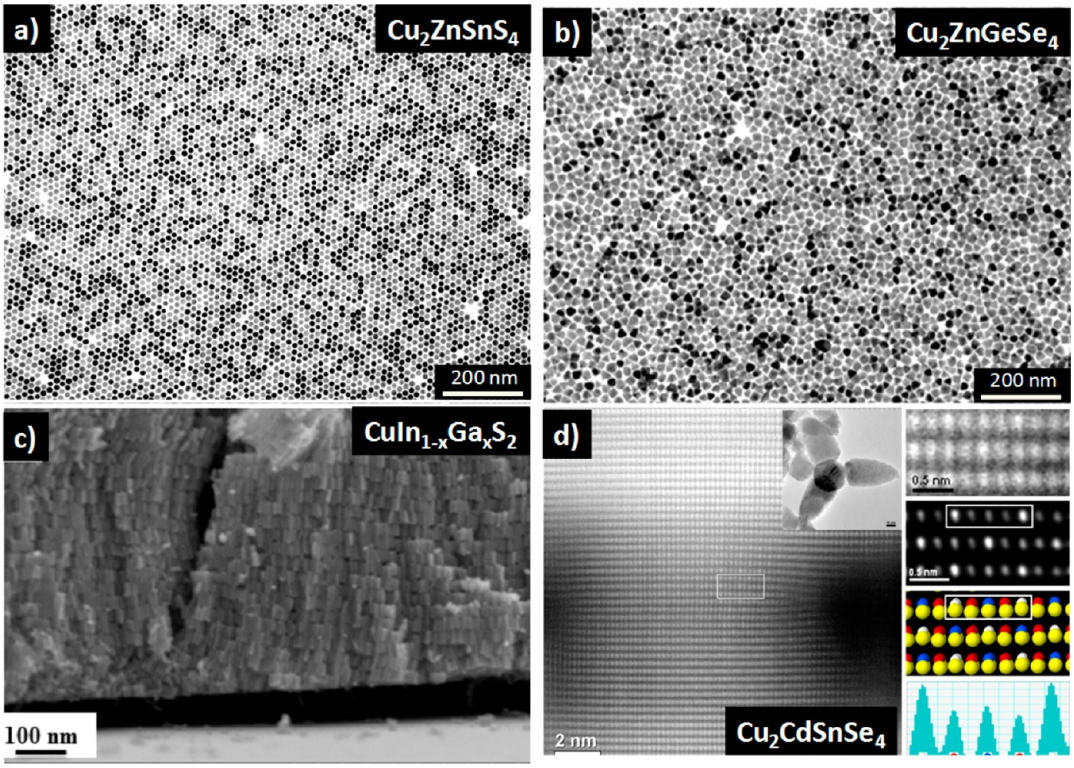

Figure 2. Examples of quaternary Cu-based chalcogenide colloidal nanocrystals. (a) TEM image of wurtzite Cu_2ZnSnS_4 NCs. Reprinted from ref 89. Copyright 2014 American Chemical Society. (b) TEM image of zinc-blende-like $Cu_2ZnGeSe_4$ NCs. Reprinted from ref 78. Copyright 2012 American Chemical Society. (c) Scanning electron microscopy image of aligned wurtzite $CuIn_{1-x}Ga_xS_2$ nanorods. Reprinted from ref 74. Copyright 2012 American Chemical Society. (d) Atomic-resolution HAADF-STEM images, three-dimensional atomic model, and intensity profile from the $[111]_{ZB}$ zone axis of a $Cu_2CdSnSe_4$ tetrapod. Reprinted from ref 76. Copyright 2014 American Chemical Society.

abundant and nontoxic elements. In multinary NCs, the band gap can be tuned not only by means of quantum size effects[60,81,87,108] but also by compositional control at the anion and cation sites.[79,83,106,109−119] Both anionic (S, Se, Te) and cationic (*e.g.*, the In/Ga ratio in CIGS) adjustments have been used in these studies.

Exciting compositional tunability of complex multinary NCs is often accompanied by considerable stoichiometric deviations, leading to large densities of donor−acceptor states within the band gap, both shallow and deep with respect to the edges of the conduction and valence bands. The multiple possibilities for radiative recombination through these donor−acceptor pairs result in broad photoluminescence peaks, long radiative lifetimes, and significant Stokes shifts.[71,120] One first consequence of PL based on donor−acceptor recombination is that no precise band gap information can be obtained from PL measurements in these materials. This PL mechanism makes the emission of multinary NCs strongly dependent not only on size but also on composition, phase, and ordering. The large density of defects also results in nonradiative recombination pathways, significantly lowering PL quantum yields. In fact, contrary to ternary I−III−VI_2 NCs, quaternary I_2−II−IV−VI_4 NCs show no PL emission at room temperature.[50,51] Substantial progress in controlling defects may allow the use of low-cost and environmentally friendly I_2−II−IV−VI_4 NCs in bioimaging,[71,121] light-emitting diodes (LEDs),[119] photocatalysis,[89,110,122−126] and NC-based solar cells operated as quantum dot devices (*e.g.*, without annealing-induced recrystallization into the bulk).[127,128]

Nonmetallic Plasmonic NCs. An emerging area of research in NCs is that of non-noble-metal plasmonic materials.[129−131] In these materials, free carriers can arise from the presence of dopant species in a metal oxide host (for example, tin dopants in indium oxide[132]) or from a large number of metal vacancies in metal chalcogenides (*e.g.*, copper vacancies in copper chalcogenide NCs)[133−138] or as a result of a redox reaction.[139] The rapidly growing interest in these types of particles stems from the fact that their densities of free carriers can readily be tuned by composition. As a consequence of this, their localized surface plasmon resonance (LSPR) can be tuned over a relatively wide spectral range (in the near- and mid-infrared spectral regions). This tunability adds an extra facet to plasmonic nanomaterials, something that traditional metals such as gold do not have, as the numbers of free carriers in the latter stay fixed. Taking into account that, in the majority of cases, the elements composing these new plasmonic materials are cheaper than gold,

these NCs have been proposed in a wide variety of applications including photothermal therapy,[134,140] sensing,[141,142] photocatalysis,[143] imaging,[144,145] electrochromic devices,[146,147] electronics,[148] and enhancement of chemical reactions.[149] On a more fundamental level, all these new generations of NCs represent interesting testing grounds on which it is possible to benchmark and to refine theories and models that so far have been applied mainly to particles of more traditional materials, such as gold, silver, and copper.[150−152] Recent exciting advances for metal oxide NPs came from the possibility to achieve cation−anion codoping, which increases free carrier densities even further, thus pushing the plasmon resonance to higher frequencies.[153] Coupling together two or more domains of materials with different plasmonic properties in a single NC, as recently shown by Liu *et al.*,[145] is certainly one way forward. Such hybrids provide an opportunity to tune the optical response further, for instance, to have a plasmon resonance spanning a larger spectral region. Another exciting direction is represented by the possibility of eliciting plasmonic resonances in nanomaterials by photoexcitation, that is, without the need to add dopants or to create vacancies.[154] On the other side, several fundamental questions are receiving deep scrutiny, such as how dopant distributions influence the plasmonic properties,[132] or in which cases the carriers are really free (as in the more traditional metal NCs) *versus* localized,[155] which have strong implications for the potential applications.

An emerging area of research in NCs is that of non-noble-metal plasmonic materials.

Organic Pigment Nanocrystals. Besides more traditional colloidal QDs composed of inorganic semiconductors, NPs made from organic semiconductors also have great potential for applications in optoelectronics.[156−167] Nanoparticles from small organic molecules are believed to allow greater variability and flexibility in materials synthesis than do their inorganic counterparts.[159] The development of organic NPs, however, is not yet as advanced as that of inorganic NCs. The systematic investigation of fluorescent organic NPs[168−173] resulted in organic NPs with size-dependent fluorescent properties, which are significantly different from those of bulk samples.[167,168,170,172] There are also striking similarities in the syntheses of NPs from organic small molecules and inorganic QDs. Perylenes and their derivatives represent a showcase example: they are synthesized *via* colloidal chemical reactions in the presence of functional ligands, in a synthesis route showing the typical features of inorganic QD syntheses—a discrete nucleation event is followed by a slower controlled growth on the existing particles, which enables control over the sizes of quasi-spherical NPs and helps to obtain narrow size distributions (<10%).[157] By tuning the synthesis conditions, precise shape control can also be achieved, and for two-dimensional perylene nanosheets, even high crystallinity could be confirmed by electron diffraction.[166] Thus, in some cases, organic NPs also represent real colloidal NCs, whose crystallization is governed not only by intermolecular interactions but also by the synthetic conditions. Recently, the collection of organic colloidal NCs has been expanded through the introduction of a general procedure that transforms commercially available insoluble microcrystalline hydrogen-bonded organic pigment powders into colloidal solutions of variously sized and shaped semiconductor microcrystals and NCs.[174] Hydrogen-bonded organic pigments such as indigos, quinacridones, and phthalocyanines are widely produced industrially as colorants for everyday products in various cosmetic and printing inks.[175] The synthesis of microcrystals and NCs is based on the transformation of the pigments into soluble dyes, so-called latent pigments (Figure 3a,b), by introducing transient protecting groups on the secondary amine moieties, followed by controlled deprotection in solution. Three deprotection methods have been demonstrated so far: thermal cleavage, acid-catalyzed deprotection, and amine-induced deprotection. During these processes, ligands are introduced to afford colloidal stability, to provide dedicated surface functionality, and for size and shape control. The resulting microcrystals and NCs have optical absorption and photoluminescence that are widely tunable across the visible (vis) to near-infrared range. Due to the excellent colloidal solubility offered by the ligands, the obtained organic pigment NCs are suitable for solution processing of (opto-)electronic devices. As examples, phthalocyanine nanowire transistors as well as quinacridone NC photodetectors (Figure 3c) with photoresponsivity values up to 1 A/W, far outperforming those of vacuum-deposited reference samples, have been demonstrated. The high responsivity was enabled by photoinduced charge transfer between the pigment NCs and the directly attached electron-accepting vitamin B2 ligands. These semiconducting NCs provide a new paradigm for preparing organic semiconductor materials from commercial colorants, and they offer a cheap, nontoxic, and environmentally friendly alternative to inorganic NCs.

***In Situ* Methods for Studying Nanocrystal Growth.** Monitoring the nucleation and growth of NCs *in situ* opens important perspectives and opportunities for the control of size, shape, and composition through the design and optimization of synthetic methods. The growth mechanism is believed to govern the morphology of the initial crystalline

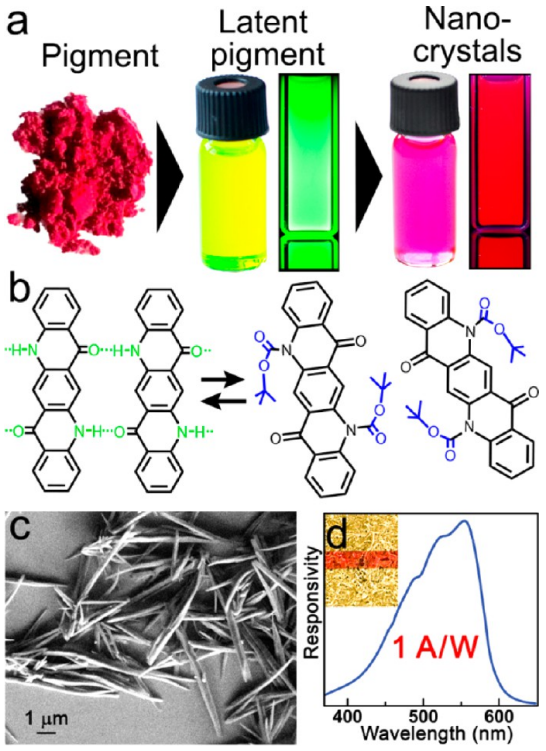

Figure 3. Quinacridone organic pigment nanocrystals. (a) Insoluble organic pigment powder is converted into a strongly luminescent latent pigment solution, which is used as a precursor for the subsequent synthesis of ligand-protected NC colloids. (b) Hydrogen-bonded pigment crystals are solubilized *via* protection of the secondary amines by *tert*-butoxycarbonyl groups. Controlled deprotection in the presence of ligands results in shape-controlled NCs (secondary electron microscopy image in (c)). (d) Photoresponsivity spectrum of a quinacridone organic pigment NC film, deposited on a paper substrate. The photoconducting device is shown in the inset; two gold electrodes are connected to the NC film, seen as a red stripe. Reproduced from ref 174. Copyright 2014 American Chemical Society.

seed, which, in turn, dictates the morphology of the final NC.[176] However, suitable *in situ* methods are scarce due to the restricted choice of observables and the stringent requirements for monitoring the chemical syntheses of NCs. First, the acquisition time must be fast, as the initial growth kinetics often take place on time scales in the range of seconds. Second, the method must be compatible with the specific reaction conditions (*e.g.*, high temperature, inert atmosphere, *etc.*). Third, the measurement must not disturb the reaction itself, which poses problems when using high-energy electron beams or X-ray radiation, for example.

The most direct method for *in situ* observation of NC growth is the use of electron microscopy on liquids, giving access to the kinetics of size and shape evolution with reaction time.[177] In this case, the precursor solution is placed in a special sample holder, containing, for example, silicon nitride windows, which are transparent for the electron beam. Alternatively, graphene sheets have been used for entrapping the liquid precursor film and recording the first real-time movies of the growth of platinum NPs.[178] In order to minimize beam-induced NC growth and other artifacts, scanning transmission electron microscopy (STEM) techniques at relatively low doses have to be applied.[179] Because mixing or even injection of precursors inside the sample holder is difficult to realize, these techniques have thus far mainly been applied to metal NPs, using a homogeneous precursor solution and triggering nucleation and growth by means of the electron beam or by supplying thermal energy.

In the case of semiconductor NCs, their distinct size-dependent optical properties can be exploited by means of *in situ* UV–vis absorption measurements to determine NC growth kinetics.[180–183] An advantage of this method is its high temporal resolution, on the order of microseconds. On the other hand, this method is restricted to systems presenting a gradual color change or at least gradual changes in optical density of the reaction medium during growth. This technique has been proven useful in combination with (*ex situ*) NMR spectroscopy for the elucidation of the detailed reaction mechanisms taking place in different syntheses of CdSe NCs.[184–188]

Finally, *in situ* X-ray diffraction experiments provide a powerful tool for assessing NC nucleation and growth kinetics. Small-angle X-ray scattering (SAXS) can give access to precursor organization in prenucleation stages as well as to the mean size and auto-assembly of crystallites in postnucleation stages. Wide-angle (WAXS) measurements, on the other hand, enable identification of the crystal structure. High-energy synchrotron radiation is necessary for obtaining sufficient signal intensity during *in situ* X-ray studies on solutions enclosed in or flown through thin glass capillaries. Sample damage is minimized by using a beam shutter and short acquisition times (typically tens of milliseconds for SAXS and seconds for WAXS, depending on the detectors used). In one of the first examples, Abecassis *et al.* investigated the nucleation and growth of gold NPs by means of a combined SAXS/WAXS and UV–vis study.[189] Meanwhile, (extended) X-ray absorption fine structure (XAFS, EXAFS) measurements have been used to study the nucleation of gold[191] and CdSe NCs.[190] Reiss *et al.* investigated the nucleation and growth of Cu_2ZnSnS_4 (CZTS) NPs.[192] As the performance of CZTS-based devices derived from CZTS NPs strongly depends on the stoichiometry of the absorber material,[193] the fine

control of the crystal structure and absence of detrimental secondary phases are crucial. *In situ* SAXS measurements on the CZTS precursor solution revealed that during the initial heating stage (110 °C, 30 min) ~10 nm NPs are formed, which self-assemble into face-centered cubic superlattice at lower temperature (25 °C). While the SAXS signal disappears when going to higher temperature (280 °C), the evolution of the reaction can be monitored with the Bragg peaks in the WAXS spectrum. The initially formed NPs, having a nominal composition of $Cu_{3.1}Zn_{1.5}S_4$ (determined *ex situ*), undergo a fast phase transition and cation exchange within the first 10 min, leading to the "self-adjustment" of composition to $Cu_{2.1}Zn_{1.14}SnS_4$ and PMCA crystal structure (space group $P\bar{4}2m$), while no change in NP size is observed. These results demonstrate that *in situ* X-ray studies using synchrotron radiation are particularly useful for probing transient crystalline phases in multinary NCs. The complementary data obtained with SAXS and WAXS measurements shed light on the nucleation and growth mechanisms, and the fast acquisition times give access to reaction kinetics.

***In Situ* Electron Microscopy Methods for Monitoring Chemical and Structural Transformations in Individual Nanocrystals.** Hand-in-hand with approaches for following the growth kinetics of NCs, various attempts have been made to monitor chemical and structural transformations in individual NCs directly in an electron microscope, with time resolution and often also with atomic resolution, when perturbations such as thermal annealing and/or irradiation are applied to the NCs.[194−199] These studies have been made possible by recent advances in electron microscopy tools. Examples of phenomena that have been studied include (but are not limited to) atomic-scale resolution imaging of phase transitions and transformations in morphology (including sublimation) in gold and PbSe NCs,[194] thermal annealing of Au−CdSe NCs with formation of metal−semiconductor epitaxial interfaces,[195] reorganization of Au−CdS NCs to AuS/Cd core−shell structures by combined annealing and electron irradiation,[196] transformation of CdSe/Cu_3P sandwich NCs to Cu_2Se NCs following combined Cd and P sublimation upon annealing,[197] direct observation of structural fluctuations in a single rod-shaped Cu_2S NC,[198] and imaging, with atomic resolution, of intra-NC cation exchange reactions starting from CdSe−PbSe segmented NCs.[199] *In situ* studies of transformations in nanomaterials will receive a further boost in the near future thanks to the advent of cameras with direct detection technology, which enable the recording of thousands of electron microscopy frames at high resolution with low electron doses. These upcoming advances will make it possible to follow nanoscale processes with millisecond and submillisecond resolution. Aside from the fundamental science uncovered by such studies, these experiments will be important for evaluating the long-term stability of materials and devices using NCs as key components, especially when such materials and devices are expected to withstand extreme conditions in terms of irradiation and heating.

SURFACE CHEMISTRY—A GATEWAY TO APPLICATIONS OF NANOCRYSTALS

Nanocrystal surface chemistry is garnering increasing attention. Surface-bound capping ligands have profound effects on optical properties and dictate electronic transport in dense NC solids, besides their role in the synthesis of NCs. Understanding, controlling, and adjusting the termination of NC surfaces—a field called NC surface chemistry, in short—is therefore a major enabler of NC-based applications. The two primary trends in NC surface chemistry research are the molecular-level characterization of currently prevailing organic capping ligands and the development of novel inorganic surface functionalizations that are more suitable for NC integration into solid-state devices. Important steps have also been undertaken toward atomistic computational modeling of the whole NCs, including their surface capping ligands, and to link surface chemistry to NC properties.[200,201]

Toward Molecular-Level Understanding of Organic Surface Ligands: Importance of Nuclear Magnetic Resonance Spectroscopy. About half of the atoms in a 3 nm NC are surface atoms. Progress in surface chemistry relies on experimental techniques giving insight into the composition of NC surfaces, a conceptual framework to describe surface termination or coordination, and rational methods to modify NC surfaces. The introduction of one-dimensional (1D) and two-dimensional (2D) solution NMR spectroscopy techniques (see Figure 4a−c) initiated in-depth surface chemistry studies of NCs of binary II−VI, IV−VI, and III−V semiconductors (denoted as ME) such as CdE (E = S,Se,Te), PbE, and InP synthesized in apolar media by hot injection or heating up is especially important.[202] These synthetic approaches make use of M and E precursors, coordinating agents such as carboxylic or phosphonic acids, thiols or amines, and a noncoordinating solvent. Taking the specific example of CdSe NCs synthesized in the presence of carboxylic acids,[203] it was found that these carboxylic acids end up as ligands tightly bound to the NC surface (see Figure 4a−c). Moreover, it could be demonstrated that the actual ligand is a carboxylate moiety rather than a carboxylic acid where the negative charge on these anionic ligands is compensated by an excess of metal cations on the NC surface.[204]

A variety of studies show that the classification of ligands as L-type, X-type, or Z-type, depending on the number of electrons the NC−ligand bond takes from the NC (0, 1, and 2, respectively) to form a two-electron bond, provides a convenient

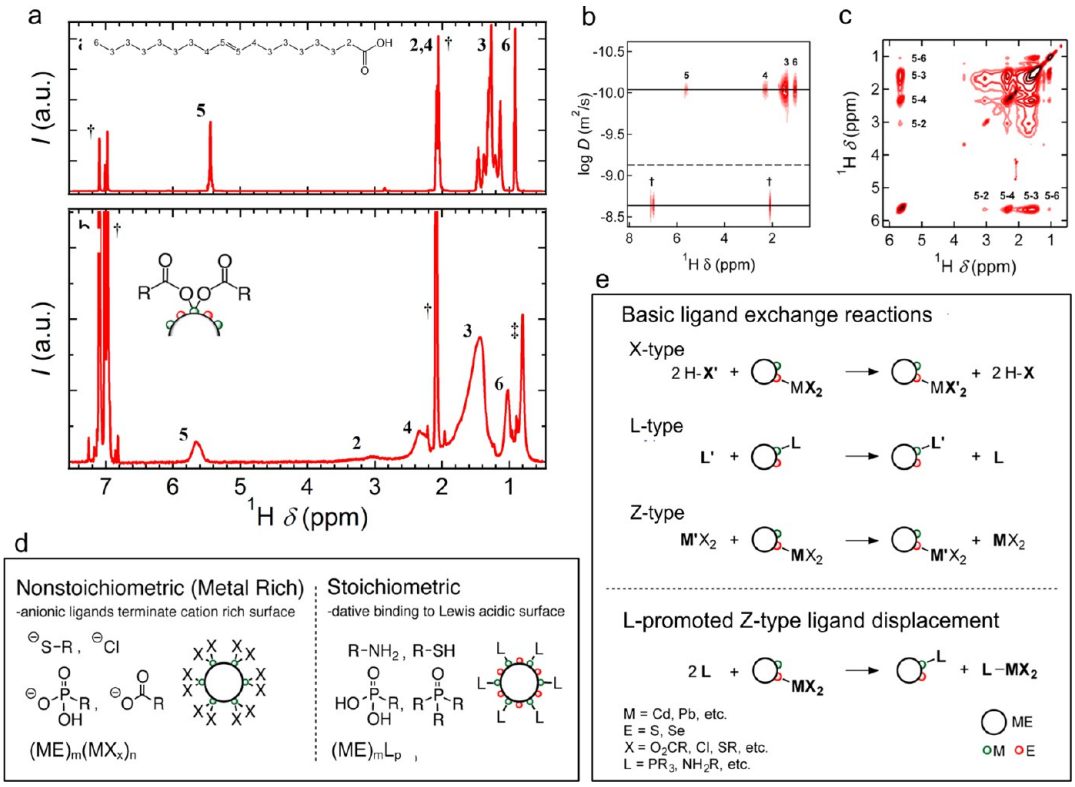

Figure 4. (a) One-dimensional ^{1}H nuclear magnetic resonance spectrum of (top) oleic acid and (bottom) CdSe nanocrystals in toluene-d_8, synthesized in the presence of oleic acid (see inset). The NC spectrum features broadened resonances that correspond to those of free oleic acid and point to the binding of oleate moieties to the CdSe surface. (b) Diffusion-ordered spectrum of CdSe NCs in toluene-d_8, showing that the broadened resonances are related to species that adopt the small diffusion coefficient characteristics of the CdSe NCs and are thus bound to the NCs. (c) Nuclear Overhauser effect spectroscopy, where strongly negative cross-peaks are characteristic of species interacting with the NCs. (a–c) Reprinted from ref 204. Copyright 2010 American Chemical Society. (d) Representation of the two classes of NCs, depending on their surface chemistry. Reprinted from ref 205. Copyright 2013 American Chemical Society. (e) Overview of different ligand exchange reaction possibilities, depending on the NC surface chemistry. Reprinted from ref 217. Copyright 2013 American Chemical Society.

framework to understand these ligand–NC interactions.[204−207] In combination with the need to form charge-neutral NCs in apolar environments, the results can be split into two extreme classes (Figure 4d). The first describes NCs where the formal charge on the metal cations M and anions E is balanced—for binary NCs, this corresponds to the bulk stoichiometry—and which are passivated by L-type ligands [(NC)(L)$_n$)]. The second are NCs that have a positive formal charge—corresponding to an excess of metal cations—that is balanced by the formal negative charge of X-type ligands [(NC)(MX$_x$)$_n$]. Remarkably, all detailed, quantitative studies addressing stoichiometry and ligand binding published thus far showed as-synthesized and purified NCs behaving according to the (NC)(MX$_x$)$_n$ class,[204−211] like the CdSe NCs discussed above, where X$^-$ moieties correspond, for example, to carboxylates[204,207,209,211] or phosphonates.[206,208,210,212] L-type ligands such as amines or phosphines, however, typically exhibit a dynamic adsorption/desorption equilibrium, suggesting that the [(NC)(L)$_n$)] class results in labile NCs that are lost upon repetitive sample purification.[213−215]

Currently, the framework established to describe ligand–NC interactions in apolar media is being extended to different material systems, where the first question is whether the prevailing [(NC)(MX$_x$)$_n$] class remains valid. In the case of metal oxide NCs such as HfO_2 and ZrO_2, for example, it was found that carboxylic acids still bind as carboxylates, yet charge compensation is accomplished by the coadsorption of protons onto surface oxygen atoms, rather than by a cation excess.[216] In addition, the classification of ligands as L-, X-, or Z-type underlines the development of rational ligand exchange schemes (Figure 4e). For instance, the charge neutrality

Progress in surface chemistry relies on experimental techniques giving insight into the composition of NC surfaces, a conceptual framework to describe surface termination or coordination, and rational methods to modify NC surfaces.

condition makes L−L′ and X−X′ exchange feasible, such as the replacement of carboxylates by hydrogen phosphonates, whereas L−X exchange is not.[217] In addition, the MX_x unit can be seen as one effective Z-type ligand. As a result, it can be replaced by other $M'X_x$ complexes, or its displacement can be promoted by L-type ligands, including amines and phosphines, but also alcohols and ethers.[217] This enables NCs with a wide range of surface terminations and M:E stoichiometries to be purposely formed, and it explains why, for example, exposure to amines has been deemed effective to remove X-type ligands from PbS or PbSe NCs.[218]

The intrinsically different surface chemistry related to L-type and X-type ligands has consequences for the design of hot-injection syntheses. Especially in the case of phosphine oxides, which are supposed to bind as L-type ligands, it has been shown that the actual surface-bound moieties are X-type ligands, resulting from phosphonic and phosphinic acid impurities.[219,220] As a result, NC stoichiometry and surface chemistry were shown to depend on the purity of the chemicals used.[212] In much the same way, the possible exchange reactions of X-type ligands point toward the need for careful NC purification methods. Taking the examples of short-chain alcohols, which are often used to purify reaction mixtures, it has been found that they can displace carboxylates by both X−X′ replacement and L-type-promoted MX_x replacement.[217,221] As ligand coverage affects NC properties such as the photoluminescence quantum yield,[215,222] it follows that the road toward NC applications will benefit from robust synthesis methods and carefully designed purification and surface functionalization schemes.

Inorganic Surface Ligands for Nanocrystal Integration into Solid-State Devices. Most of the NC applications (LEDs, solar cells, electronic circuits, photodetectors, *etc.*) relate directly to the ability to control NC surface properties. Classical synthetic routes, such as the Murray, Norris, and Bawendi synthesis of CdSe QDs[13] or the Brust synthesis of Au NPs[223] used surface ligands with long hydrocarbon chains (Figure 5A). Such ligands provide steric colloidal stabilization in nonpolar solvents and made NCs compatible with organic solvents and polymers. However, the presence of insulating organic molecules at NC surfaces introduces bottlenecks for charge transport and does not permit seamless integration of chemically synthesized NCs into inorganic glasses, ceramics, *etc.*

Recent developments of inorganic ligands provide a complementary toolbox to traditional nanomaterials. The scope of inorganic ligands has significantly diversified in recent years. Thus, small nucleophilic ions like chalcogenides (S^{2-}, Se^{2-}, Te^{2-}),[224] halides (Cl^-, Br^-, I^-),[206,225,226] and pseudohalides (CN^-, SCN^-, N_3^-)[226,227] have been used to bind electrophilic metal sites at the NC surface (Figure 5B,C,D). These negatively charged ions created NCs with negatively charged surfaces balanced by an ionic cloud of counterions. More elaborate inorganic surface ligands included molecular metal chalcogenide (MCC), also called chalcogenidometallate,[228,229] and metal halide complexes[230] (Figure 5E,F). In addition to stronger multidentate binding, these ligands could form conductive "bridges" between NCs to facilitate charge transport. Oxometallate and even more complex polyoxometalates (*e.g.*, $[Nb_{10}O_{28}]^{6-}$, $[PMo_{12}O_{40}]^{3-}$) can also be used as functional surface ligands for colloidal NCs (Figure 5G).[231−235] Yet another approach to prepare NCs without a shell of covalently bound organic ligands is shown in Figure 5H.[224,236,237] Negatively charged organic ligands (*e.g.*, carboxylate or phosphonate) can be removed, leaving behind a positively charged NC surface and weakly coordinating anions like BF_4^- that do not bind to the NC surface.[236,237]

Inorganically capped NCs introduce a viable alternative to NCs capped with organic ligands, significantly expanding the scope of applications for this class of materials. Inorganic ligands typically provide colloidal stability in polar solvents, which is needed for solution-based fabrication of electronic and optoelectronic devices. At the same time, inorganic ligands do not block electron transport, enabling efficient solution-processed field-effect transistors (FETs),[238−240] solar cells,[241,242] and photodetectors.[238] Colloidal NCs with inorganic ligands can be used for making various composite materials where size- and shape-tuned NCs are integrated into amorphous inorganic hosts. Examples include mixed ionic and electronic conducting Ag_2S NCs in GeS_2

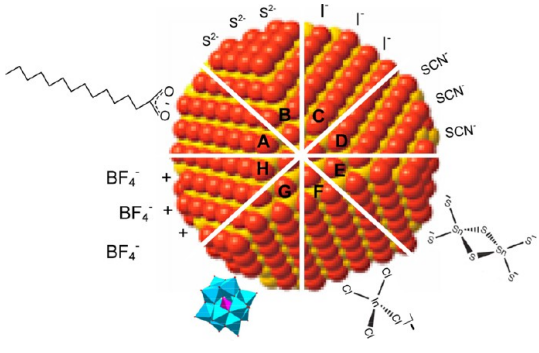

Figure 5. Approaches to nanocrystal surface chemistry: (A) Traditional organic surface ligands with long hydrocarbon chains, *e.g.*, myristate. (B−D) Monodentate inorganic ligands including chalcogenide (B), halide (C), and pseudohalide (D) ions. (E−G) Multidentate inorganic ligands including metal chalcogenide complexes (*i.e.*, chalcogenidometallates) (E), halometallates (F), and polyoxometalates (G). (H) Bare NC surface with positive surface charge balanced with non-nucleophilic BF_4^- ions.

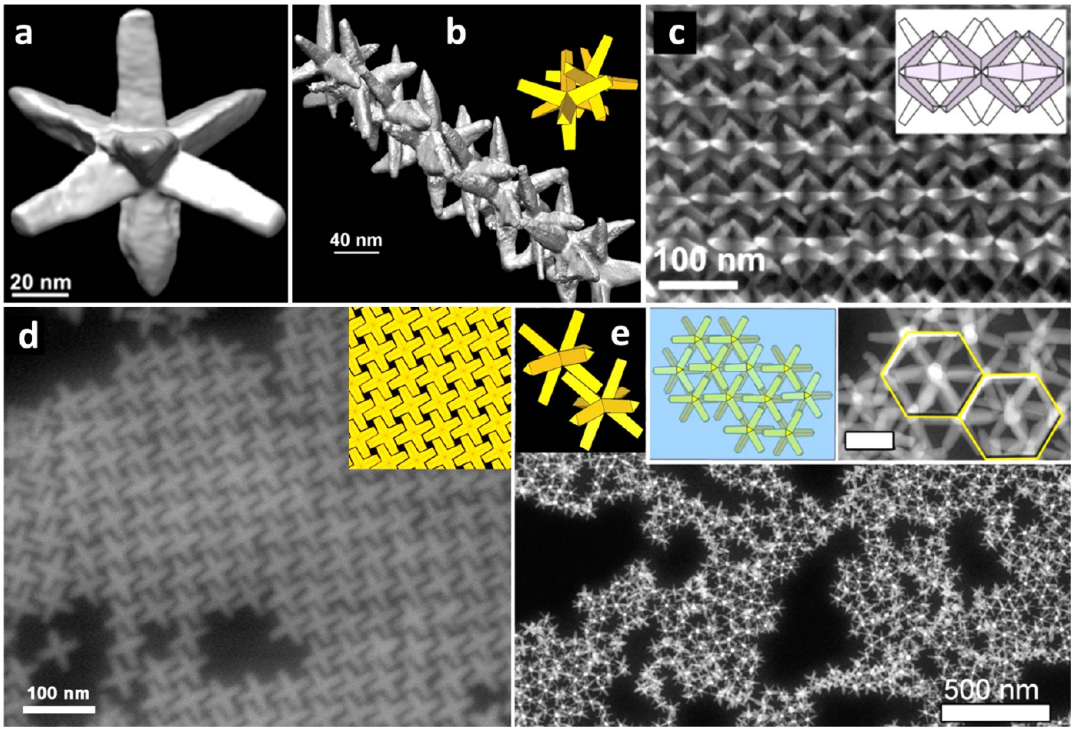

Figure 6. Various self-assembled structures of octapods. Three-dimensional reconstruction of (a) a single branched nanocrystal (octapod) from scanning transmission electron microscopy projections, revealing octahedral symmetry, and (b) a single chain of octapods, demonstrating their interlocking sequence. (c) 3D-ordered octapods in a hierarchical structure. Panels (a–c) are reprinted with permission from ref 250. Copyright 2011 Nature Publishing Group. (d) Quasi-2D self-assembly of octapods forming a square lattice. The scale bar in the top right inset is 50 nm. Reprinted from ref 251. Copyright 2012 American Chemical Society. (e) 2D hexagonal assembly of octapods with pod–pod parallel configuration. Reprinted from ref 252. Copyright 2014 American Chemical Society.

glasses derived from $[Ge_2S_6]^{4-}$ ligands[243] or luminescent PbS/CdS core–shell NCs capped by AsS_3^{3-} ligands that were integrated into As_2S_3 chalcogenide glasses.[244] Advanced electrochromic materials have been prepared from plasmonic indium–tin oxide NCs integrated into NbO_x glass.[235] Finally, one can design chemical reactions between NCs and inorganic ligands to create new phases. This has been shown for Cu_2Se NCs capped with $In_2Se_4^{2-}$ ligands: annealing a film of these NCs resulted in the formation of a pure $CuInSe_2$ phase, suitable for solar cell applications.[245]

LONG-RANGE-ORDERED NANOCRYSTAL ASSEMBLIES

Shape-Engineered Superlattices. Several advances have been made recently in the understanding and experimental realization of ordered superstructures of nonspherical, but well-defined, polyhedral NPs. In the case of most polyhedral shapes, researchers recently demonstrated the ability to make accurate computational predictions on their assembly behavior.[246,247] Predictions, however, turn out to be much more complicated for objects of more complex forms, such as branched NPs. One example in this category is represented by colloidal octapod-shaped semiconductor NCs with a central core of CdSe and pods of CdS, for which elaborate control over size, shape, and shape distribution has been achieved.[248,249] Figure 6a is an electron tomography reconstruction of a single octapod. In this case, the experimental observations of the possible organizational pathways preceded the theory and, furthermore, provided a benchmark for testing existing and new computational tools on self-assembly. Miszta *et al.*, for example, found that when octapods aggregate in the solution phase they self-organize first into linear chains of NCs.[250] This is shown in Figure 6b, which reports a tomographic reconstruction of a chain. This type of organization is driven by the maximization of van der Waals interactions between neighboring octapods when they are in a so-called "interlocked configuration", that is, when neighboring octapods are rotated by 90° with respect to each other, as shown in the yellow sketch of Figure 6b (simple geometrical considerations show that this configuration maximizes the contact area between octapods). Under appropriate solvent conditions, chains of interlocked octapods can reach up to several tens of particles, and these chains then interact with each other side-by-side, leading to the formation of ordered three-dimensional (3D) superstructures of octapods (Figure 6c). This type of assembly is therefore hierarchical: first, one type of ordered unit is formed (a chain of particles); at a second stage, such linear units self-organize to form 3D structures. Modeling based

on anisotropic van der Waals forces between the particles was able to reproduce the formation of chains but failed to reproduce the chain–chain interactions.[250] Electrical transport experiments on such 3D-ordered octapod assemblies showed that their regular structure results in cold-field-emission-dominated photoconductivity.[253]

For objects as complex as octapods, the experimental conditions under which their aggregation is triggered are extremely critical in dictating a specific assembly pathway. An interesting case study was reported by Qi *et al.*,[254] who explored the dynamics of the assembly of octapods that are constrained to move on a surface (and are therefore in a 2D space) with four of their eight pod tips forced to touch the surface at all times. This can be experimentally realized by depositing a solution of octapods and letting the solvent evaporate quickly so that not all octapods have time to interlock into chains, leaving many octapods as individual particles at the last stages of solvent evaporation. As they are not entirely free to rotate in 3D, these individual octapods end up forming square superlattices of the kind displayed in Figure 6d (see also inset). In this particular type of quasi-2D system, it was possible to model the complete phase diagram in the 2D parameter space of volume fraction of octapods and aspect ratio of their pods, in very good agreement with the experiments.[254]

Several advances have been made recently in the understanding and experimental realization of ordered superstructures of nonspherical, but well-defined polyhedral NPs.

Based on calculations, two configurations of neighboring octapods are found to be low energy:[250] one is the interlocked case discussed earlier and sketched in Figure 6d, and the other configuration is sketched in the top left inset of Figure 6e. In this latter case, the particles are spatially organized such that two of their respective pods are parallel to each other. Assemblies based on this configuration, which result in an open framework of the type displayed in the central inset of Figure 6e, have not thus far been realized in the solution phase. This is most likely because the interlocked configuration is more favorable over the parallel pod–pod one, and therefore, the octapods quickly form chains. Recently, however, Arciniegas *et al.*[252] experimentally prepared a 2D version of such an open type of assembly, at least locally (see Figure 6e and its top left inset). This was done by depositing a droplet of a solution containing both octapods and poly(methyl methacrylate) on a substrate and again letting the solvent evaporate quickly. During solvent evaporation, the octapods were dragged at the droplet–air interface and remained there, partially immersed in the liquid and partially protruding from it. In this situation, the octapods appeared to have a degree of rotational freedom. Since the particles were neither completely inside the liquid nor completely out of it, neighboring octapods seemed not to prefer to interlock, but instead, they adopted the parallel pod-to-pod configuration.[252]

Octapods are perhaps one of the most revealing examples of how objects of complex shapes can be strongly influenced by their local environment to choose a specific organization pathway. In the future, much higher levels of complexity and functionality in self-assembled nanomaterials are likely to be achieved as we learn how to combine different objects having complex yet complementary shapes. This field is truly in its infancy. One beautiful example in this direction was recently given by Paik and Murray,[255] who prepared binary superlattices of particles having shapes that interlock with each other like in a puzzle. These were planar tripodal NPs of Gd_2O_3 shape and rhombohedral GdF_3 platelets. The complementarity in the shapes enabled their organization into ordered superstructures, with both control over position and orientation of the two types of particles over micrometer scales.

Octapods are perhaps one of the most revealing examples of how objects of complex shapes can be strongly influenced by their local environment to choose a specific organization pathway.

Converting Superlattices into Two-Dimensional Honeycomb Crystals. By evaporating a solution of PbSe NCs capped with oleic acid over a liquid ethylene glycol surface, Vanmaekelbergh *et al.* formed an ordered 2D superlattice. Further, by the action of gentle heating, the PbSe cores fused into a honeycomb architecture (Figure 7).[256] Electron microscopy, combined with grazing-incidence SAXS and STEM, revealed that the NCs attach *via* the (100) facets into a honeycomb structure with octahedral symmetry, despite the fact that two other honeycomb symmetries are also possible (tetrahedral and trigonal). The honeycomb superlattices are atomically coherent and have octahedral symmetry that is buckled; the NCs occupy two parallel planes, leading to a silicene-like lattice. Taking into account recent computer simulations using density functional

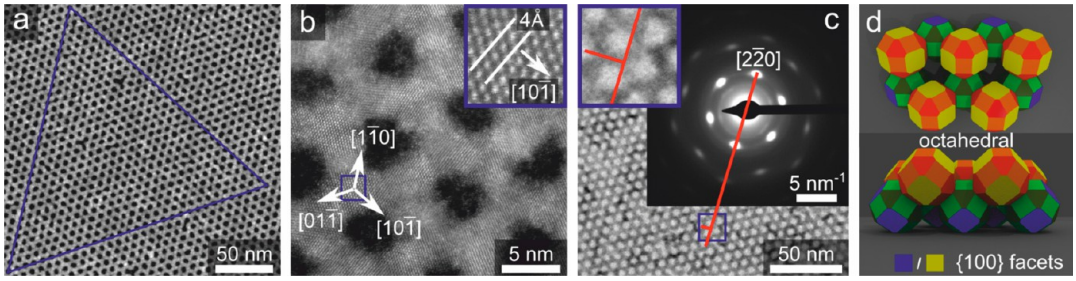

Figure 7. Single-crystalline two-dimensional PbSe honeycomb structure created by means of oriented attachment during self-assembly. (a) HAADF-STEM image, with PbSe being the bright part. The equilateral triangle shows the long-range ordering of the structure. (b) High-resolution HAADF-STEM image, showing that the ⟨111⟩ nanocrystal axes are perpendicular to the honeycomb plane, and three of the ⟨110⟩ axes are perpendicular to the NC bonds. (Inset) Zoomed-in image on the atomic columns indicated by the blue box. (c) Electron diffraction pattern showing the high degree of crystallinity. The transmission electron microscopy image in the background shows the area on which the electron diffraction pattern was recorded. The red line and the inset show the orientation of the diffraction spots with respect to the honeycomb structure, confirming that the ⟨110⟩ axes are perpendicular to the NC bonds. (d) Model of the honeycomb structure (top and side view), with truncated cubes as NCs. The two inequivalent sites in the honeycomb lattice are indicated by yellow/red and blue/green NCs. Rectangles (orange and light green) represent (110) facets; triangles (red and dark green) represent (111) facets, and squares (yellow, blue) represent (100) facets. Reprinted with permission from ref 256. Copyright 2014 American Association for the Advancement of Science.

theory by Zherebetskyy *et al.* for ligand-capped PbS NCs,[257] Boles and Talapin explained the preferred attachment *via* (100) facets:[258] the binding energy of oleic acid to the (100) facet is too low to keep surfactant molecules in place for a long time. Binding of oleate/hydroxyl pairs to the (111) surface is much stronger. Surfactants are less likely to desorb from a (111) surface than from a (001) surface by a factor of $\sim 10^6$. The rather fast ligand desorption is assisted by the ethylene glycol, used as a liquid substrate for 2D assembly by Vanmaekelbergh *et al.* Once the (100) facets are bare, they also become reactive, causing fast oriented attachment. Considerable necking and large-scale atomic motion occurred during the oriented attachment process, leading to 2D single crystals with hexagonal arrangements of holes (honeycombs). Such a lattice is a mesoscale analogue of atomic graphene or MoS_2 sheets. These structures are also remarkably robust: Pb ions can be replaced with Cd ions, retaining the integrity of the selenium sublattice and the overall structure. It has been predicted that honeycomb semiconductors of zinc blende compounds (such as CdSe) will show a truly new electronic band structure, with a valence hole Dirac band and one or two conduction electron Dirac bands combined with strong spin−orbit coupling.[259]

NOVEL APPLICATIONS OF NANOCRYSTALS

Nanocrystal-Derived Thermoelectrics. Due to the importance of grain boundaries for attaining low thermal conductivities, colloidal NCs are particularly well-suited as solution-processable thermoelectric materials. The performance of a thermoelectric material depends on its Seebeck coefficient (S), electrical conductivity (σ), and thermal conductivity (κ) and is measured by means of a dimensionless figure of merit, defined as $ZT = \sigma S^2 T/\kappa$, where T is the absolute temperature. Nanomaterials and, particularly, nanocomposites provide several mechanisms to enhance ZT.[260−268] First, phonon scattering at grain boundaries and at the interface between two acoustically mismatched phases significantly decreases thermal conductivity. Second, selective scattering of low-energy charge carriers at interfacial energy barriers increases the average excess energy per carrier and thus increases the Seebeck coefficient. Preferential scattering of the minority carriers further increases the Seebeck coefficient. At the same time, interface scattering also reduces the electronic and bipolar contributions to the thermal conductivity, potentially accounting for a significant reduction in the total thermal conductivity.[264,269] Third, the sharply peaked electronic density of states in quantum-confined materials may also result in higher Seebeck coefficients[270] and in lower electronic contributions to thermal conductivity, well below those predicted by the Wiedemann−Franz law.[271,272]

Clear evidence of the advantages of nanostructured materials for thermoelectricity was obtained by vacuum-based thin-film technologies, which are neither particularly cost-effective nor suitable for large-scale production or for those applications that require bulk materials.[273,274] Alternative cost-effective bulk composites[262,275] are produced by thermal processing of metastable solid solutions,[276,277] consolidation using spark plasma sintering or hot pressing of nanopowders obtained by hydrothermal and solvothermal routes,[278] or mechanical milling.[279] None of these processes allow accurate control of the sizes and shapes of the nanocrystalline domains. Colloidal NCs allow combining the best of the two worlds—control over composition, interfaces, and distribution of phases at the nanometer scale of vacuum-based technologies with the capacity to produce cost-effective materials in bulk form.[280] Either mechanical mixtures

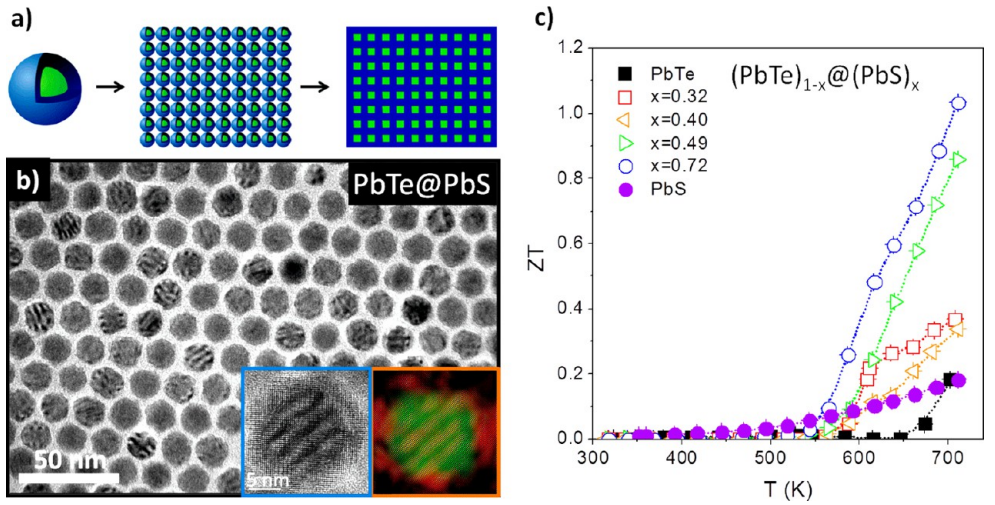

Figure 8. Thermoelectric nanocomposites from the bottom-up assembly of colloidal nanocrystals. (a) Scheme of the nanocomposite preparation from the bottom-up assembly of core–shell nanoparticles. (b) Transmission electron microscopy and high-resolution transmission electron microscopy image and crystallographic color maps of $(PbTe)_{0.28}@(PbS)_{0.72}$ core–shell NPs. (c) Thermoelectric figure of merit of $(PbTe)_{1-x}(PbS)_x$ nanocomposites obtained from hot pressing $(PbTe)_{1-x}@(PbS)_x$ core–shell NCs. Reproduced from ref 282. Copyright 2013 American Chemical Society.

or controlled assemblies of single-phase NCs or heterostructured NCs can be used to produce bulk nanocomposites with well-defined distribution of phases (Figure 8).[281−284] Furthermore, colloidal NCs are especially well-suited for producing conformable thermoelectric devices capable of fine temperature adjustments and for harvesting small amounts of energy.

One major challenge for NC-derived thermoelectrics is the removal of the native organic ligands. In this regard, inorganic ligands such as the MCCs discussed above are highly promising, as they can be applied *via* low-temperature ligand-exchange reactions, thus eliminating thermal pyrolysis of organic ligands at high temperatures.[227,238,284−292] Another challenge is fine-tuning of the electronic properties of the resulting NC solids, in particular, the doping level, carrier mobility, and type of majority carriers.[293] Different strategies have been proposed, including the introduction of external dopants in the precursor solution,[294] postsynthesis diffusion and zion-exchange doping and control of composition in multinary NCs,[73,77,78,94,95,295,296] or mixing of several kinds of NCs followed by thermal densification.[297,298]

Another challenge to overcome in order to take full advantage of NC-based nanocomposites is maintaining the integrity (composition, size, and shape) of the NCs in the final nanocomposites after film deposition/bulk nanomaterial consolidation. Addressing this challenge involves minimizing the temperature and duration of thermal treatments by using efficient ligand-exchange processes. Operation temperatures should also be reduced to ensure long-term stability as one main advantage of thermoelectric solid-state conversion devices. To this end, those materials that have their efficiency peak at ambient temperature, such as Bi−Sb−Se−Te alloys, have been the focus of research.[299−302] These are also the materials that are the most promising for applications. The coating of the NCs with ion diffusion blocking layers could also help to prevent crystal growth. In this sense, the production of nanocomposites with dissimilar ionic mobilities could allow adjustments of the crystallinity of each component in the nanocomposites, with different regions providing different functionality. As an example, most efficient bulk nanostructured materials are made by a host material, in which charge carriers flow with high mobility, containing nanocrystalline inclusions that inject charge to the host, scatter phonons, and filter low-energy and minority charge carriers. Such nanocomposites can be obtained by mixing NPs made of low-melting-point materials with NPs made of low-diffusivity ions and using rapid crystallization processes to prevent phase segregation.

Another challenge of bottom-up assembly techniques is producing textured nanomaterials. Several of the best thermoelectric materials are highly anisotropic with properties that are strongly dependent on the crystallographic orientation. Therefore, preferential alignment of the crystals along favorable transport directions is necessary.[303] This requirement calls for anisotropic nanostructures and/or for the consolidation of the material within a magnetic or electric field.

Finally, the selection of the appropriate material system, component distribution, and impurities is crucial. The high versatility of colloidal synthesis routes should allow the production of almost any nanocomposite, even those beyond the reach of other technologies. While nanocomposites with reported high efficiencies are an excellent reference beyond these systems, versatility and particularities of bottom-up

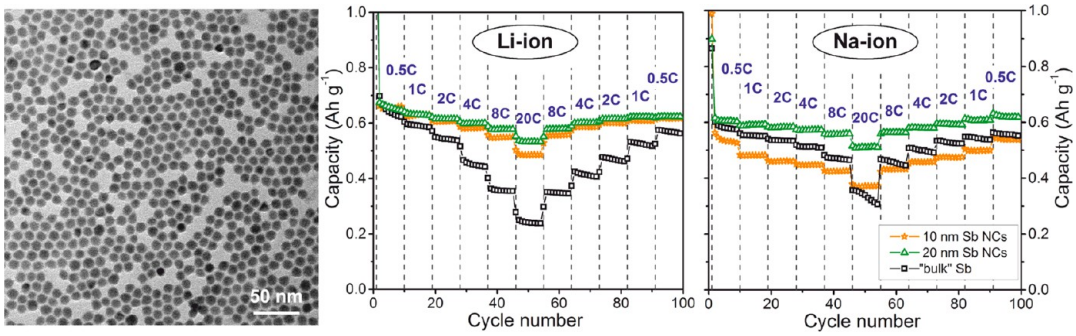

Figure 9. Transmission electron microscopy image of colloidally synthesized ~10 nm Sb nanocrystals; rate capability tests of anodes containing Sb NCs in Li ion and Na ion half-cells (1C = 0.66 A g^{-1}, 64% of active material). Reproduced from ref 316. Copyright 2014 American Chemical Society.

methods may be able to produce novel high-performance nanocomposites not previously tested. Although the reduction of thermal conductivity is a tempting easy-to-reach goal for bottom-up assembled nanomaterials, in order to produce the high-performance nanomaterials that are needed for thermoelectric devices to have a high economic and social impact, an overall improvement of the thermoelectric parameters is required, including electrical conductivities in the 10^5 Sm^{-1} range and Seebeck coefficients above 200 μV/K.

Highly Uniform Colloidal Nanocrystals in Battery Research. The benefits of precise NC engineering were recently recognized in the field of rechargeable Li ion batteries and for the emerging conceptually identical Na ion technology.[304−316] In recent years, the search for new electrode materials with higher charge storage capacity (*e.g.*, greater number of Li ions stored per unit mass or unit volume) has undergone a drastic shift toward nanomaterials. Due to the short internal diffusion paths, nanoscale materials are far less limited by their ionic or electronic conductivities than are their bulk counterparts. Nanoscopic particles can also withstand much greater mechanical deformation caused by large (100−300%) volumetric changes during charge/discharge cycling, observed in high-energy-density anode materials based on Si, Sn, Sb, and Ge. Overall, nanostructuring significantly enlarges the variety of inorganic compounds that can be utilized as Li and Na ion storage media.

Uniform NCs as electrode materials provide better understood structure−property relationships, especially when it comes to resolving the NC size effect on electrochemical performance. As an example, it has recently been shown that Sn and Sb NCs exhibit very different size effects on cycling stability.[315−317] While the performance of Sn NCs is strongly size-dependent and may be satisfactory only at sizes of 10 nm or below, Sb NCs exhibit stable and near-theoretical capacity as long as their size is in the 20−100 nm range and, surprisingly, display significantly decreased capacities for particles smaller than 20 nm (Figure 9). Antimony is a viable alternative to Sn cost-wise and had been much less explored than Sn, Ge, and Si. Antimony's theoretical specific capacity (660 mAh g^{-1} for conversion to Li_3Sb) is lower than that for Si and Sn, but the volumetric capacities are very similar (1890 mAh cm^{-3} for Sb, 2200 mAh cm^{-3} for Si, and 2000 mAh cm^{-3} for Sn). All three elements exhibit theoretical capacities much higher than that of commercially employed graphite (372 and 843 mAh cm^{-3}).[318]

Perhaps the most important feature of Sb is that insertion of Na ions into Sb is just as efficient and as fast as for Li ions.[319] Furthermore, exceptional rate capability and 80−85% retention of the initial capacity (580−640 mAh g^{-1} at 0.5−1C) when cycled with a current density of 13.2 A g^{-1} (20C rate, Figure 9) were observed for both ions.[316] This makes nanoscale Sb the best-performing Na ion anode material identified thus far and comparable to the fastest Li ion intercalation materials such as graphite[320] and lithium titanates.[321]

Metal Oxide Nanocrystals for Designing Electrochromic Windows. As discussed above, the past few years have seen rapid progress in the development of synthetic protocols for doped metal oxide NCs[322,323] that can exhibit plasmon resonance phenomena in the near- and mid-infrared spectral ranges (Figure 10a).[324] Distinct from metal NPs, the composition of these new particles can be synthetically varied to tune the wavelength of their LSPR. The latter is controlled *via* the carrier concentration, which is controlled by aliovalent substitutional doping in transparent conducting oxides, such as indium tin oxide (ITO), indium cadmium oxide (ICO), or aluminum zinc oxide (AZO). Several oxides, such as anatase titanium dioxide or tungsten oxide, can also be "self"-doped, by formation of oxygen vacancies.[325,326] Recent investigations have found that, analogous to metal NPs, metal oxides also show shape-dependent LSPR spectra;[327,328] highly uniform ICO NCs (*e.g.*, with octahedral and spherical NCs) even show infrared LSPRs with quality factors comparable to that of metallic NPs in the visible spectra region.

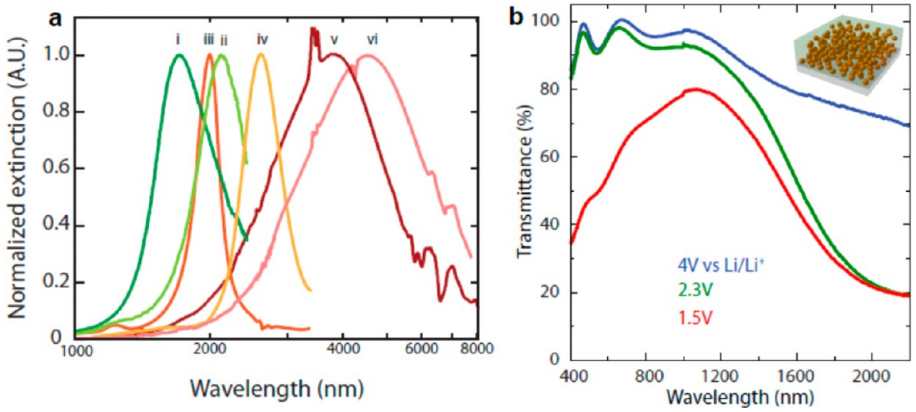

Figure 10. (a) Extinction spectra of various doped oxide nanocrystals demonstrating the synthetic tunability of their localized surface plasmon resonances. (i,ii) Tin-doped indium oxide, (iii,iv) indium-doped cadmium oxide, and (v,vi) aluminum-doped zinc oxide with different doping levels are shown. Reprinted from ref 324. Copyright 2014 American Chemical Society. (b) Dynamic modulation of near-infrared and visible light transmittance by an ITO-in-niobia nanocomposite film under applied electrochemical potential. Reprinted from ref 332. Copyright 2013 American Chemical Society.

Further, the metal oxide NPs' LSPRs also exhibit nuances that are unique to semiconductor plasmonic particles, in which the LSPR also depends on the radial dopant distribution.[329] This effect was shown for ITO NCs, where the segregation of tin near the NP's surface results in symmetric line shapes that suggest weak or no damping of the plasmon by ionized impurities, whereas uniformly doped NPs exhibit strongly asymmetric resonances.

Beyond synthetic tunability, an exciting opportunity lies in the responsive nature of plasmonic resonances in doped oxide NCs. As they exchange electrons with their environment, the plasma frequency shifts and the LSPR intensity is strongly modulated. The chemical stability of metal oxides enables the dynamic modulation of the LSPR in films of NCs through electrochemical doping.[330,331] In ITO NPs, for example, dynamic shifts by >1200 nm were obtained by electrochemically controlling the NPs' carrier concentration by almost a factor of 3. By embedding plasmonic ITO NCs in an amorphous niobium oxide matrix,[233] nanocomposites were created that can dynamically control near-infrared and visible light transmittance independently as a function of the applied electrochemical voltage (Figure 10b).[235] Coatings of these nanocomposites switch progressively between three optical states: fully transparent, selectively near-infrared blocking, and broad-band blocking of visible and infrared light. It should also be noted that the modest visible light modulation in the pure material of the amorphous matrix, the NbOx, was increased by a factor of 5 by the incorporation of the NCs into the glass composite, with an optimal NC content of about 40%. This enhancement of the optical contrast in the visible spectral region was attributed to structural reconstruction of the NbO_x matrix, as a consequence of the covalent linkage to the embedded NCs. This high electrochromic response of the NC−glass nanocomposite could enable energy-saving "smart" windows that uniquely manage thermal loads and daylighting in buildings, cars, aircrafts, ships, and so on. The responsive nature of metal oxide NC plasmons will undoubtedly find additional applications in the near future. For instance, these NCs could be deployed in biological environments to sense and mediate redox events.

Building Nanocrystal-Based Electronics. Colloidal semiconductor NCs introduce a new, solution-based material class from which solid-state electronic materials can be assembled. These assembled NC solids provide a playground to probe the collective interactions that give rise to charge transport in solid-state materials and a route to design n-type and p-type semiconductors for integration in low-cost, large-area electronic, optoelectronic, and thermoelectric devices. Charge transport in semiconductor NC solids has advanced from early foundational measurements of dark and photoconductivity, using solid-state and electrochemical platforms.[333−335] Today, high-mobility, high-conductivity charge transport has been reported with electron mobilities of >10 cm^2/Vs and hole mobilities of >1 cm^2/Vs in II−VI,[240,336] III−V,[337] and IV−VI[239,338,339] semiconductor NC solids, using electrical measurements in the field-effect transistor[239,240,336,337] (Figure 11) and Hall geometries[227,340] and in time-resolved microwave conductivity measurements.[338]

This high-mobility charge transport has been achieved by (i) taking advantage of the synthesis of monodisperse NC building blocks to reduce site-to-site energy dispersion; (ii) strong electronic coupling, through exchange of the ligands used in synthesis with the compact ligand chemistries described above; and (iii) doping and passivation at the NC surface, by introducing extrinsic atoms (*e.g.*, indium in CdSe NC solids),[240,336] additional atoms to shift the NC stoichiometry (*e.g.*, excess metal or chalcogen in II−VI and IV−VI solids),[339,341−344] ligands (*e.g.*, halides),[345,346] and oxide layers (*e.g.*,

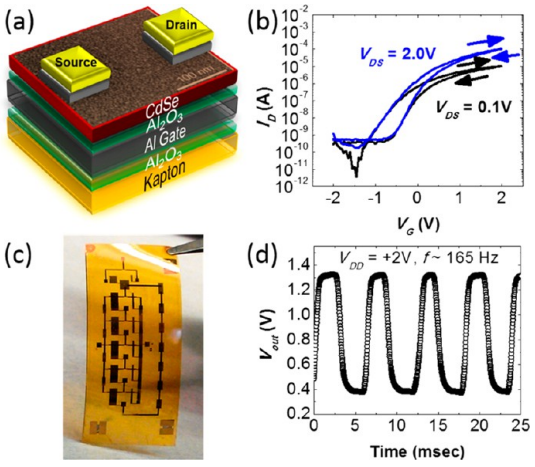

Figure 11. (a) Schematic and (b) transfer characteristics in the linear and saturation regimes of a thiocyanate-exchanged, solution-deposited, CdSe nanocrystal transistor fabricated on a flexible Kapton substrate. (c) Photograph and (d) output characteristics of five-stage, CdSe NC-integrated circuit ring oscillator. Reprinted with permission from ref 350. Copyright 2012 Nature Publishing Group.

Al_2O_3)[239,347] either during or post-synthesis and using solution and physical vapor deposition methods. The combination of strong coupling, doping, and passivation enables control over the carrier type, concentration, and mobility; the trap density and energy; and, therefore, the Fermi energy in NC solids, which is important for device design. There are still remaining opportunities to improve charge transport in NC solids. For example, while there is early evidence of small domains of ordering in lead chalcogenide NC solids, long-range order promises improved charge transport by overcoming Anderson localization.[342,348] The most stable, high-mobility NC solids are realized for metal-rich and halide-passivated NC surfaces that yield n-type NC solids. Development of comparable p-doped materials is important to improve the performance of NC-based devices, most notably to fabricate p−n junctions or complementary metal oxide semiconductor (CMOS) circuits with balanced electron and hole transport.

These high-mobility semiconductor NC solids have been incorporated into electronic and optoelectronic devices. The noncorrosive, low-temperature processing used to form high-mobility NC solids has enabled their fabrication on flexible plastics.[349] For example, Figure 11a, b shows the device schematic and transfer characteristics of an n-type CdSe NC field-effect transistor constructed on flexible Kapton substrates.[350] This device geometry has been scaled to enable device operation at low voltages. These flexible NC FETs have been integrated into circuitry by fabricating vertical interconnect access holes to connect device terminals and construct n-type metal oxide semiconductor field-effect transistor (MOSFET) analogues and digital NC-based electronics. Figure 11c,d shows a photograph and output characteristics of a five-stage, NC-integrated circuit ring oscillator, composed of 10 transistors to form the oscillator and two additional transistors that serve as a buffer. All NC FETs across the 2 cm × 6 cm substrate have similar device parameters to enable their operation in concert as a ring oscillator. Recent demonstrations of NC device fabrication using common cleanroom techniques[351] allow the device dimensions to be scaled down and suggest that future large-area, complex, higher bandwidth, and higher speed analog and digital NC-based circuits are feasible. Encapsulation of NC devices by atomic layer deposition improves the device performance, which is important for circuitry and enables device operation in ambient air.[239,351] Nanocrystals are emerging as a promising material class for low-cost, large-area, and flexible electronic circuitry. Opportunities to improve circuit speed, to decrease power, and to decrease noise may be realized through advances in material, device, and circuit design, fabrication, and characterization. Furthermore, it was recently found that, when films of surfactant-coated NCs are irradiated with an electron beam or with X-rays, they become inert toward cation exchange.[352] Initial studies have indicated that irradiation cross-links the ligands at the surface of the NCs to the extent that a cross-linked ligand shell creates a barrier to the flow of ions to/from the NCs. This enables the patterning of NC films into chemically different components with different physical properties by locally (that is, in the irradiated regions) inhibiting cation exchange. This "masked" cation exchange process can, in principle, be employed to fabricate electrical circuits in NC films with no alteration of their initial morphology.

> Nanocrystals are emerging as a promising material class for low-cost, large-area, and flexible electronic circuitry.

Nanocrystal Quantum Dots with Engineered Interfaces for Light-Emitting Diodes. The improvement in lighting efficiency is an important element of today's energy-saving strategies. One approach toward more efficient lighting involves the use of LEDs where electric current is directly converted into a stream of photons. Chemically synthesized QDs have emerged as a new promising class of materials for low-cost yet efficient LEDs.[35,353] Quantum dot LEDs have advanced tremendously over the past two decades, evolving from proof-of-principle polymer−QD structures[354]

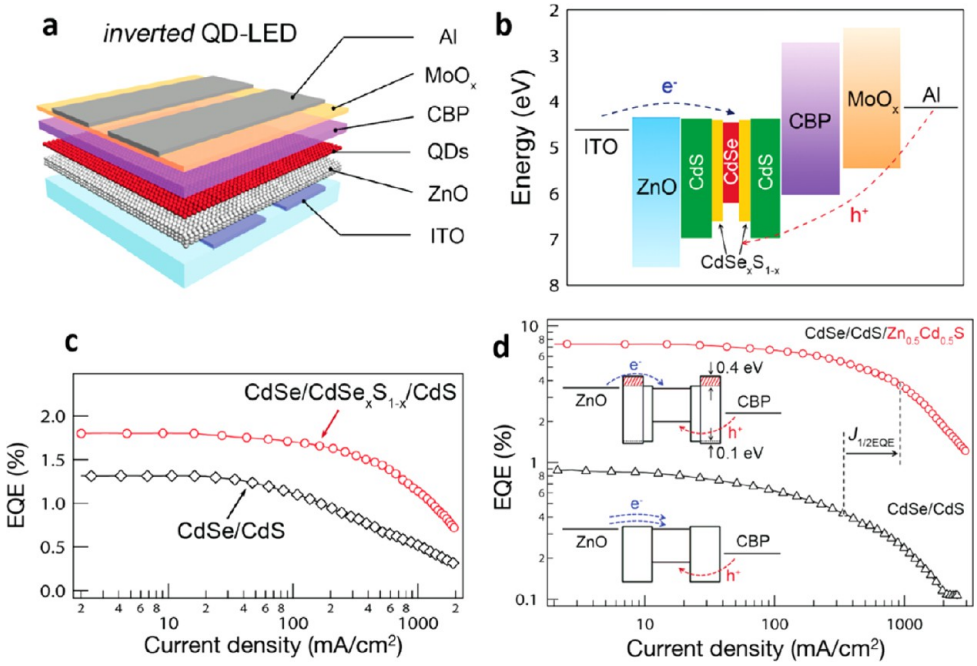

Figure 12. QD-based light-emitting diodes.[361] (a) Inverted LED comprising an active layer of engineered QDs contacted by electron (bottom) and hole (top) transport/injection layers. The bottom contact is based on zinc oxide (ZnO) nanoparticles deposited onto indium tin oxide; the top contact is based on 4,4′-bis(*N*-carbazolyl)-1,1′-biphenyl on aluminum capped with molybdenum oxide. (b) Energy band diagram of the inverted QD-LED with an active emitting layer based on CdSe/CdSe$_x$S$_{1-x}$/CdS QDs with an alloyed interface. (c) External quantum efficiency (EQE) *versus* current density for two QD-LEDs: one employing CdSe/CdS QDs with an abrupt interface (black diamonds) and the other, CdSe/CdSe$_x$S$_{1-x}$/CdS QDs (*x* is *ca.* 0.5), with an alloyed interface (red circles). Both samples have the same CdSe core radius (r = 1.5 nm) and the same total radius (R = 7 nm); the thickness of the CdSe$_x$S$_{1-x}$ alloy layer is 1.5 nm. (d) EQE *versus* current density of QD-LEDs with CdSe/CdS QDs (r = 1.5 nm and R = 3.5 nm; lower inset and the trace shown by black triangles) and CdSe/CdS/Zn$_{0.5}$Cd$_{0.5}$S QDs (r = 1.5 nm, R = 3.5 nm, and the Zn$_{0.5}$Cd$_{0.5}$S layer thickness is 1.5 nm; top inset and the trace shown by red circles). Vertical dashed lines indicate EQE roll-off onsets defined as the current density for which EQE drops by one-half ($J_{1/2EQE}$). Reprinted with permission from ref 361. Copyright 2013 Nature Publishing Group.

to modern devices employing direct charge injection from finely tuned electron and hole transport layers.[337,355−359] Outstanding challenges in the field of QD-LEDs are associated with still insufficient long-term stability of devices and efficiency losses at high currents (so-called, efficiency roll-off or droop).

There is ample evidence that reversible degradation of the LED efficiency at high currents originates from nonradiative Auger recombination, whereby the electron−hole recombination energy is not released as a photon but instead dissipates as kinetic energy of the extra carrier.[359−361] For example, recent studies of inverted LEDs (Figure 12a,b) demonstrate the propensity of these devices to generate excess electrons in the emitting layer.[361] As a result, a significant contribution to emission is provided by negatively charged excitons (that is, negative trions) that are subject to fast Auger recombination.[362−364] Recently, two approaches have been proposed to mitigate this problem.[361,365] The first approach involves the use of thick-shell CdSe/CdS QDs with an intermediate CdSe$_x$S$_{1-x}$ alloy layer at the core−shell interface, which helps to suppress Auger recombination and thus to increase the emission efficiency of charged species (Figure 12c). As indicated by theoretical modeling[366] as well as experimental spectroscopic studies,[367] this effect is linked to "smoothing" of the confinement potential, which reduces the matrix element of a nonradiative intraband transition involved in Auger decay. In the second approach, the conduction band edge of a QD is raised using an additional layer of a higher band gap Zn$_x$Cd$_{1-x}$S alloy (Figure 12d). This enables one to impede electron injection moderately and thus to improve the charge-injection balance within the QD active layer. Use of either of these strategies enhances peak emission efficiency (EQE up to 1.8% for the first approach and 7.5% for the second) and also significantly increases the threshold current of efficiency roll-off (Figure 12c,d).[361] These studies demonstrate a large promise of interface engineering for optimizing QD performance in LEDs by reducing nonradiative losses associated with Auger recombination. At the same time, for practical applications, the lessons learned from II−VI materials need to be translated to cadmium-free NCs.

LASER EMISSION FROM NANOCRYSTAL QUANTUM DOTS

Nanocrystal Lasing. Due to high, near-unity emission efficiencies and size-dependent emission wavelengths,

NCs are attractive materials for the realization of highly flexible, solution-processed lasing media. Paradoxically, despite their favorable light-emitting properties, NCs are difficult to use in optical amplification. Because of nearly exact balance between absorption and stimulated emission in NCs excited with single electron–hole pairs (single excitons), the condition for optical amplification can only be achieved by exciting two excitons (that is, biexcitons) in at least a fraction of the NCs in the ensemble.[368] The resulting complication is associated with nonradiative Auger recombination, which leads to fast optical gain decay. In this process, instead of being emitted as a photon, the electron–hole pair recombination energy is transferred to a third carrier (an electron or a hole) on extremely short time scales of tens to hundreds of picoseconds.[369,370]

To resolve the problem of Auger recombination, the first successful demonstration of amplified spontaneous emission (ASE) from the NCs utilized a short-pulse laser as an excitation source and a dense close-packed NC solid as a gain medium.[368] Ultrafast charge carrier injection was essential for avoiding population losses during the pumping stage, while a high density of NC emitters allowed for a fast buildup of ASE, which could compete with Auger decay. After the elucidation of the principal mechanism for optical gain decay, additional progress in NC lasing has been associated with the development of structures with suppressed Auger recombination (*e.g.*, nanorods,[371,372] thick-shell CdSe/CdS NCs ["giant" quantum dots],[373] or dot-in-rod NCs[374]) and exploration of novel lasing concepts such as "single-exciton" gain realized in NCs with strong exciton–exciton repulsion.[375−377] The principles of single-exciton gain, originally introduced in ref 375, were implemented practically in ref 378 using type-II CdS/ZnSe NCs. These structures enabled strong exciton–exciton repulsion (on the order of 100 meV), which produced transient displacement of a band-edge absorbing transition away from the emission line in the case when a single exciton was injected into a NC. As a result, population inversion could be realized with single excitons without complications associated with Auger recombination.

Several recent efforts have focused on the structures with suppressed Auger recombination. An interesting development in this area has come from the exploitation of CdSe/CdS dot-in-rod NCs, in which the localization of holes in the CdSe core and the substantial delocalization of electrons throughout the whole NC creates a quasi-type-II system,[377] which leads to a considerable decrease in the Auger recombination rate[379] and, as a result, facilitates ASE. Furthermore, engineering of the CdSe core and of the CdS shell in these NCs allows one to realize ASE from either the core, the shell, or both,[374] and the strong confinement of both electrons and holes within the inorganic core leads to an enhanced temperature stability of the ASE threshold, a signature of true QD ASE/lasing.[355] The integration of these NCs into microresonators, for example, *via* the deposition of films of NCs onto silica microspheres[380] or the creation of coffee-stain rings of close-packed NC multilayers by self-assembly[381,382] has recently paved the way to new concepts of NC-based lasers. Novel prototype lasing devices have recently been fabricated with other types of core–shell NCs (*e.g.*, CdZnS/ZnS).[383]

Interesting opportunities in the field of NC lasing are associated with the use of 2D nanostructures (nanosheets and nanoplatelets) that have been under active development during the last 2–3 years. Especially in the case of CdSe, much work has been done to optimize the fabrication of core (*i.e.*, "CdSe" only) and core–shell architectures.[384−387] The interest in these materials stems from the fact that they can be considered as the colloidal analogues of epitaxial quantum wells: excitons are strongly confined in one dimension, while the in-plane confinement is much weaker.[388] Apart from interesting effects observed in CdSe nanoplatelets, like narrow emission line widths, high fluorescence quantum yields, and ultrafast fluorescence lifetimes, one key aspect distinguishes them from the corresponding CdSe quantum dots (0D) and quantum rods/wires (1D): the quantization of levels only in one direction imposes stricter restrictions on momentum conservation and therefore results in a lower rate of Auger recombination. CdSe and CdSe/CdS nanoplatelets thus represent interesting candidates for the realization of low-threshold (potentially, lower than for quantum dots and rods) ASE and lasing.[389−391] A significant promise of these materials for lasing applications has been indicated by the recent demonstration of continuous-wave stimulated emission and lasing using close-packed films of colloidal CdSe nanoplatelets.[391]

Carbon-Based Nanoparticles for Light-Emitting Devices. Carbon-based dots (CDs)[392] have emerged as an active area of research due to their broad-band optical absorption, strong photoluminescence, low toxicity, and high chemical stability. Recently, great progress has been made in the large-scale preparation of CDs by methods such as electrochemical oxidation processes, hydrothermal

Carbon-based dots have emerged as an active area of research due to their broad-band optical absorption, strong photoluminescence, low toxicity, and high chemical stability.

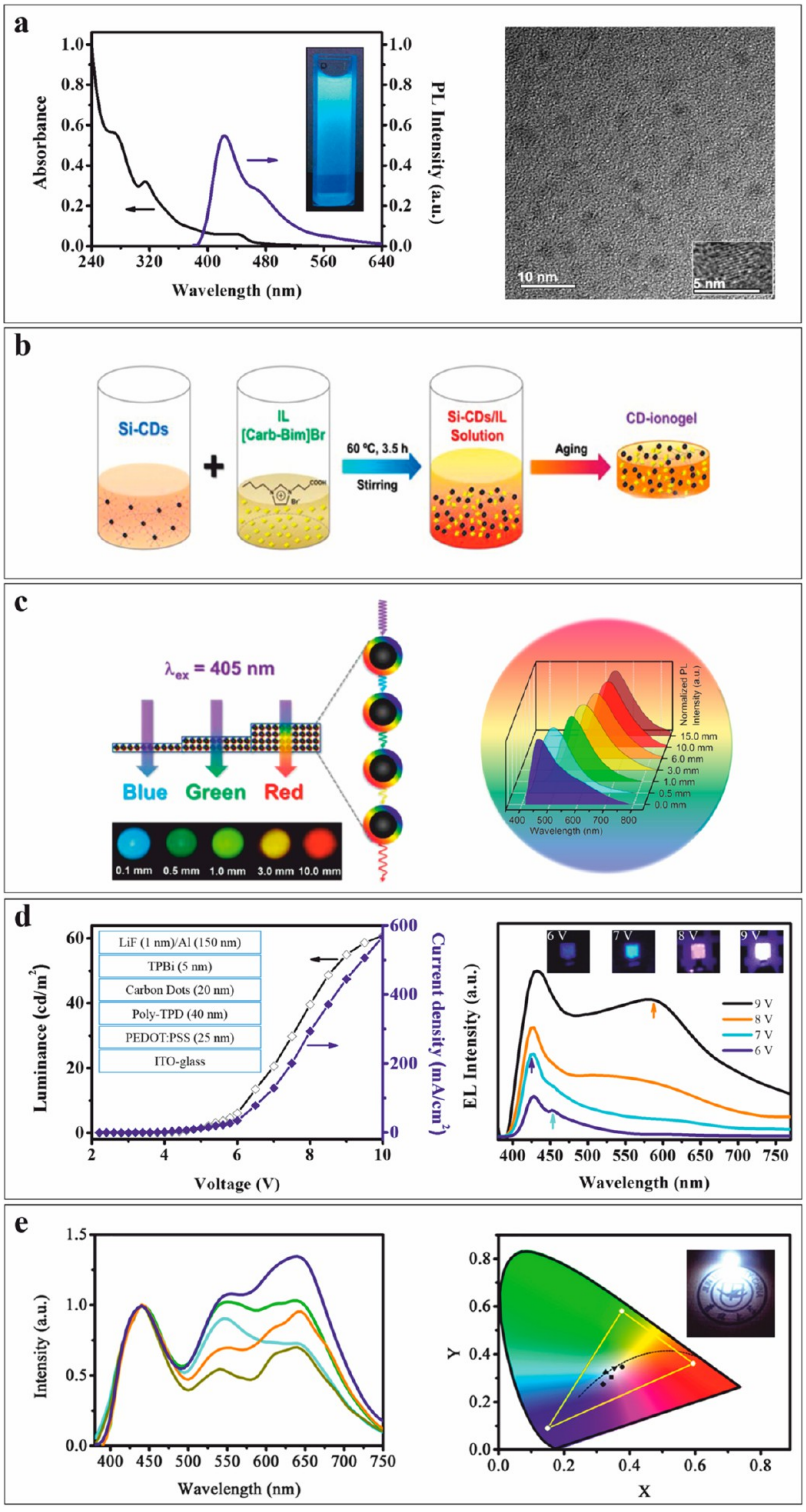

Figure 13. (a) Absorption and photoluminescence (340 nm excitation wavelength) spectra of carbon-based dots and a TEM/HRTEM image of CDs. Reprinted from ref 399. Copyright 2013 American Chemical Society. (b) Schematic illustration of the preparation of the CD ionogel using organosilane-functionalized CDs (Si-CDs) through sol−gel processing in the presence of ionic liquid 1-(3-carboxypropyl)-3-butylimidazolium bromide. (c) Schematic illustration of the light propagation through the increasingly thicker layers of the CD ionogel, resulting in the different emission color as a consequence of multiple light reabsorption and the subsequent emission steps. Reprinted from ref 398. Copyright 2014 American Chemical Society. (d) Current density and brightness of the CD light-emitting diodes (structure shown in inset) emitting blue, cyan, magenta, and white light, with the corresponding electroluminescence (EL) spectra. Reprinted from ref 399. Copyright 2013 American Chemical Society. (e) EL spectra of a white LED fabricated from a mixture of blue-emitting CDs and green and red emitting zinc copper indium sulfide quantum dots, with the corresponding color triangle and a white LED photograph. Reprinted with permission from ref 400. Copyright 2014 AIP Publishing LLC.

scission strategies, chemical oxidation methods, and carbonizing organic precursor syntheses. These low-cost, mild, and green synthetic methods have also served as a platform for further manipulation of their properties, enabling customized design of novel functional materials. Reported by Sun *et al.* in 2006,[393] these fluorophores combine several attributes of traditional semiconductor QDs such as tunable luminescence emission and high resistance to photobleaching without incurring the burden of intrinsic toxicity or being hostage to elemental scarcity. In recent years, CDs have been demonstrated to possess high (up to 60−80%) emission quantum yields[394,395] in the blue spectral region (Figure 13a), making them competitive in light-emitting performance with QDs. Several reports have shown that the efficient and excitation-dependent photo- and electroluminescence of CDs is promising in the fabrication of hybrid LEDs and thus has potential applications for displays and solid-state lighting.[396,397] It was recently shown[398] how the surfaces of CDs can be functionalized with organosilanes and incorporated into highly flexible hybrid materials when combined with ionic liquids within silica gel networks to form CD ionogels (Figure 13b) with properties that are promising for the fabrication of flexible displays and other optical technologies. The emission from such CD ionogels can be tuned across a large range of the CIE display gamut as a result of the sequential multiple light reabsorption and subsequent emission, resulting in the thickness-dependent red shift of the emitted light (Figure 13c) and, thus, full-color performance. Furthermore, CD-based LEDs with driving-current-controlled color change were introduced.[399] These devices consist of a CD emissive layer sandwiched between an organic hole transport layer and an organic or inorganic electron transport layer fabricated by solution processing (Figure 13d). By tuning the device structure and the injecting current density (by changing the applied voltage), multicolor emission of blue, cyan, magenta, and white can be obtained from the same CDs (Figure 13d). By combining CDs that emit blue light and zinc copper indium sulfide QDs that emit in the green and red regions of the electromagnetic spectrum, white LEDs (Figure 13e) with a high color-rendering index of 93 have been realized.[400] These examples highlight the promise of CD-based composites with controlled chromaticity photo- and electroluminescence. Future comprehensive studies using ultrafast spectroscopy techniques, linked with the synthetic design of the CD-based hybrid materials at the nanometer scale, will help to elucidate the mechanisms and kinetics of charge transfer and recombination processes in such composites. Material design of CD-based LED devices and carefully engineered LED device structures will lead to optimized, efficient next-generation color displays and solid-state lighting.

Infrared Photodetectors—From Interband to Intraband. The thermal infrared imaging ranges are the mid-wave infrared (MWIR, 3−5 μm) and long-wave infrared (LWIR, 8−12 μm). Many current infrared devices are based on bulk semiconductor or nanostructured materials grown by epitaxy and cost in excess of $50 000 for cameras, which leaves the door open for disruptive technologies. Infrared semiconductor devices use interband transitions as well as all possible manners of band gap engineering including inter-sub-band transitions with quantum wells or intraband transitions with QDs and type-II structures.[401] Epitaxial QDs should have significant advantages due to the expected slower carrier relaxation compared to wells,[402] but the epitaxial QD devices realized so far have remained inferior to the bulk technology.

Colloidal QDs show promise because they can be assembled as close-packed solids and with narrow (5%) size dispersion. As discussed above, they afford the possibility of low-cost liquid processing at moderate temperatures, a characteristic shared with organic materials, but with the possibility of sustaining infrared electronic transitions. The first step in exploring their potential as infrared detectors or emitters is therefore to develop colloidal QDs with infrared electronic transitions. These could be interband or intraband, as shown in Figure 14. Intraband transitions in CdSe were the first instance of MWIR electronic transitions in colloidal QDs.[403] However, the ultrafast excitonic relaxation[404] suggested ultrafast nonradiative intraband relaxation. It is now understood that, in the absence of a multicarrier mechanism or without coupling to the vibrational modes of the ligand shells, slower intraband relaxation can be obtained.[405] Another limitation was that an intraband infrared photoresponse requires the precise filling of intraband states, but controlled doping in colloidal quantum dots has remained difficult.[406]

On the contrary, interband transitions require only an appropriate band gap energy to begin, and the past decade has seen much improvement in making colloidal QDs with infrared interband transitions, first using small gap lead salts[407] such as PbSe[408] (bulk gap of 0.3 eV) and then HgTe (0 eV gap).[409,410] In parallel, the conductivity improvement brought about by ligand exchange after QD film formation[411] and the ohmic conductivity[412] achieved in such films enabled efficient photoconductivity that evolved from visible to near-IR detection,[413−416] eventually into the MWIR with HgTe[417] and recently into the LWIR.[418] The development of HgTe colloidal QDs now focuses on improving the infrared detectivity through the device structure, the material processing, and the emission properties, and it may well lead to a disruptive IR technology.

Interest in intraband photoconduction was renewed in the past

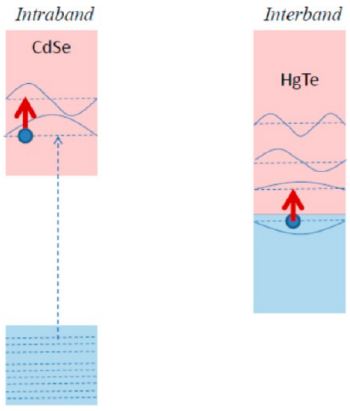

Figure 14. Possible schemes for obtaining infrared electronic absorption in single-component colloidal quantum dots. The intraband scheme allows the use of wide band gap semiconductors if they can be doped. They could then be transparent in the visible and absorbing in the IR, which is potentially useful for enhanced vision. The interband scheme relies on small gap semiconductors. One could also envision core−shell nanocrystals of type-II structures.

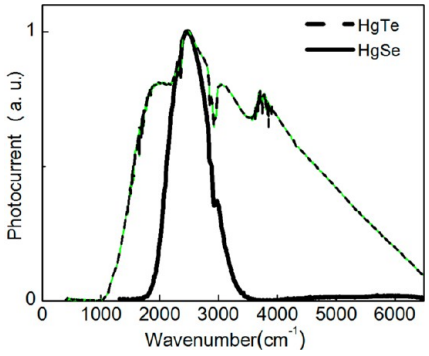

Figure 15. Photocurrent of films of HgTe and n-HgSe colloidal quantum dots of ~15 and ~6 nm, respectively. The films are deposited on interdigitated electrodes and treated in air with ethanedithiol. The measurements are done at 80 K. The intraband photoresponse of n-HgSe just covers the midwave infrared. Reprinted from ref 419. Copyright 2014 American Chemical Society.

year with the discovery of air-stable n-doping of β-HgS QDs.[420] Indeed, β-HgS QDs exhibit a surface-tunable occupation of the lowest $1S_e$ conduction band state with a strong absorption and weak luminescence of the $1S_e-1P_e$ intraband transition in the MWIR. The same properties were also observed for HgSe QDs, which can be made with better size control. As a result of the stable doping, colloidal HgS and HgSe QD intraband photodetectors have recently been demonstrated in the MWIR, and their best performance is similar to the best interband detectors at similar wavelengths.[419] Figure 15 shows photocurrent spectra taken with interband HgTe and intraband HgSe. Both systems show similar signal-to-noise ratios, but the intraband response is much narrower, being restricted to the $1S_e-1P_e$ transition. When other systems are successfully doped with carriers, intraband devices may allow the use of wider gap semiconductors for infrared applications, such as using n-ZnO or n-CdS. Using either interband or intraband transitions, colloidal QDs have interesting infrared properties for infrared detection or emission. The n-HgSe QDs' intraband photodetector is also conceptually significant since it is the first instance of using the intraband transitions of a colloidal semiconductor structure, and one can now add the intraband transitions to the range of colloidal QD design.

Hybrid Two- and Zero-Dimensional Quantum Dot Photodetectors. Colloidal QD photodetectors have seen tremendous progress over the past decade and have emerged as a novel sensing platform for high sensitivity, low-cost photodetectors, whose spectral coverage can readily extend from the UV to the short-wave and mid-IR spectrum.[414,421−424] Photoconductive detectors[414,421] and photodiodes[422] based on QDs have both been reported, showing distinct exciting features: photodiodes are detectors with fast response (determined by the transit time of carriers) and responsivity that cannot exceed the 100% quantum efficiency limit; on the other hand, photoconductive detectors have shown significant photoconductive gain on the order of 10^3 or higher, determined by the ratio of carrier lifetime over carrier transit time. Photoconductive detectors tend to be slower in time response, as determined by the carrier lifetime, but they offer significant promise for sensing with higher sensitivity because they have the potential to overcome the read-out noise floor. Improving the performance of photoconductive detectors will rely on two advances: (1) identifying material processing methods that introduce shallower trap states/sensitizing centers to accelerate the carrier lifetime and thereby the temporal response of the detector,[425] and (2) decreasing the transit correspondingly to account for the reduction of lifetime so that gain is not considerably affected. Significant efforts have been undertaken to increase carrier mobility in colloidal QD solids and have reached impressive values of 10−30 cm^2/Vs.[238] The mobility values, however, still fall well below the ones met in single-crystalline counterparts.

A potential solution to this road block was recently demonstrated by exploiting the synergism of colloidal QDs with graphene. Colloidal QDs offer unprecedented opportunities to tailor optical absorption across a broad range, whereas graphene provides carrier mobilities that cannot be matched in any other

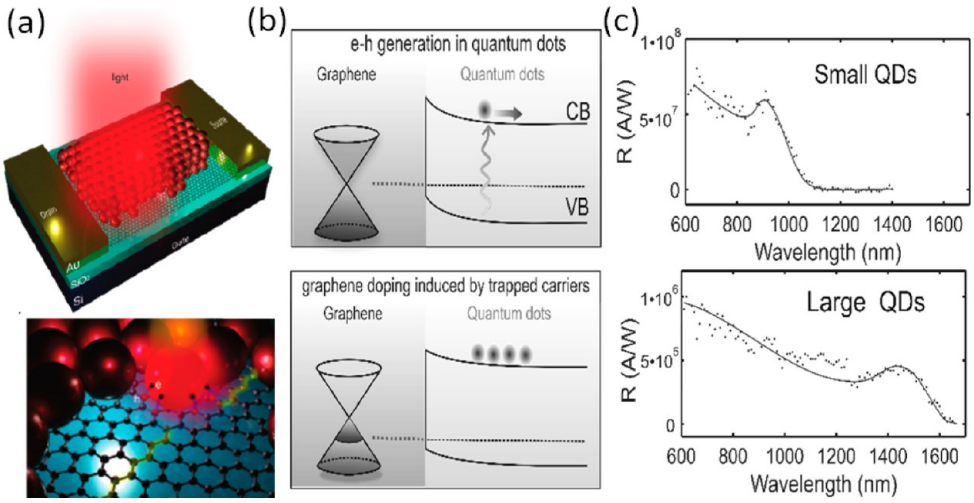

Figure 16. High-gain, high-sensitivity graphene–quantum dot photodetectors. (a) Device structure of the graphene–QD phototransistor. (b) Band alignment at the graphene–PbS QD interface. (c) Spectral responsivity of QD–graphene phototransistors employing two different sizes of QDs to cover the vis–NIR (top panel) and SWIR–vis (bottom panel) parts of the spectrum. The achieved responsivities in both cases are in excess of 10^6 A/W. Reprinted with permission from ref 428. Copyright 2012 Nature Publishing Group.

Colloidal QD photodetectors have seen tremendous progress over the past decade and have emerged as a novel sensing platform for high sensitivity, low-cost photodetectors, whose spectral coverage can readily extend from the UV to the short-wave and mid-IR spectrum.

single-crystalline or nanocrystalline material.[426,427] It was recently shown that efficient charge transfer of photogenerated carriers in a QD solid placed atop a graphene transistor offers an advantageous platform for achieving record gains (on the order of 10^7) as a result of the prolonged carrier lifetime in the QD layer and the ultrahigh mobility (on the order of 500–1000 cm^2/Vs) of the graphene channel.[428] In this architecture (Figure 16a), the QD layer acts as an efficient sensitizer for graphene in which photogenerated holes are transferred to the graphene channel, whereas electrons remain trapped in the QD layer (Figure 16b). With an applied electric field, holes recirculate within the graphene channel as long as the electrons remain in the colloidal QD layer. This gain was achieved with low applied electric fields, on the order of 10^3 V/cm, and both material platforms are fully compatible with large-area manufacturing and CMOS processing, opening the way toward monolithic integration to CMOS or flexible electronic technologies to cover both the visible and infrared spectra (Figure 16c). The presence of the back-gate electrode also offers additional functionalities, as it can electrostatically modulate the band alignment of the graphene–QD interface and therefore acts as a local electric knob that can tune gain in this transistor from its maximum value to zero, offering the possibility of resetting the detector.

At present, one of the major challenges is the existence of a high dark current due to the lack of a band gap in graphene. However, a new realm of opportunities has emerged with the advent of other 2D semiconductors that enable high in-plane carrier mobilities at atomically thin layers with the added benefit of the presence of a band gap.[429] The latter enables control of the carrier density in the channel over a much broader range; as a result, similarly performing photodetectors with significantly lower dark current rates are within reach. Further co-optimization of the integrated amplification stage offered by the 2D channel with the sensitizing photogating CQD layer may pave the way for achieving even higher performance in sensitivity and functionalities offered by this hybrid platform.

Novel Architectures for Colloidal Nanocrystal Solar Cells Based on Inorganic Bulk Heterojunctions. Quantum dot solar cells have emerged as one of the most promising technologies for solution-processed thin-film photovoltaics, leveraging their solution processing and facile band gap tunability.[430] The latter possibility has been a major driving force toward third-generation photovoltaics, as well, exploiting both multiple exciton generation effects[431] and the development of tandem solar cells.[432] Recent advances in the control of surface passivation have led to dramatic performance improvement in power conversion efficiencies, now reported to reach nearly

9%.[433−436] These improvements are the result of tuning the surface properties of QDs in order to passivate deep traps with reflected effects on improved carrier mobility and suppressed trap-recombination.[434,435] Modification of the surface dipole moment has also been suggested as a novel strategy to tune the band energy levels of QD solids and has been shown to result in highly efficient heterojunction QD solar cells.[436] Tailoring the electronic properties of QD solids, in particular, controlling doping, has been considered a major challenge, as robust doping techniques had remained elusive. Multiple recent reports have shown that transforming p-type PbS QDs into an n-type electron acceptor material is now within reach. This has been demonstrated both by controlling the cation−anion stoichiometry, employment of monovalent halide anions replacing surface sulfur atoms, as well as through employment of heterovalent cations that replace Pb.[373,374] The last two approaches have been successfully demonstrated in operational QD homojunction solar cells, and the cation substitution has also yielded robust n-type PbS QDs under extended exposure to air.[363] This avenue is expected to pave the way toward advanced design methodologies for controlling the electronic properties of QDs at the atomic level and advanced QD functionalities including intraband transition-based applications. Key challenges that remain include understanding the introduction of dopants in QDs, their incorporation into the crystal structure, and the alleviation of adverse effects that this may have in terms of introducing additional states within the band gap. Advanced codoping/passivation techniques need to be sought to unleash the potential of atomically engineered QD solids.

At present, the main body of work on high-performance QD solar cells has been based on PbS QDs. The presence of Pb may pose environmental concerns; therefore, there is an eminent need to explore alternative semiconductor compounds for use in environmentally friendly green photovoltaics (PVs). Some of the key features that have led to successful employment of PbS QDs in solar cells include its large dielectric constant and therefore small exciton binding energy that allows exciton dissociation at room temperature in the absence of a junction, its favorably long carrier lifetime that can effectively compete with the currently achieved carrier mobilities for efficient charge collection, and its mild doping that allows the formation of depletion widths in excess of 200 nm. Caution is therefore required, as alternative semiconductor materials may not possess such features. The employment of traditional planar heterojunctions may not serve as a promising architecture for high-efficiency NC solar cells. Recently, and following the paradigm of polymer-based solar cells, the introduction of bulk heterojunctions for inorganic NC solar cells has been shown to be a novel architectural platform for QD and NC solar cells.[437] In this architecture, the photoactive layer consists of two types of NCs, an n-type electron acceptor and a p-type electron donor material, that have been blended on the nanoscale so that the charge separation interface is extended throughout the bulk heterojunction (Figure 17a). One of the key aspects of this approach is that charge transfer of minority carriers to the corresponding collecting medium takes place at the nanoscale, suppressing minority carrier transport, and leads to a significant increase in effective carrier lifetime and, consequently, to charge collection efficiency (Figure 17b). The employment of an inorganic bulk heterojunction has also enabled remote trap passivation in QD solar cells, resulting in higher open circuit voltages as a result of suppressed trap-assisted recombination (Figure 17c). Similar to the advanced atomic passivation techniques previously employed, it has been shown that majority electrons from ZnO NCs can be utilized to fill electron trap states in PbS QDs when the bulk heterojunction of ZnO and PbS NCs is employed.[438] This may enable both new remote passivation techniques for colloidal NC materials for which atomic/ligand passivation schemes may not be available and also engineered properties of NC composites at the supra-nanocrystalline level. Last but not least, the presence of a distributed heterojunction at the nanoscale may potentially expand the available quantum-confined materials whose exciton binding energy has been prohibitively high for their use in bilayer heterojunction arhictectures (*e.g.*, CIS(Se) QDs).

Carrier Multiplication for High-Efficiency Solar Cells. Semiconductor NCs offer a number of functionalities that are attractive for solar energy conversion. A size-controlled tunable band gap in combination with low-temperature synthesis and processing can enable low-cost, high-efficiency single- and multiple-junction PV cells based on NCs of various formulations and sizes.[439−442] High emission efficiencies and tunable emission colors along with a large engineered Stokes shift can help to realize new types of luminescent solar concentrators and new schemes for spectral reshaping of solar radiation.[443−445] Attractive prospects are also associated with use of novel processes such as carrier multiplication (CM) for boosting PV efficiencies above traditional thermodynamic limits.[446−448]

CM is a process by which absorption of a single photon produces multiple electron−hole pairs (excitons). It can potentially increase the power conversion efficiency of single-junction PVs to above 40% *via* increased photocurrent.[449,450] The first spectroscopic observation of CM in PbSe NCs[451] and follow-up studies of this process in NCs of various compositions[452−457] have demonstrated that CM can indeed be enhanced in nanomaterials compared to bulk solids. This assessment is based

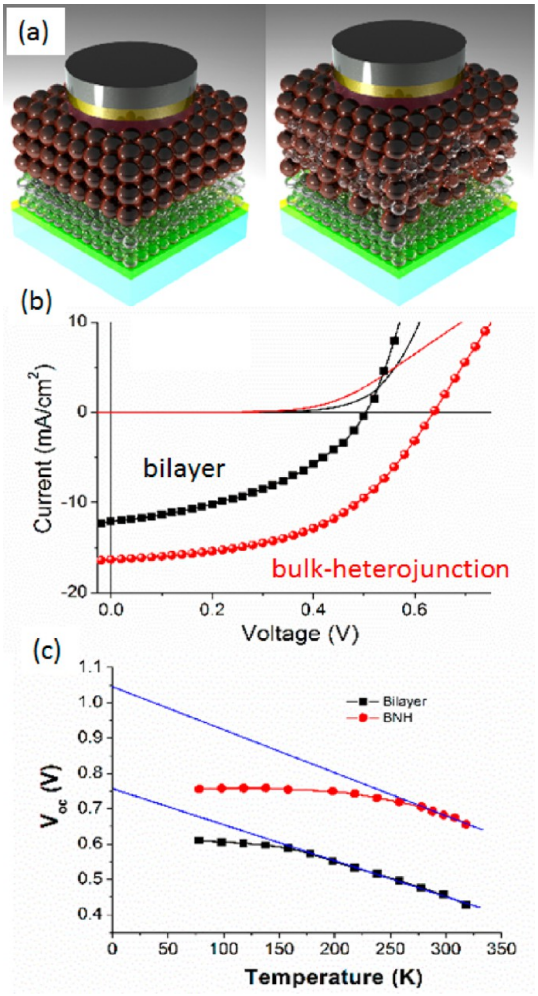

Figure 17. More efficient charge collection and suppressed trap recombination in colloidal quantum dot solar cells is achieved by means of a bulk nano-heterojunction structure in which p-type and n-type materials are blended on the nanometer scale. (a) Schematic of the bilayer (left) and the bulk nano-heterojunction solar cell devices (right) consisting of n-type ZnO nanocrystals and p-type PbS QDs. The improved performance of the heterojunction devices, compared with that of bilayer devices, is displayed in higher photocurrents (b) and higher open circuit voltages (c) (resulting from a trap passivation mechanism at the supra-nanocrystalline level). Reprinted with permission from ref 438. Copyright 2014 John Wiley and Sons.

on the observed reduction of both the spectral onset of this effect (CM threshold; $\hbar\omega_{th}$) and the electron–hole (e–h) pair creation energy (ε_{eh}), that is, the energy in excess of $\hbar\omega_{th}$ required to create an extra exciton. Other types of nanostructures including quasi-1D nanorods[458,459] and 1D carbon nanotubes[460] as well as quasi-2D nanoplatelets[461] and 2D graphene[462] have also shown significant CM efficiencies. Furthermore, studies of QD-based devices such as photodetectors[423] and PV cells[431,463] have demonstrated that CM can produce greater-than-unity quantum efficiencies in a generated photocurrent, which firmly establishes the relevance of this phenomenon to practical solar energy conversion technologies.

A current challenge in the CM field is the development of structures operating at or near the limit defined by energy conservation. As applied to the CM threshold and the e–h pair creation energy, the corresponding targets are $\varepsilon_{eh} = E_g$ and $\hbar\omega_{th} = 2E_g$. A "window-of-opportunity" model[43] relates ε_{eh} to the non-CM (*e.g.*, phonon-related) energy loss rate (k_{cool}; energy dissipated per unity time) and the CM rate ($r_{CM} = 1/\tau_{CM}$; τ_{CM} is the characteristic CM time) by $\varepsilon_{eh} = k_{cool}/r_{CM} = k_{cool}\tau_{CM}$. Hence a smaller ε_{eh} can be achieved by either increasing the CM rate or decreasing the cooling rate.

Recently, the role of intraband cooling in CM was evaluated *via* a comparative study of PbS, PbSe, and PbTe QDs.[43,75,76] These studies indicated that the measured CM yields are directly correlated with the energy loss rates inferred either from direct measurements of intraband relaxation or from estimated phonon emission rates. This suggested the possibility of enhancing CM yields by designing NCs with slowed intraband cooling.

The concept of "cooling-rate engineering" was recently tested by Cirloganu *et al.* using PbSe/CdSe core–shell QDs with exceptionally thick shells (Figure 18a).[464] Theoretical modeling of these structures indicates that a large valence band offset between PbSe and CdSe (Figure 18b) and a significant disparity between hole masses lead to strong backscattering of hole wave functions at the PbSe/CdSe interface. Therefore, at large shell thicknesses and correspondingly large aspect ratios (ρ, defined as the ratio between the shell thickness and the total NC radius), the higher energy holes are almost entirely shell-localized, while the lower energy states remain primarily confined to the core. As a result, these two types of states become electronically decoupled, which is further emphasized by a sizable energetic gap separating them at large ρ (Figure 18b). These effects are expected to slow the cooling of a "hot" shell-localized hole, which, in turn, should enhance the CM channel associated with scattering of this long-lived energetic hole with a pre-existing electron in the band-edge core-localized states (Figure 18b).

A prominent signature of reduced rates of hole cooling was the observation of shell-related PL in the visible spectrum, which emerged for

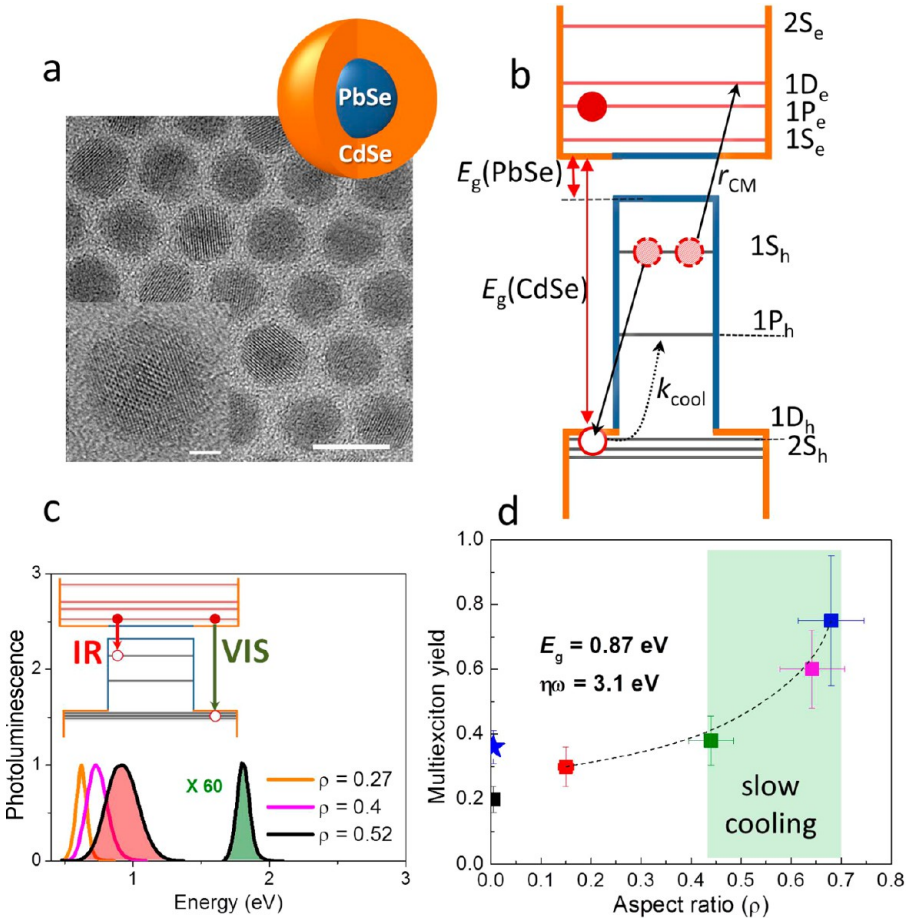

Figure 18. Thick-shell PbSe/CdSe nanocrystals with enhanced carrier multiplication yields.[464] (a) TEM image of a sample of PbSe/CdSe NCs with an overall radius of 4 nm and an aspect ratio of 0.52 (10 nm scale bar). Inset: Higher-resolution image of an individual NC (2 nm scale bar). (b) Approximate structure of electronic states for the NC with a 2 nm core radius and a 2 nm shell thickness. The quantum dot energy spectrum features closely spaced electron levels and sparsely distributed hole core levels. Relaxation of a hot hole from a shell-based state to a core-localized level can happen either *via* a CM process (straight black lines) or by thermalization (dotted black line); the photogenerated and pre-existing carriers are shown by solid and dashed circles, respectively. (c) Photoluminescence spectra of the PbSe/CdSe NCs with aspect ratios of 0.27, 0.4, and 0.52 and a constant overall radius of 4 nm, showing progressive blue shifts with increasing shell size and the emergence of visible emission for the NCs with the thickest shell (shaded spectra); all IR spectra are normalized, while for the thick shell structure, the visible emission amplitude is multiplied by a factor of 60 for the purpose of comparison. Inset: Schematic representation of the band structure indicating the transitions associated with the IR and visible emission. (d) Multiexciton yields measured for PbSe/CdSe core/shell structures with progressively increasing shell thicknesses (3.1 eV excitation). The QDs have slightly different total sizes but similar band gaps (~0.87 eV) for proper comparison and are represented by different color squares on the plot (black dashed line is a guide for the eye). The region where energy conservation is met and simultaneously slow cooling is observed (green shading) corresponds to the highest CM yields. The CM yields for core-only PbSe QDs and PbSe nanorods of similar band gaps are shown by the black square and the blue star, respectively.

large aspect ratios of about 0.4−0.5 (Figure 18c). The appearance of this new emission band correlated with a sharp, almost 4-fold increase of the CM yield (Figure 18d). Specifically, the studies of the PbSe/CdSe NC samples with similar band gaps (0.87 ± 0.02 eV) but different aspect ratios revealed the increase in the CM yield from ~20% for the core-only samples (ρ = 0) to ~75% for the core−shell NCs with ρ = 0.68. The measurements of CM efficiency as a function of photon energy also indicated a considerable reduction of the CM onset almost down the fundamental $2E_g$ limit.[464] These findings suggest that the control of intraband cooling in combination with other demonstrated approaches for enhancing CM yields, such as shape control[459] and/or use of semiconductors with reduced rates of phonon emission (*e.g.*, PbTe),[465] might provide a practical route for reaching the ideal energy-conservation-defined limit in the CM performance.

Theranostic Applications of Nanocrystals. Recently, NCs have been discussed frequently in the context of theranostics. Theranostics involves a platform combining medical diagnostics/analysis with subsequent treatment. From the materials point of view, NCs exhibit significant potential because many different functionalities can be combined in one NC. Nanocrystals comprise an inorganic crystalline core (which can contain core−shell structures such as in the case of CdSe/ZnS) and, in

the context of biological environments, an organic coating (either by design or by adsorption of proteins).[466] Thus, even when the inorganic NC cores act only as passive carriers, the possibility to link different functional molecules to their organic surface coating enables multifunctionality straightforwardly. Functional molecules may involve ligands for specific targeting, for reducing interactions with the immune system, and for providing contrast for imaging, *etc*. However, the NC cores may also introduce functionality, such as fluorescence, super-paramagnetism, or plasmon resonance. Thus, with inorganic cores and organic shells together, NCs are suitable for combining different functionalities. For example, by combining fluorescent, magnetic, or radioactive cores with fluorescent, magnetic, or radioactive shells, NCs that can be detected with several imaging modalities such as fluorescence microscopy, magnetic resonance imaging (MRI), or single-photon emission computed tomography were demonstrated.[467−470]

In order to be truly theranostic, NCs would need to comprise sensing as well as actuating capabilities. In principle, such NCs are available, such as super-paramagnetic iron oxide NPs (SPIONs). Super-paramagnetic iron oxide NPs can be used as T_2 contrast agents for MRI, for example, to indicate the presence of tumors.[336] In the same manner, upon irradiation with alternating magnetic fields, SPIONs can also be used to heat locally and thus to destroy tumor tissue by hyperthermia.[471] Efforts in this direction are aimed at preparing SPIONs that are optimized for hyperthermia, that is, characterized by high values of specific absorption rates in order to minimize the NP dose to be administered and, therefore, to reduce toxic side effects. In this context, successful approaches have been demonstrated in terms of exchange-coupled core−shell architectures[472] and optimized shapes.[473,474] Thus, SPIONs fulfill theranostic purposes, first, by helping to diagnose tumor tissue by providing contrast in MRI to visualize it and, second, by facilitating therapy (*i.e.*, tumor ablation) by local hyperthermia. Similar principles can be extended to more complex applications. Nanocrystals, such as SPIONs, with ion-sensitive fluorophores integrated into their organic surface coating can optically quantify local ion concentrations.[475] Upon local creation of heat, SPIONs can also be used to gate ion channels and thus to control ion concentrations.[476] The same NCs can both detect irregularities in ion concentration (*via* integrated ion-sensitive fluorophores) and correct them *via* heat-mediated control of ion channels. In addition to ions, this idea has been indicated for glucose. Again, glucose-sensitive fluorophores on the NC surface could report local glucose concentration,[477] and upon diagnosis of increased glucose levels, the levels could be corrected therapeutically by triggering release of insulin *via* local hyperthermia.[478]

The above-mentioned examples are based on particles that report data for diagnosis to a physician (*e.g.*, images of tissue, local analyte concentrations) and can, upon switching on an external trigger (*e.g.*, local exposure to alternating magnetic fields), initiate treatment. However, one can also envisage NCs with a direct feedback loop. In such stimuli-responsive NCs, a local trigger (*i.e.*, diagnosis) would transform the properties of the NCs, thus leading to a therapeutic effect. One example is pH-sensitive NCs, which, upon exposure to acidic tumor tissue (diagnosis), locally release drug molecules against the tumor (therapy). Analogous to this approach, pH-sensitive, magnetic, so-called "nanogrenades" (NGs), which are self-assembled NPs composed of iron oxide NPs immobilized in a pH-sensitive polymer, were recently fabricated as theranostic anticancer agents.[479] Based on pH-dependent assembly/disassembly, magnetic resonance imaging and the photodynamic activity are enhanced when these NGs are present in the tumor environment, where the pH value is lower than elsewhere. Small tumors of only 3 mm implanted in mice were successfully visualized *via* pH-responsive T_1 magnetic resonance and fluorescence imaging, demonstrating early stage diagnosis of tumors.[479] Furthermore, the pH-triggered generation of singlet oxygen enabled pH-dependent photodynamic therapy to kill the cancer cells selectively. The enhanced photoactivation of the NGs within the tumor parenchyma enabled superior photodynamic therapeutic efficacy in both human colorectal carcinoma xenografts and in highly drug-resistant heterogeneous tumors. For this purpose, a tumor pH-sensitive nanoformulated triptolide coated with folate targeting ligands was synthesized to treat hepatocellular carcinoma (HCC), which has one of the worst prognoses for survival as it is poorly responsive to both conventional chemotherapy and mechanism-directed therapy (Figure 19).[480] Screening hundreds of compounds against a panel of HCC cells showed that triptolide, a natural product, is much more effective than the current standards of therapy. However, its poor solubility and high toxicity prevented triptolide from potential clinical application. Incorporating triptolide into pH-sensitive polymer NPs coated with folate-targeting ligands led to greatly increased progression-free survival in mice with mitigated side effects.

All of these examples demonstrate that, from the materials point of view, NCs and NPs are capable of combining diagnostic and therapeutic function in one entity. However, there is still almost no clinical use of theranostic NCs. Setting aside the problem of potential cytotoxic effects, the main hurdle is targeting. NCs enable passive tumor targeting governed by the

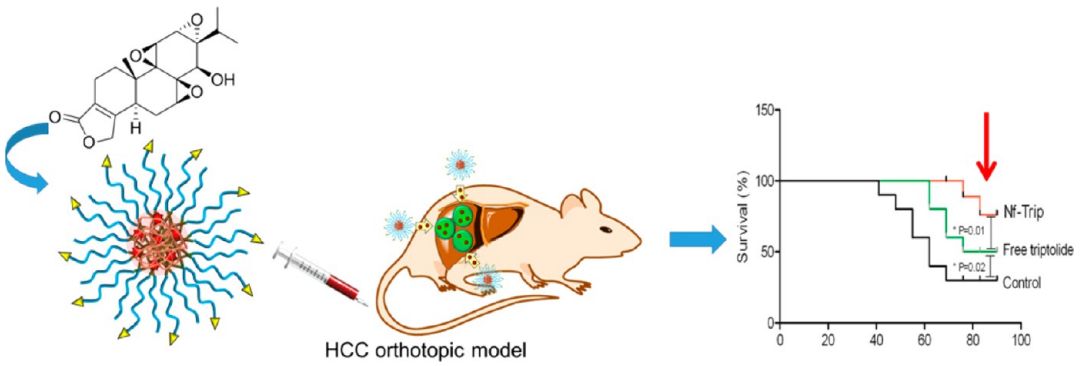

Figure 19. Triptolide-based anticancer theranostic nanoparticles for the treatment of hepatocellular carcinoma (HCC). Left: Structure formula of triptolide, a natural bioactive molecule, and schematic of tumor pH-sensitive nanoformulated triptolide, coated with folate, for use in an HCC subpopulation that overexpresses the folate receptor. Right: While triptolide can prevent disease progression, the pH-sensitive nanoformulated triptolide (Nf-Trip) NPs facilitate uptake into the tumor, and specifically tumor cells, leading to increased efficacy while mitigating systemic toxicity, resulting in increased survival rates. Reprinted from ref 480. Copyright 2014 American Chemical Society.

size and the enhanced permeation and retention effect.[481] This effect is dominant in mice but less pronounced in humans; thus, passive targeting often is not sufficient and involves significant side effects, such as clearance of the NCs by the immune system, leading to their accumulation in the liver. Active targeting of NCs, for example, by the attachment of ligands specific to the target tissue, however, adds little specificity on top of passive targeting.[482]

Thus, controlled biodistribution is one key issue that remains to be resolved. The general problem to solve is not in the functionality of the materials but rather the basic issue of many pharmaceutical agents: targeted biodistribution. Having made this statement, one has to question critically some recent developments concerning the design of theranostic NCs. In the literature, there are increased reports combining as many functional properties into one NC as possible. However, in many reports, the usefulness of all these different components is not demonstrated. Are all these functions needed? Are the effects of the respective functionalities additive, or is the synergistic effect negligible? To justify the integration of many functionalities into one NC, one would first have to investigate experimentally the effects of all functionalities individually, then paired functionalities, *etc.*, and finally benchmark the NC with all combined functionalities. Unfortunately, in many reports, authors do not undertake this effort, and thus the practical use of multifunctionality remains in question. One should also keep in mind that, for clinical use, each theranostic NC-based system should be kept as simple as possible. There is no doubt that NCs are well-suited to offer multifunctional properties with the potential for theranostic use. However, in order to translate from laboratory to bedside, one has to go back to solve the basic remaining issues such as biodistribution and biocompatibility,[483] instead of aiming only to make the NCs increasingly complex.

CONCLUSIONS AND OUTLOOK

Some tens of years ago, NC research existed as an individual field, with its main focus on the synthesis and basic optical and structural characterization. Contemporary NC research has expanded, impacting many research fields and promising a wide scope of applications, as a broad range of inorganic materials has become accessible in NC form. Topics that unite all researchers dealing with NCs are the advances in synthesis, structural characterization, and surface chemistry; basic optical, magnetic, and electronic properties; and the construction of nanosolids composed of NCs as building blocks. In this Nano Focus article, we aimed to provide a snapshot of the current developments and trends in NC research. For more specific information on the topics that we could only briefly discuss here, we refer to recent reviews on NC synthesis,[30,33,71,129,323,484−489] simulation of NC growth,[490] QD photovoltaics,[491] QD electronics,[492] QD LEDs,[493] near- and mid-IR active colloidal QDs,[494,417,495] exciton dynamics,[496,497] semiconductor NC plasmonics,[131,498] surface chemistry,[202] biomedical applications of NCs,[499] and electrochromic applications of NCs.[500]

Being at the forefront of NC research, QDs are at an advanced stage of development in terms of the precision of their syntheses as well as control of their surface chemistries. In fact, it is the effect of the surface chemistry on the individual optical properties of QDs and on QD-based optoelectronic devices that will continue to motivate research about inorganic surface capping and simulation of NC surfaces and the enitre NC entity using density functional theory. The advent of inorganically capped NCs was recent, but we foresee it impacting all fields of applications based on NC solids, including electronics, thermoelectrics, and batteries, and triggering a wave of device improvements and new applications

enabled by their low-cost, low-temperature, and large-area integration and compatibility with flexible and nonplanar substrates.[350,351,501] Novel NMR techniques such as dynamic nuclear polarization–surface-enhanced NMR spectroscopy will facilitate acquisition of well-resolved spectra from surface-bound organic or inorganic capping ligands and outermost NC atomic layers.[502]

Understanding the mechanisms of NC synthesis supports the community's ability to design NC materials with controlled size, shape, and composition. Concerning the synthesis of NCs, a particularly difficult task remains: the *in situ* observation of NC formation at the nucleation stage and at the very early stage of growth. Despite the great potential of *in situ* XRD, an inherent limitation is the mass transport during the mixing of reagents. We believe that this task may be facilitated by the deployment of microfluidic methods,[503−506] combined with online monitoring by optical absorption and emission spectroscopy and with *in situ* structural characterization by synchrotron XRD. Furthermore, microfluidics may enable fast screening of reaction conditions and more repeatable synthesis outputs than in conventional batch syntheses performed in reaction flasks. Some of the key principles of colloidal synthesis of inorganic NCs, such as the use of surfactants, also enter other fields of material developments, including colloidal graphene nanoribbons[507] and the synthesis of organic pigment NCs, as discussed above.[174]

A frequently debated issue in the field of nanomaterials is the question of toxicity[508−512] and environmental friendliness. The use of the most promising QD materials—those exhibiting record photoluminescence quantum yields,[35] record charge transport properties,[513] or long photoluminescence wavelengths[424]—might be restricted by legislation because of the toxicity of their constituents (Pb, Cd, Hg).[511]

Understanding the mechanisms of NC synthesis supports the community's ability to design NC materials with controlled size, shape, and composition.

Promising and substantially less-toxic replacements of the currently favored Cd- or Pb-containing compounds include not only ionically bound compound semiconductors but also covalently bound group IV NPs. The latter (silicon, diamond, silicon carbide, and germanium NPs) benefit from their fluorescence, observed over wide spectral regions covering the near-infrared, visible, and near-ultraviolet ranges and are thus favored for *in vivo* and *in vitro* biomedical experiments.[514] Also, "carbon dots" exhibit color-tunable emission properties, which are excitation-dependent in this case, making these nanomaterials promising for applications predominantly in the fields of bioimaging, cancer therapy, printing inks, photocatalysis, and optoelectronic devices.[515,516]

When it comes to real-world applications, the NC research community will soon face significant challenges in commercially competitive areas such as photovoltaics. The power conversion efficiencies of QD-based solar cells have advanced from sub-1% levels in 2005 to over 8.5% in 2013–2014.[436,491,517,518] However, this breakthrough is now challenged by the discovery of highly efficient photovoltaics in lead halide perovskites with power conversion efficiencies approaching 20%, yet with even simpler fabrication procedures than the synthesis and processing of QDs.[519] A common problem of both technologies is chemical instability, which limits long-term operation required for commercial solar cells and should be addressed in the future.

Applications in which the integration of NCs into well-established technologies results in significant improvement in the performance of the latter are certainly beneficial. An example of such an application is the QD color TV, representing LCD screens with improved back-lighting, provided by colloidal QDs. The color conversion back-lighting provides a larger range of possible colors than the standard phosphor coatings used for color conversion from the LED back-light, making the LCD screens as powerful as the old vacuum-tube electron ray TV sets. Even though this innovative product was technically ready for the market, it was offered for sale only for a period of a few months in 2013, indicating harsh competition with other technologies and, eventually, restricted market penetration in Europe related to the presence of cadmium in the QDs. Another promising optoelectronic application is the implementation of infrared-active QDs onto CMOS-based readout electronics to obtain highly integrated infrared imagers and cameras, operated at wavelengths not accessible for Si-based devices.[520] Also, the incorporation of QDs in place of organic dye molecules in conventional OLEDs[521] is being actively pursued as a technology with the potential for fast commercialization, owing to extensive developments in hole- and electron-transporting and injecting layers for OLEDs.

Exciting progress with respect to NC applications has been obtained in the wide field of biomedicine and especially in theranostics. We have discussed NP-based approaches here, highlighting their advantages in comparison to traditional medications in cancer treatments—mouse models with increased survival rates are encouraging results.[480] Similarly successful was the demonstration of gold NPs in cancer-cell-specific, on-demand intracellular amplification of chemoradiation therapy,

obtained by laser-induced mechanical impact.[522] With a laser pulse, the gold NPs provide a plasmonic nanobubble, a mechanical explosion that destroys the host cancer cell or ejects drugs into the cytoplasm. The same NPs locally enhance external X-rays, leading to a "quadrapeutic" effect, which improves the efficacy of standard chemoradiation therapy by a factor of 10−1000×. Thus, theranostic NPs have the potential to become powerful tools in cancer treatment, as indicated in studies on animals (mice). While there are no doubts that research in these directions will provide a multitude of further treatment routes to heal a wide range of diseases, challenges remain in the transfer of these developments to applications for humans, which includes finding appropriate dosages, ruling out pharmacological interactions, studying side effects and innocuousness, licensing novel NP medicines, and gaining regulatory approval. Less critical, and therefore much more straightforward for clinical use, might be medical applications for which the NPs are applied outside of the body. An example of such promising applications is an extracorporeal blood-cleansing device for sepsis therapy, presented recently by Kang *et al.*[523] In this device, magnetic NPs are used, coated with an engineered human protein, which captures a broad range of pathogens and toxins. Magnets are then used to pull out the toxins and pathogens bound to the magnetic NPs in the blood, which is then returned back to the patient after cleansing. The extracorporeal device is called "biospleen", and it removes multiple-gram doses of bacteria, fungi, and endotoxins from human blood at a flow rate of 1.25 L per h *in vitro*. Thus, it represents a dialysis-like blood cleansing system, which could also be applied in parallel with targeted antibiotic therapy to heal diseases and to prolong life.

As mentioned in the introduction, photoelectrochemistry was one of the original driving forces for the development of NC research. While this field had stagnated somewhat over the last 20 years, there have been significant advances in understanding photocatalytic processes required for the conversion of solar energy into fuels. In particular, Ni-decorated CdS nanorods have been shown to generate H_2 (with ethanol as a sacrificial agent) photocatalytically with an external quantum efficiency of above 50%, which is an unprecedented value for chalcogenide NCs with non-noble cocatalysts under visible light.[524] This high value was suggested to be achieved through a two-step mechanism of hole transfer *via* a redox couple $^{\bullet}OH/OH^{-}$ at high pH, operating as a highly mobile molecular shuttle between the NC surface and the hole scavenger (ethanol).

Prior to applied considerations, NC research is often (if not primarily) dominated by pure curiosity and always has the potential to provide surprising fundamental discoveries. Questions such as to what extent energetic interactions are responsible for the NC self-assembly into more- or less-ordered structures[525] are being debated and explored. Superstructures of increasing complexity and/or beauty will be assembled, independent of their impact on device performance. Also, NPs with more elaborate shapes and specific properties will be developed by direct synthesis or with the assistance of galvanic- or cation-exchange reactions.[526] Hybrid superlattices of NCs with large inorganic (atomically defined) molecules such as polyoxometallates will bridge the gap between atomically precise and colloidal crystals.[527] The increased availability of *in situ* characterization tools will deliver deeper insights into the formation mechanisms of NCs, their seeds, their shape evolution, and the dynamics of their growth for increased numbers of materials. Nanocrystals will continue to provide a playground to make the unimaginable come closer, such as cold electron transport at room temperature by energy filtering through the quantum-confined states of NCs.[528] Such basic research will certainly continue to lead to novel concepts for devices and applications in the coming years.

Conflict of Interest: The authors declare no competing financial interest.

Acknowledgment. This article was inspired by the discussions and presentations at the NaNaX6 conference held in Bad-Hofgastein, Austria, May 18-23, 2014. M.K. acknowledges partial financial support by the European Union (EU) *via* ERC Starting Grant 2012 (Project NANOSOLID, GA No. 306733). L.M. acknowledges partial financial support by the EU *via* ERC Consolidator Grant 2013 (Project TRANS-NANO, GA No. 614897) and CNECT-ICT-604391 (Graphene Flagship). Z.H. acknowledges Ghent University (GOA Detavernier-Hens), the FWO-Vlaanderen (G.0760.12), SIM (SIBO SoPPoM), BelSPo (IAP 7.35, photonics@be) and EH-H2020 (ETN Phonsi) for research funding. B.A.K. acknowledges financial support from the Robert A. Welch Foundation (F-1464) and the NSF (CHE-1308813). A.C. acknowledges financial support from the EU FP7 under project UNION (FP7-NMP 310250). A.L.R. acknowledges financial support from the Guandong Province Technology Council, China (Project R-IND4601). W.H. thanks the "Gesellschaft für Mikro- und Nanoelektronik (GMe)", the Austrian Science fund FWF, for financial support *via* the SFB project IR_ON and acknowledges the use of the services and facilities of the "Energie Campus Nürnberg" and financial support through the "Aufbruch Bayern" initiative of the state of Bavaria. P.R. acknowledges financial support from French National Research Agency (NANOFRET, Grant No. ANR-12-NANO-0007; NIRA, Grant No. ANR-13-BS08-0011). V.I.K. acknowledges financial support from the Center for Advanced Solar Photophysics (CASP), an Energy Frontier Research Center of the U.S. Department of Energy (DOE), Office of Science (OS) and Office of Basic Energy Sciences (OBES). W.J.P. acknowledges funding for the EU (project FutureNanoNeeds). C.R.K. and C.B.M. acknowledge financial support from the U.S. Department of Energy Office of Basic Energy Sciences, Division of Materials Science and Engineering (Award No. DE-SC0002158). D.V.T. and P.G.-S. acknowledge financial support from the NSF MRSEC Program under Award No. DMR 08-20054.

REFERENCES AND NOTES

1. Faraday, M. The Bakerian Lecture: Experimental Relations of Gold (and Other Metals) to Light. *Philos. Trans. R. Soc.* **1857**, *147*, 145–181.
2. Nozik, A. J. Photoelectrochemistry—Applications to Solar Energy Conversion. *Annu. Rev. Phys. Chem.* **1978**, *29*, 189–222.
3. Grätzel, M. Photochemical Methods for the Conversion of Light into Chemical Energy. *Berichte der*

Bunsengesellschaft für physikalische Chemie **1980**, *84*, 981–991.
4. Weller, H.; Koch, U.; Gutiérrez, M.; Henglein, A. Photochemistry of Colloidal Metal Sulfides. 7. Absorption and Fluorescence of Extremely Small ZnS Particles (The World of the Neglected Dimensions). *Ber. Bunsen-Ges. Phys. Chem.* **1984**, *88*, 649–656.
5. Alfassi, Z.; Bahnemann, D.; Henglein, A. Photochemistry Of Colloidal Metal Sulfides. 3. Photoelectron Emission from Cadmium Sulfide and Cadmium Sulfide-Zinc Sulfide Cocolloids. *J. Phys. Chem.* **1982**, *86*, 4656–4657.
6. Rossetti, R.; Nakahara, S.; Brus, L. E. Quantum Size Effects in the Redox Potentials, Resonance Raman Spectra, and Electronic Spectra of CdS Crystallites in Aqueous Solution. *J. Chem. Phys.* **1983**, *79*, 1086–1088.
7. Brus, L. Electronic Wave Functions in Semiconductor Clusters: Experiment and Theory. *J. Phys. Chem.* **1986**, *90*, 2555–2560.
8. Brus, L. E. Electron−Electron and Electron−Hole Interactions in Small Semiconductor Crystallites: The Size Dependence of the Lowest Excited Electronic State. *J. Chem. Phys.* **1984**, *80*, 4403–4409.
9. Henglein, A. Catalysis of Photochemical-Reactions By Colloidal Semiconductors. *Pure Appl. Chem.* **1984**, *56*, 1215–1224.
10. Ekimov, A. I.; Onushchenko, A. A. Quantum Size Effects in 3-Dimensional Microscopic Semiconductor Crystals. *JETP Lett.* **1981**, *34*, 345–349.
11. Efros, A. L. Interband Absorption of Light in a Semiconductor Sphere. *Sov. Phys. Semicond.* **1982**, *16*, 772–775.
12. Itoh, T.; Kirihara, T. Excitons in CuCl Microcrystals Embedded in NaCl. *J. Lumin.* **1984**, *31−32*, 120–122.
13. Murray, C. B.; Norris, D. J.; Bawendi, M. G. Synthesis and Characterization of Nearly Monodisperse CdE (E = Sulfur, Selenium, Tellurium) Semiconductor Nanocrystallites. *J. Am. Chem. Soc.* **1993**, *115*, 8706–8715.
14. Gaponik, N.; Talapin, D. V.; Rogach, A. L.; Hoppe, K.; Shevchenko, E. V.; Kornowski, A.; Eychmüller, A.; Weller, H. Thiol-Capping of CdTe Nanocrystals: An Alternative to Organometallic Synthetic Routes. *J. Phys. Chem. B* **2002**, *106*, 7177–7185.
15. Hines, M. A.; Guyot-Sionnest, P. Synthesis and Characterization of Strongly Luminescing ZnS-Capped CdSe Nanocrystals. *J. Phys. Chem.* **1996**, *100*, 468–471.
16. Schaak, R. E.; Williams, M. E. Full Disclosure: The Practical Side of Nanoscale Total Synthesis. *ACS Nano* **2012**, *6*, 8492–8497.
17. Parak, W. J. Complex Colloidal Assembly. *Science* **2011**, *334*, 1359–1360.
18. Yarema, M.; Wörle, M.; Rossell, M. D.; Erni, R.; Caputo, R.; Protesescu, L.; Kravchyk, K. V.; Dirin, D. N.; Lienau, K.; von Rohr, F.; *et al.* Monodisperse Colloidal Gallium Nanoparticles: Synthesis, Low Temperature Crystallization, Surface Plasmon Resonance and Li-Ion Storage. *J. Am. Chem. Soc.* **2014**, *136*, 12422–12430.
19. Yu, Y. X.; Bosoy, C. A.; Hessel, C. M.; Smilgies, D. M.; Korgel, B. A. Silicon Nanocrystal Superlattices. *ChemPhysChem* **2013**, *14*, 84–87.
20. Lu, X.; Hessel, C. M.; Yu, Y.; Bogart, T. D.; Korgel, B. A. Colloidal Luminescent Silicon Nanorods. *Nano Lett.* **2013**, *13*, 3101–3105.
21. Lu, X. T.; Korgel, B. A. A Single-Step Reaction for Silicon and Germanium Nanorods. *Chem.—Eur. J.* **2014**, *20*, 5874–5879.
22. Yang, Z. Y.; Iqbal, M.; Dobbie, A. R.; Veinot, J. G. C. Surface-Induced Alkene Oligomerization: Does Thermal Hydrosilylation Really Lead to Monolayer Protected Silicon Nanocrystals? *J. Am. Chem. Soc.* **2013**, *135*, 17595–17601.
23. Maurice, A.; Haro, M. L.; Hyot, B.; Reiss, P. Synthesis of Colloidal Indium Antimonide Nanocrystals Using Stibine. *Part. Part. Syst. Char.* **2013**, *30*, 828–831.
24. Beberwyck, B. J.; Alivisatos, A. P. Ion Exchange Synthesis of III-V Nanocrystals. *J. Am. Chem. Soc.* **2012**, *134*, 19977–19980.
25. Liu, W. Y.; Chang, A. Y.; Schaller, R. D.; Talapin, D. V. Colloidal InSb Nanocrystals. *J. Am. Chem. Soc.* **2012**, *134*, 20258–20261.
26. Yarema, M.; Kovalenko, M. V. Colloidal Synthesis of InSb Nanocrystals with Controlled Polymorphism Using Indium and Antimony Amides. *Chem. Mater.* **2013**, *25*, 1788–1792.
27. Oh, M. H.; Yu, T.; Yu, S.-H.; Lim, B.; Ko, K.-T.; Willinger, M.-G.; Seo, D.-H.; Kim, B. H.; Cho, M. G.; Park, J.-H.; *et al.* Galvanic Replacement Reactions in Metal Oxide Nanocrystals. *Science* **2013**, *340*, 964–968.
28. Xia, X.; Wang, Y.; Ruditskiy, A.; Xia, Y. 25th Anniversary Article: Galvanic Replacement: A Simple and Versatile Route to Hollow Nanostructures with Tunable and Well-Controlled Properties. *Adv. Mater.* **2013**, *25*, 6313–6333.
29. Li, H. B.; Zanella, M.; Genovese, A.; Povia, M.; Falqui, A.; Giannini, C.; Manna, L. Sequential Cation Exchange in Nanocrystals: Preservation of Crystal Phase and Formation of Metastable Phases. *Nano Lett.* **2011**, *11*, 4964–4970.
30. Gupta, S.; Kershaw, S. V.; Rogach, A. L. 25th Anniversary Article: Ion Exchange in Colloidal Nanocrystals. *Adv. Mater.* **2013**, *25*, 6923–6944.
31. Rivest, J. B.; Jain, P. K. Cation Exchange on the Nanoscale: An Emerging Technique for New Material Synthesis, Device Fabrication, and Chemical Sensing. *Chem. Soc. Rev.* **2013**, *42*, 89–96.
32. Sytnyk, M.; Kirchschlager, R.; Bodnarchuk, M. I.; Primetzhofer, D.; Kriegner, D.; Enser, H.; Stangl, J.; Bauer, P.; Voith, M.; Hassel, A. W.; *et al.* Tuning the Magnetic Properties of Metal Oxide Nanocrystal Heterostructures by Cation Exchange. *Nano Lett.* **2013**, *13*, 586–593.
33. Wang, W. S.; Dahl, M.; Yin, Y. D. Hollow Nanocrystals through the Nanoscale Kirkendall Effect. *Chem. Mater.* **2013**, *25*, 1179–1189.
34. El Mel, A. A.; Buffiere, M.; Tessier, P. Y.; Konstantinidis, S.; Xu, W.; Du, K.; Wathuthanthri, I.; Choi, C. H.; Bittencourt, C.; Snyders, R. Highly Ordered Hollow Oxide Nanostructures: The Kirkendall Effect at the Nanoscale. *Small* **2013**, *9*, 2838–2843.
35. Chen, O.; Zhao, J.; Chauhan, V. P.; Cui, J.; Wong, C.; Harris, D. K.; Wei, H.; Han, H.-S.; Fukumura, D.; Jain, R. K.; Bawendi, M. G. Compact High-Quality CdSe−CdS Core−Shell Nanocrystals with Narrow Emission Linewidths and Suppressed Blinking. *Nat. Mater.* **2013**, *12*, 445–451.
36. Christodoulou, S.; Vaccaro, G.; Pinchetti, V.; De Donato, F.; Grim, J. Q.; Casu, A.; Genovese, A.; Vicidomini, G.; Diaspro, A.; Brovelli, S.; *et al.* Synthesis of Highly Luminescent Wurtzite CdSe/CdS Giant-Shell Nanocrystals Using a Fast Continuous Injection Route. *J. Mater. Chem. C* **2014**, *2*, 3439–3447.
37. Wilson, W. L.; Szajowski, P. F.; Brus, L. E. Quantum Confinement in Size-Selected, Surface-Oxidized Silicon Nanocrystals. *Science* **1993**, *262*, 1242–1244.
38. Yang, C. S.; Bley, R. A.; Kauzlarich, S. M.; Lee, H. W. H.; Delgado, G. R. Synthesis of Alkyl-Terminated Silicon Nanoclusters by a Solution Route. *J. Am. Chem. Soc.* **1999**, *121*, 5191–5195.
39. Warner, J. H.; Hoshino, A.; Yamamoto, K.; Tilley, R. D. Water-Soluble Photoluminescent Silicon Quantum Dots. *Angew. Chem., Int. Ed.* **2005**, *44*, 4550–4554.
40. Holmes, J. D.; Ziegler, K. J.; Doty, R. C.; Pell, L. E.; Johnston, K. P.; Korgel, B. A. Highly Luminescent Silicon Nanocrystals with Discrete Optical Transitions. *J. Am. Chem. Soc.* **2001**, *123*, 3743–3748.
41. Li, X. G.; He, Y. Q.; Talukdar, S. S.; Swihart, M. T. Process for Preparing Macroscopic Quantities of Brightly Photoluminescent Silicon Nanoparticles with Emission Spanning the Visible Spectrum. *Langmuir* **2003**, *19*, 8490–8496.

42. Li, X. G.; He, Y. Q.; Swihart, M. T. Surface Functionalization of Silicon Nanoparticles Produced by Laser-Driven Pyrolysis of Silane Followed by HF-HNO_3 Etching. *Langmuir* **2004**, *20*, 4720–4727.
43. Mangolini, L.; Thimsen, E.; Kortshagen, U. High-Yield Plasma Synthesis of Luminescent Silicon Nanocrystals. *Nano Lett.* **2005**, *5*, 655–659.
44. Jurbergs, D.; Rogojina, E.; Mangolini, L.; Kortshagen, U. Silicon Nanocrystals with Ensemble Quantum Yields Exceeding 60%. *Appl. Phys. Lett.* **2006**, *88*, 233116.
45. Hessel, C. M.; Henderson, E. J.; Veinot, J. G. C. Hydrogen Silsesquioxane: A Molecular Precursor for Nanocrystalline Si–SiO_2 Composites and Freestanding Hydride-Surface-Terminated Silicon Nanoparticles. *Chem. Mater.* **2006**, *18*, 6139–6146.
46. Hessel, C. M.; Reid, D.; Panthani, M. G.; Rasch, M. R.; Goodfellow, B. W.; Wei, J.; Fujii, H.; Akhavan, V.; Korgel, B. A. Synthesis of Ligand-Stabilized Silicon Nanocrystals with Size-Dependent Photoluminescence Spanning Visible to Near-Infrared Wavelengths. *Chem. Mater.* **2012**, *24*, 393–401.
47. Locritani, M.; Yu, Y.; Bergamini, G.; Baroncini, M.; Molloy, J. K.; Korgel, B. A.; Ceroni, P. Silicon Nanocrystals Functionalized with Pyrene Units: Efficient Light-Harvesting Antennae with Bright Near-Infrared Emission. *J. Phys. Chem. Lett.* **2014**, *5*, 3325–3329.
48. Yu, Y.; Bosoy, C. A.; Smilgies, D.-M.; Korgel, B. A. Self-Assembly and Thermal Stability of Binary Superlattices of Gold and Silicon Nanocrystals. *J. Phys. Chem. Lett.* **2013**, *4*, 3677–3682.
49. Yu, Y.; Hessel, C. M.; Bogart, T. D.; Panthani, M. G.; Rasch, M. R.; Korgel, B. A. Room Temperature Hydrosilylation of Silicon Nanocrystals with Bifunctional Terminal Alkenes. *Langmuir* **2013**, *29*, 1533–1540.
50. Panthani, M. G.; Hessel, C. M.; Reid, D.; Casillas, G.; Jose-Yacaman, M.; Korgel, B. A. Graphene-Supported High-Resolution TEM and STEM Imaging of Silicon Nanocrystals and Their Capping Ligands. *J. Phys. Chem. C* **2012**, *116*, 22463–22468.
51. Heitsch, A. T.; Hessel, C. M.; Akhavan, V. A.; Korgel, B. A. Colloidal Silicon Nanorod Synthesis. *Nano Lett.* **2009**, *9*, 3042–3047.
52. Holmes, J. D.; Johnston, K. P.; Doty, R. C.; Korgel, B. A. Control of Thickness and Orientation of Solution-Grown Silicon Nanowires. *Science* **2000**, *287*, 1471–1473.
53. Heitsch, A. T.; Fanfair, D. D.; Tuan, H.-Y.; Korgel, B. A. Solution–Liquid–Solid (SLS) Growth of Silicon Nanowires. *J. Am. Chem. Soc.* **2008**, *130*, 5436–5437.
54. Trentler, T. J.; Hickman, K. M.; Goel, S. C.; Viano, A. M.; Gibbons, P. C.; Buhro, W. E. Solution–Liquid–Solid Growth of Crystalline III–V Semiconductors—An Analogy to Vapor–Liquid–Solid Growth. *Science* **1995**, *270*, 1791–1794.
55. Wang, F.; Dong, A.; Sun, J.; Tang, R.; Yu, H.; Buhro, W. E. Solution–Liquid–Solid Growth of Semiconductor Nanowires. *Inorg. Chem.* **2006**, *45*, 7511–7521.
56. Hessel, C. M.; Heitsch, A. T.; Korgel, B. A. Gold Seed Removal from the Tips of Silicon Nanorods. *Nano Lett.* **2010**, *10*, 176–180.
57. Chockla, A. M.; Harris, J. T.; Akhavan, V. A.; Bogart, T. D.; Holmberg, V. C.; Steinhagen, C.; Mullins, C. B.; Stevenson, K. J.; Korgel, B. A. Silicon Nanowire Fabric as a Lithium Ion Battery Electrode Material. *J. Am. Chem. Soc.* **2011**, *133*, 20914–20921.
58. Bogart, T. D.; Oka, D.; Lu, X.; Gu, M.; Wang, C.; Korgel, B. A. Lithium Ion Battery Peformance of Silicon Nanowires with Carbon Skin. *ACS Nano* **2014**, *8*, 915–922.
59. Bogart, T. D.; Lu, X.; Gu, M.; Wang, C.; Korgel, B. A. Enhancing the Lithiation Rate of Silicon Nanowires by the Inclusion of Tin. *RSC Adv.* **2014**, *4*, 42022–42028.
60. Allen, P. M.; Bawendi, M. G. Ternary I–III–VI Quantum Dots Luminescent in the Red to Near-Infrared. *J. Am. Chem. Soc.* **2008**, *130*, 9240–9241.
61. Guo, Q.; Kim, S. J.; Kar, M.; Shafarman, W. N.; Birkmire, R. W.; Stach, E. A.; Agrawal, R.; Hillhouse, H. W. Development of $CuInSe_2$ Nanocrystal and Nanoring Inks for Low-Cost Solar Cells. *Nano Lett.* **2008**, *8*, 2982–2987.
62. Han, W.; Yi, L.; Zhao, N.; Tang, A.; Gao, M.; Tang, Z. Synthesis and Shape-Tailoring of Copper Sulfide/Indium Sulfide-Based Nanocrystals. *J. Am. Chem. Soc.* **2008**, *130*, 13152–13161.
63. Pan, D.; An, L.; Sun, Z.; Hou, W.; Yang, Y.; Yang, Z.; Lu, Y. Synthesis of Cu–In–S Ternary Nanocrystals with Tunable Structure and Composition. *J. Am. Chem. Soc.* **2008**, *130*, 5620–5621.
64. Panthani, M. G.; Akhavan, V.; Goodfellow, B.; Schmidtke, J. P.; Dunn, L.; Dodabalapur, A.; Barbara, P. F.; Korgel, B. A. Synthesis of $CuInS_2$, $CuInSe_2$, and $Cu(In_xGa_{1-x})Se_2$ (CIGS) Nanocrystal "Inks" for Printable Photovoltaics. *J. Am. Chem. Soc.* **2008**, *130*, 16770–16777.
65. Guo, Q.; Ford, G. M.; Hillhouse, H. W.; Agrawal, R. Sulfide Nanocrystal Inks for Dense $Cu(In_{1-x}Ga_x)(S_{1-y}Se_y)_2$ Absorber Films and Their Photovoltaic Performance. *Nano Lett.* **2009**, *9*, 3060–3065.
66. Riha, S. C.; Parkinson, B. A.; Prieto, A. L. Solution-Based Synthesis and Characterization of Cu_2ZnSnS_4 Nanocrystals. *J. Am. Chem. Soc.* **2009**, *131*, 12054–12055.
67. Steinhagen, C.; Panthani, M. G.; Akhavan, V.; Goodfellow, B.; Koo, B.; Korgel, B. A. Synthesis of Cu_2ZnSnS_4 Nanocrystals for Use in Low-Cost Photovoltaics. *J. Am. Chem. Soc.* **2009**, *131*, 12554–12555.
68. Ibáñez, M.; Zamani, R.; Li, W.; Shavel, A.; Arbiol, J.; Morante, J. R.; Cabot, A. Extending the Nanocrystal Synthesis Control to Quaternary Compositions. *Cryst. Growth Des.* **2012**, *12*, 1085–1090.
69. Chang, J.; Waclawik, E. R. Colloidal Semiconductor Nanocrystals: Controlled Synthesis and Surface Chemistry in Organic Media. *RSC Adv.* **2014**, *4*, 23505–23527.
70. Fan, F.-J.; Wu, L.; Yu, S.-H. Energetic I–III–VI_2 and I_2–II–IV–VI_4 Nanocrystals: Synthesis, Photovoltaic and Thermoelectric Applications. *Energy Environ. Sci.* **2014**, *7*, 190–208.
71. Aldakov, D.; Lefrancois, A.; Reiss, P. Ternary and Quaternary Metal Chalcogenide Nanocrystals: Synthesis, Properties and Applications. *J. Mater. Chem. C* **2013**, *1*, 3756–3776.
72. Shavel, A.; Arbiol, J.; Cabot, A. Synthesis of Quaternary Chalcogenide Nanocrystals: Stannite $Cu_2Zn_xSn_ySe_{1+x+2y}$. *J. Am. Chem. Soc.* **2010**, *132*, 4514–4515.
73. Ibáñez, M.; Zamani, R.; Li, W.; Cadavid, D.; Gorsse, S.; Katcho, N. A.; Shavel, A.; López, A. M.; Morante, J. R.; Arbiol, J.; *et al.* Crystallographic Control at the Nanoscale To Enhance Functionality: Polytypic Cu_2GeSe_3 Nanoparticles as Thermoelectric Materials. *Chem. Mater.* **2012**, *24*, 4615–4622.
74. Singh, A.; Coughlan, C.; Laffir, F.; Ryan, K. M. Assembly of $CuIn_{1-x}Ga_xS_2$ Nanorods into Highly Ordered 2D and 3D Superstructures. *ACS Nano* **2012**, *6*, 6977–6983.
75. Singh, A.; Geaney, H.; Laffir, F.; Ryan, K. M. Colloidal Synthesis of Wurtzite Cu_2ZnSnS_4 Nanorods and Their Perpendicular Assembly. *J. Am. Chem. Soc.* **2012**, *134*, 2910–2913.
76. Zamani, R. R.; Ibáñez, M.; Luysberg, M.; García-Castelló, N.; Houben, L.; Prades, J. D.; Grillo, V.; Dunin-Borkowski, R. E.; Morante, J. R.; Cabot, A.; Arbiol, J. Polarity-Driven Polytypic Branching in Cu-Based Quaternary Chalcogenide Nanostructures. *ACS Nano* **2014**, *8*, 2290–2301.
77. Ibáñez, M.; Cadavid, D.; Zamani, R.; García-Castelló, N.; Izquierdo-Roca, V.; Li, W.; Fairbrother, A.; Prades, J. D.; Shavel, A.; Arbiol, J.; Pérez-Rodríguez, A.; *et al.* Composition Control and Thermoelectric Properties of Quaternary Chalcogenide Nanocrystals: The Case of Stannite $Cu_2CdSnSe_4$. *Chem. Mater.* **2012**, *24*, 562–570.

78. Ibáñez, M.; Zamani, R.; Lalonde, A.; Cadavid, D.; Li, W.; Shavel, A.; Arbiol, J.; Morante, J. R.; Gorsse, S.; Snyder, G. J.; *et al.* $Cu_2ZnGeSe_4$ Nanocrystals: Synthesis and Thermoelectric Properties. *J. Am. Chem. Soc.* **2012**, *134*, 4060–4063.
79. Dilena, E.; Xie, Y.; Brescia, R.; Prato, M.; Maserati, L.; Krahne, R.; Paolella, A.; Bertoni, G.; Povia, M.; Moreels, I.; *et al.* $CuIn_xGa_{1-x}S_2$ Nanocrystals with Tunable Composition and Band Gap Synthesized *via* a Phosphine-Free and Scalable Procedure. *Chem. Mater.* **2013**, *25*, 3180–3187.
80. Lesnyak, V.; George, C.; Genovese, A.; Prato, M.; Casu, A.; Ayyappan, S.; Scarpellini, A.; Manna, L. Alloyed Copper Chalcogenide Nanoplatelets *via* Partial Cation Exchange Reactions. *ACS Nano* **2014**, *8*, 8407–8418.
81. Khare, A.; Wills, A. W.; Ammerman, L. M.; Norris, D. J.; Aydil, E. S. Size Control and Quantum Confinement in Cu_2ZnSnS_4 Nanocrystals. *Chem. Commun.* **2011**, *47*, 11721–11723.
82. Nishi, H.; Nagano, T.; Kuwabata, S.; Torimoto, T. Controllable Electronic Energy Structure of Size-Controlled Cu_2ZnSnS_4 Nanoparticles Prepared by a Solution-Based Approach. *Phys. Chem. Chem. Phys.* **2014**, *16*, 672–675.
83. Wang, Y.-H. A.; Zhang, X.; Bao, N.; Lin, B.; Gupta, A. Synthesis of Shape-Controlled Monodisperse Wurtzite $CuIn_xGa_{1-x}S_2$ Semiconductor Nanocrystals with Tunable Band Gap. *J. Am. Chem. Soc.* **2011**, *133*, 11072–11075.
84. Lu, X.; Zhuang, Z.; Peng, Q.; Li, Y. Controlled Synthesis of Wurtzite $CuInS_2$ Nanocrystals and Their Side-by-Side Nanorod Assemblies. *CrystEngComm* **2011**, *13*, 4039–4045.
85. Koo, B.; Patel, R. N.; Korgel, B. A. Wurtzite−Chalcopyrite Polytypism in $CuInS_2$ Nanodisks. *Chem. Mater.* **2009**, *21*, 1962–1966.
86. Wang, J.-J.; Wang, Y.-Q.; Cao, F.-F.; Guo, Y.-G.; Wan, L.-J. Synthesis of Monodispersed Wurtzite Structure $CuInSe_2$ Nanocrystals and Their Application in High-Performance Organic−Inorganic Hybrid Photodetectors. *J. Am. Chem. Soc.* **2010**, *132*, 12218–12221.
87. Zhong, H.; Lo, S. S.; Mirkovic, T.; Li, Y.; Ding, Y.; Li, Y.; Scholes, G. D. Noninjection Gram-Scale Synthesis of Monodisperse Pyramidal $CuInS_2$ Nanocrystals and Their Size-Dependent Properties. *ACS Nano* **2010**, *4*, 5253–5262.
88. Koo, B.; Patel, R. N.; Korgel, B. A. Synthesis of $CuInSe_2$ Nanocrystals with Trigonal Pyramidal Shape. *J. Am. Chem. Soc.* **2009**, *131*, 3134–3135.
89. Yu, X.; Shavel, A.; An, X.; Luo, Z.; Ibáñez, M.; Cabot, A. Cu_2ZnSnS_4-Pt and Cu_2ZnSnS_4-Au Heterostructured Nanoparticles for Photocatalytic Water Splitting and Pollutant Degradation. *J. Am. Chem. Soc.* **2014**, *136*, 9236–9239.
90. Lu, X.; Zhuang, Z.; Peng, Q.; Li, Y. Wurtzite Cu_2ZnSnS_4 Nanocrystals: A Novel Quaternary Semiconductor. *Chem. Commun.* **2011**, *47*, 3141–3143.
91. Shavel, A.; Cadavid, D.; Ibáñez, M.; Carrete, A.; Cabot, A. Continuous Production of Cu_2ZnSnS_4 Nanocrystals in a Flow Reactor. *J. Am. Chem. Soc.* **2012**, *134*, 1438–1441.
92. Haas, W.; Rath, T.; Pein, A.; Rattenberger, J.; Trimmel, G.; Hofer, F. The Stoichiometry of Single Nanoparticles of Copper Zinc Tin Selenide. *Chem. Commun.* **2011**, *47*, 2050–2052.
93. Pamplin, B. The Adamantine Family of Compounds. *Prog. Cryst. Growth Charact.* **1980**, *3*, 179–192.
94. Li, W.; Ibáñez, M.; Cadavid, D.; Zamani, R.; Rubio-Garcia, J.; Gorsse, S.; Morante, J.; Arbiol, J.; Cabot, A. Colloidal Synthesis and Functional Properties of Quaternary Cu-Based Semiconductors: $Cu_2HgGeSe_4$. *J. Nanopart. Res.* **2014**, *16*, 1–6.
95. Li, W.; Ibáñez, M.; Zamani, R. R.; Garcia-Castello, N.; Gorsse, S.; Cadavid, D.; Prades, J. D.; Arbiol, J.; Cabot, A. $Cu_2HgSnSe_4$ Nanoparticles: Synthesis and Thermoelectric Properties. *CrystEngComm* **2013**, *15*, 8966–8971.
96. Goodman, C. H. L. The Prediction of Semiconducting Properties in Inorganic Compounds. *J. Phys. Chem. Solids* **1958**, *6*, 305–314.
97. Pamplin, B. R. A Systematic Method of Deriving New Semiconducting Compounds by Structural Analogy. *J. Phys. Chem. Solids* **1964**, *25*, 675–684.
98. Batabyal, S. K.; Tian, L.; Venkatram, N.; Ji, W.; Vittal, J. J. Phase-Selective Synthesis of $CuInS_2$ Nanocrystals. *J. Phys. Chem. C* **2009**, *113*, 15037–15042.
99. Regulacio, M. D.; Ye, C.; Lim, S. H.; Bosman, M.; Ye, E.; Chen, S.; Xu, Q.-H.; Han, M.-Y. Colloidal Nanocrystals of Wurtzite-Type Cu_2ZnSnS_4: Facile Noninjection Synthesis and Formation Mechanism. *Chem.—Eur. J.* **2012**, *18*, 3127–3131.
100. Chang, J.; Waclawik, E. R. Controlled Synthesis of $CuInS_2$, $Cu2SnS_3$ and Cu_2ZnSnS_4 Nano-Structures: Insight into the Universal Phase-Selectivity Mechanism. *CrystEngComm* **2013**, *15*, 5612–5619.
101. Zou, Y.; Su, X.; Jiang, J. Phase-Controlled Synthesis of Cu_2ZnSnS_4 Nanocrystals: The Role of Reactivity between Zn and S. *J. Am. Chem. Soc.* **2013**, *135*, 18377–18384.
102. Nose, K.; Soma, Y.; Omata, T.; Otsuka-Yao-Matsuo, S. Synthesis of Ternary $CuInS_2$ Nanocrystals; Phase Determination by Complex Ligand Species. *Chem. Mater.* **2009**, *21*, 2607–2613.
103. Wang, J.-j.; Liu, P.; Seaton, C. C.; Ryan, K. M. Complete Colloidal Synthesis of Cu_2SnSe_3 Nanocrystals with Crystal Phase and Shape Control. *J. Am. Chem. Soc.* **2014**, *136*, 7954–7960.
104. Fan, F.-J.; Wu, L.; Gong, M.; Chen, S. Y.; Liu, G. Y.; Yao, H.-B.; Liang, H.-W.; Wang, Y.-X.; Yu, S.-H. Linearly Arranged Polytypic CZTSSe Nanocrystals. *Sci. Rep.* **2012**, *2*, 952.
105. Jiang, H.; Dai, P.; Feng, Z.; Fan, W.; Zhan, J. Phase Selective Synthesis of Metastable Orthorhombic Cu_2ZnSnS_4. *J. Mater. Chem.* **2012**, *22*, 7502–7506.
106. Chen, S.; Gong, X. G.; Walsh, A.; Wei, S.-H. Crystal and Electronic Band Structure of Cu_2ZnSnX_4 (X = S and Se) Photovoltaic Absorbers: First-Principles Insights. *Appl. Phys. Lett.* **2009**, *94*, 041903.
107. Schorr, S. The Crystal Structure of Kesterite Type Compounds: A Neutron and X-ray Diffraction Study. *Sol. Energy Mater. Sol. Cells* **2011**, *95*, 1482–1488.
108. Li, T.-L.; Teng, H. Solution Synthesis of High-Quality $CuInS_2$ Quantum Dots as Sensitizers for TiO_2 Photoelectrodes. *J. Mater. Chem.* **2010**, *20*, 3656–3664.
109. Pan, D.; Wang, X.; Zhou, Z. H.; Chen, W.; Xu, C.; Lu, Y. Synthesis of Quaternary Semiconductor Nanocrystals with Tunable Band Gaps. *Chem. Mater.* **2009**, *21*, 2489–2493.
110. Yu, X.; An, X.; Shavel, A.; Ibáñez, M.; Cabot, A. The Effect of the Ga Content on the Photocatalytic Hydrogen Evolution of $CuIn_{1-x}Ga_xS_2$ Nanocrystals. *J. Mater. Chem. A* **2014**, *2*, 12317–12322.
111. Singh, A.; Singh, S.; Levcenko, S.; Unold, T.; Laffir, F.; Ryan, K. M. Compositionally Tunable Photoluminescence Emission in $Cu_2ZnSn(S_{1-x}Se_x)_4$ Nanocrystals. *Angew. Chem., Int. Ed.* **2013**, *52*, 9120–9124.
112. Wei, H.; Ye, Z.; Li, M.; Su, Y.; Yang, Z.; Zhang, Y. Tunable Band Gap $Cu_2ZnSnS_{4x}Se_{4(1-x)}$ Nanocrystals: Experimental and First-Principles Calculations. *CrystEngComm* **2011**, *13*, 2222–2226.
113. Riha, S. C.; Parkinson, B. A.; Prieto, A. L. Compositionally Tunable $Cu_2ZnSn(S_{(1-x)}Se_{(x)})_4$ Nanocrystals: Probing the Effect of Se-Inclusion in Mixed Chalcogenide Thin Films. *J. Am. Chem. Soc.* **2011**, *133*, 15272–15275.
114. Ou, K.-L.; Fan, J.-C.; Chen, J.-K.; Huang, C.-C.; Chen, L.-Y.; Ho, J.-H.; Chang, J.-Y. Hot-Injection Synthesis of Monodispersed $Cu_2ZnSn(S_xSe_{1-x})_4$ Nanocrystals: Tunable Composition and Optical Properties. *J. Mater. Chem.* **2012**, *22*, 14667–14673.
115. Chiang, M.-Y.; Chang, S.-H.; Chen, C.-Y.; Yuan, F.-W.; Tuan, H.-Y. Quaternary $CuIn(S_{1-x}Se_x)_2$ Nanocrystals: Facile Heating-Up Synthesis, Band Gap Tuning, and Gram-Scale

Production. *J. Phys. Chem. C* **2011**, *115*, 1592–1599.
116. Ford, G. M.; Guo, Q.; Agrawal, R.; Hillhouse, H. W. Earth Abundant Element $Cu_2Zn(Sn_{1-x}Ge_x)S_4$ Nanocrystals for Tunable Band Gap Solar Cells: 6.8% Efficient Device Fabrication. *Chem. Mater.* **2011**, *23*, 2626–2629.
117. Xu, L.-C.; Wang, R.-Z.; Liu, L.-M.; Chen, Y.-P.; Wei, X.-L.; Yan, H.; Lau, W.-M. Wurtzite-Type $CuInSe_2$ for High-Performance Solar Cell Absorber: *Ab Initio* Exploration of the New Phase Structure. *J. Mater. Chem.* **2012**, *22*, 21662–21666.
118. Chen, S.; Walsh, A.; Luo, Y.; Yang, J.-H.; Gong, X. G.; Wei, S.-H. Wurtzite-Derived Polytypes of Kesterite and Stannite Quaternary Chalcogenide Semiconductors. *Phys. Rev. B* **2010**, *82*, 195203.
119. Bozyigit, D.; Wood, V. Challenges and Solutions for High-Efficiency Quantum Dot-Based LEDs. *MRS Bull.* **2013**, *38*, 731–736.
120. De Trizio, L.; Prato, M.; Genovese, A.; Casu, A.; Povia, M.; Simonutti, R.; Alcocer, M. J. P.; D'Andrea, C.; Tassone, F.; Manna, L. Strongly Fluorescent Quaternary Cu—In—Zn—S Nanocrystals Prepared from $Cu_{1-x}InS_2$ Nanocrystals by Partial Cation Exchange. *Chem. Mater.* **2012**, *24*, 2400–2406.
121. Li, L.; Daou, T. J.; Texier, I.; Kim Chi, T. T.; Liem, N. Q.; Reiss, P. Highly Luminescent $CuInS_2$/ZnS Core/Shell Nanocrystals: Cadmium-Free Quantum Dots for *In Vivo* Imaging. *Chem. Mater.* **2009**, *21*, 2422–2429.
122. Lin, Y.; Zhang, F.; Pan, D.; Li, H.; Lu, Y. Sunlight-Driven Photodegradation of Organic Pollutants Catalyzed by $TiO_2/(ZnS)_x(CuInS_2)_{1-x}$ Nanocomposites. *J. Mater. Chem.* **2012**, *22*, 8759–8763.
123. Kang, S.-Z.; Yang, Y.-K.; Bu, W.; Mu, J. TiO_2 Nanoparticles Incorporated with $CuInS_2$ Clusters: Preparation and Photocatalytic Activity for Degradation of 4-Nitrophenol. *J. Solid State Chem.* **2009**, *182*, 2972–2976.
124. Liu, R.; Liu, Y.; Liu, C.; Luo, S.; Teng, Y.; Yang, L.; Yang, R.; Cai, Q. Enhanced Photoelectrocatalytic Degradation of 2,4-Dichlorophenoxyacetic Acid by $CuInS_2$ Nanoparticles Deposition onto TiO_2 Nanotube Arrays. *J. Alloys Compd.* **2011**, *509*, 2434–2440.
125. Shen, F.; Que, W.; He, Y.; Yuan, Y.; Yin, X.; Wang, G. Enhanced Photocatalytic Activity of ZnO Microspheres *via* Hybridization with $CuInSe_2$ and $CuInS_2$ Nanocrystals. *ACS Appl. Mater. Interfaces* **2012**, *4*, 4087–4092.
126. Shen, F.; Que, W.; Liao, Y.; Yin, X. Photocatalytic Activity of TiO_2 Nanoparticles Sensitized by $CuInS_2$ Quantum Dots. *Ind. Eng. Chem. Res.* **2011**, *50*, 9131–9137.
127. Akhavan, V. A.; Panthani, M. G.; Goodfellow, B. W.; Reid, D. K.; Korgel, B. A. Thickness-Limited Performance of $CuInSe_2$ Nanocrystal Photovoltaic Devices. *Opt. Express* **2010**, *18*, A411–A420.
128. Stolle, C. J.; Harvey, T. B.; Korgel, B. A. Nanocrystal Photovoltaics: A Review of Recent Progress. *Curr. Opin. Chem. Eng.* **2013**, *2*, 160–167.
129. Comin, A.; Manna, L. New Materials for Tunable Plasmonic Colloidal Nanocrystals. *Chem. Soc. Rev.* **2014**, *43*, 3957–3975.
130. Liu, X.; Swihart, M. T. Heavily-Doped Colloidal Semiconductor and Metal Oxide Nanocrystals: An Emerging New Class of Plasmonic Nanomaterials. *Chem. Soc. Rev.* **2014**, *43*, 3908–3920.
131. Faucheaux, J. A.; Stanton, A. L. D.; Jain, P. K. Plasmon Resonances of Semiconductor Nanocrystals: Physical Principles and New Opportunities. *J. Phys. Chem. Lett.* **2014**, *5*, 976–985.
132. Lounis, S. D.; Runnerstrom, E. L.; Bergerud, A.; Nordlund, D.; Milliron, D. J. Influence of Dopant Distribution on the Plasmonic Properties of Indium Tin Oxide Nanocrystals. *J. Am. Chem. Soc.* **2014**, *136*, 7110–7116.
133. Zhao, Y.; Pan, H.; Lou, Y.; Qiu, X.; Zhu, J.; Burda, C. Plasmonic $Cu_{2-x}S$ Nanocrystals: Optical and Structural Properties of Copper-Deficient Copper(I) Sulfides. *J. Am. Chem. Soc.* **2009**, *131*, 4253–4261.
134. Hessel, C. M.; Pattani, V.; Rasch, M.; Panthani, M. G.; Koo, B.; Tunnell, J. W.; Korgel, B. A. Copper Selenide Nanocrystals for Photothermal Therapy. *Nano Lett.* **2011**, *11*, 2560–2566.
135. Dorfs, D.; Härtling, T.; Miszta, K.; Bigall, N. C.; Kim, M. R.; Genovese, A.; Falqui, A.; Povia, M.; Manna, L. Reversible Tunability of the Near-Infrared Valence Band Plasmon Resonance in $Cu_{2-x}Se$ Nanocrystals. *J. Am. Chem. Soc.* **2011**, *133*, 11175–11180.
136. Hsu, S.-W.; Bryks, W.; Tao, A. R. Effects of Carrier Density and Shape on the Localized Surface Plasmon Resonances of $Cu_{2-x}S$ Nanodisks. *Chem. Mater.* **2012**, *24*, 3765–3771.
137. Luther, J. M.; Jain, P. K.; Ewers, T.; Alivisatos, A. P. Localized Surface Plasmon Resonances Arising from Free Carriers in Doped Quantum Dots. *Nat. Mater.* **2011**, *10*, 361–366.
138. Kriegel, I.; Jiang, C.; Rodríguez-Fernández, J.; Schaller, R. D.; Talapin, D. V.; da Como, E.; Feldmann, J. Tuning the Excitonic and Plasmonic Properties of Copper Chalcogenide Nanocrystals. *J. Am. Chem. Soc.* **2011**, *134*, 1583–1590.
139. Palomaki, P. K. B.; Miller, E. M.; Neale, N. R. Control of Plasmonic and Interband Transitions in Colloidal Indium Nitride Nanocrystals. *J. Am. Chem. Soc.* **2013**, *135*, 14142–14150.
140. Song, G.; Shen, J.; Jiang, F.; Hu, R.; Li, W.; An, L.; Zou, R.; Chen, Z.; Qin, Z.; Hu, J. Hydrophilic Molybdenum Oxide Nanomaterials with Controlled Morphology and Strong Plasmonic Absorption for Photothermal Ablation of Cancer Cells. *ACS Appl. Mater. Interfaces* **2014**, *6*, 3915–3922.
141. Jain, P. K.; Manthiram, K.; Engel, J. H.; White, S. L.; Faucheaux, J. A.; Alivisatos, A. P. Doped Nanocrystals as Plasmonic Probes of Redox Chemistry. *Angew. Chem., Int. Ed.* **2013**, *52*, 13671–13675.
142. Guo, M.; Law, W.-C.; Liu, X.; Cai, H.; Liu, L.; Swihart, M.; Zhang, X.; Prasad, P. Plasmonic Semiconductor Nanocrystals as Chemical Sensors: Pb^{2+} Quantitation *via* Aggregation-Induced Plasmon Resonance Shift. *Plasmonics* **2014**, 1–6.
143. Lou, Z.; Wang, Z.; Huang, B.; Dai, Y. Synthesis and Activity of Plasmonic Photocatalysts. *ChemCatChem* **2014**, *6*, 2456–2476.
144. Liu, X.; Law, W.-C.; Jeon, M.; Wang, X.; Liu, M.; Kim, C.; Prasad, P. N.; Swihart, M. T. $Cu_{2-x}Se$ Nanocrystals with Localized Surface Plasmon Resonance as Sensitive Contrast Agents for *In Vivo* Photoacoustic Imaging: Demonstration of Sentinel Lymph Node Mapping. *Adv. Healthcare Mater.* **2013**, *2*, 952–957.
145. Liu, X.; Lee, C.; Law, W.-C.; Zhu, D.; Liu, M.; Jeon, M.; Kim, J.; Prasad, P. N.; Kim, C.; Swihart, M. T. Au—$Cu_{2-x}Se$ Heterodimer Nanoparticles with Broad Localized Surface Plasmon Resonance as Contrast Agents for Deep Tissue Imaging. *Nano Lett.* **2013**, *13*, 4333–4339.
146. Llordes, A.; Garcia, G.; Gazquez, J.; Milliron, D. J. Tunable Near-Infrared and Visible-Light Transmittance in Nanocrystal-in-Glass Composites. *Nature* **2013**, *500*, 323–326.
147. Runnerstrom, E. L.; Llordes, A.; Lounis, S. D.; Milliron, D. J. Nanostructured Electrochromic Smart Windows: Traditional Materials and NIR-Selective Plasmonic Nanocrystals. *Chem. Commun.* **2014**, *50*, 10555–10572.
148. Bekenstein, Y.; Vinokurov, K.; Keren-Zur, S.; Hadar, I.; Schilt, Y.; Raviv, U.; Millo, O.; Banin, U. Thermal Doping by Vacancy Formation in Copper Sulfide Nanocrystal Arrays. *Nano Lett.* **2014**, *14*, 1349–1353.
149. Xiao, M.; Jiang, R.; Wang, F.; Fang, C.; Wang, J.; Yu, J. C. Plasmon-Enhanced Chemical Reactions. *J. Mater. Chem. A* **2013**, *1*, 5790–5805.
150. Mendelsberg, R. J.; Garcia, G.; Li, H.; Manna, L.; Milliron, D. J. Understanding the Plasmon Resonance in Ensembles of Degenerately Doped Semiconductor Nanocrystals. *J. Phys. Chem. C* **2012**, *116*, 12226–12231.
151. Zhang, H.; Kulkarni, V.; Prodan, E.; Nordlander, P.; Govorov, A. O. Theory of Quantum Plasmon

Resonances in Doped Semiconductor Nanocrystals. *J. Phys. Chem. C* **2014**, *118*, 16035–16042.
152. Scotognella, F.; Della Valle, G.; Srimath Kandada, A. R.; Dorfs, D.; Zavelani-Rossi, M.; Conforti, M.; Miszta, K.; Comin, A.; Korobchevskaya, K.; Lanzani, G.; Manna, L.; Tassone, F. Plasmon Dynamics in Colloidal $Cu_{2-x}Se$ Nanocrystals. *Nano Lett.* **2011**, *11*, 4711–4717.
153. Ye, X.; Fei, J.; Diroll, B. T.; Paik, T.; Murray, C. B. Expanding the Spectral Tunability of Plasmonic Resonances in Doped Metal-Oxide Nanocrystals through Cooperative Cation–Anion Codoping. *J. Am. Chem. Soc.* **2014**, *136*, 11680–11686.
154. Schimpf, A. M.; Thakkar, N.; Gunthardt, C. E.; Masiello, D. J.; Gamelin, D. R. Charge-Tunable Quantum Plasmons in Colloidal Semiconductor Nanocrystals. *ACS Nano* **2013**, *8*, 1065–1072.
155. Kriegel, I.; Rodríguez-Fernández, J.; Wisnet, A.; Zhang, H.; Waurisch, C.; Eychmüller, A.; Dubavik, A.; Govorov, A. O.; Feldmann, J. Shedding Light on Vacancy-Doped Copper Chalcogenides: Shape-Controlled Synthesis, Optical Properties, and Modeling of Copper Telluride Nanocrystals with Near-Infrared Plasmon Resonances. *ACS Nano* **2013**, *7*, 4367–4377.
156. Li, R.; Hu, W.; Liu, Y.; Zhu, D. Micro- and Nanocrystals of Organic Semiconductors. *Acc. Chem. Res.* **2010**, *43*, 529–540.
157. Kang, L.; Wang, Z.; Cao, Z.; Ma, Y.; Fu, H.; Yao, J. Colloid Chemical Reaction Route to the Preparation of Nearly Monodispersed Perylene Nanoparticles: Size-Tunable Synthesis and Three-Dimensional Self-Organization. *J. Am. Chem. Soc.* **2007**, *129*, 7305–7312.
158. Lim, S. J.; An, B. K.; Jung, S. D.; Chung, M. A.; Park, S. Y. Photoswitchable Organic Nanoparticles and a Polymer Film Employing Multifunctional Molecules with Enhanced Fluorescence Emission and Bistable Photochromism. *Angew. Chem., Int. Ed.* **2004**, *43*, 6346–6350.
159. An, B. K.; Kwon, S. K.; Jung, S. D.; Park, S. Y. Enhanced Emission and Its Switching in Fluorescent Organic Nanoparticles. *J. Am. Chem. Soc.* **2002**, *124*, 14410–14415.
160. Hu, J. S.; Guo, Y. G.; Liang, H. P.; Wan, L. J.; Jiang, L. Three-Dimensional Self-Organization of Supramolecular Self-Assembled Porphyrin Hollow Hexagonal Nanoprisms. *J. Am. Chem. Soc.* **2005**, *127*, 17090–17095.
161. Balakrishnan, K.; Datar, A.; Naddo, T.; Huang, J. L.; Oitker, R.; Yen, M.; Zhao, J. C.; Zang, L. Effect of Side-Chain Substituents on Self-Assembly of Perylene Diimide Molecules: Morphology Control. *J. Am. Chem. Soc.* **2006**, *128*, 7390–7398.
162. Balakrishnan, K.; Datar, A.; Oitker, R.; Chen, H.; Zuo, J. M.; Zang, L. Nanobelt Self-Assembly from an Organic n-Type Semiconductor: Propoxyethyl-PTCDI. *J. Am. Chem. Soc.* **2005**, *127*, 10496–10497.
163. Datar, A.; Balakrishnan, K.; Yang, X. M.; Zuo, X. B.; Huang, J. L.; Oitker, R.; Yen, M.; Zhao, J. C.; Tiede, D. M.; Zang, L. Linearly Polarized Emission of an Organic Semiconductor Nanobelt. *J. Phys. Chem. B* **2006**, *110*, 12327–12332.
164. Fu, H.; Xiao, D.; Yao, J.; Yang, G. Nanofibers of 1,3-Diphenyl-2-pyrazoline Induced by Cetyltrimethylammonium Bromide Micelles. *Angew. Chem., Int. Ed.* **2003**, *42*, 2883–2886.
165. Tian, Z.; Chen, Y.; Yang, W.; Yao, J.; Zhu, L.; Shuai, Z. Low-Dimensional Aggregates from Stilbazolium-like Dyes. *Angew. Chem., Int. Ed.* **2004**, *43*, 4060–4063.
166. Yilong, L.; Qing, L.; Hongbing, F.; Jiannian, Y. Phase and Shape-Controlled Synthesis of Single Crystalline Perylene Nanosheets and Its Optical Properties. *J. Phys. Chem. C* **2009**, *113*, 10038–10043.
167. Fu, H. B.; Yao, J. N. Size Effects on the Optical Properties of Organic Nanoparticles. *J. Am. Chem. Soc.* **2001**, *123*, 1434–1439.
168. Kasai, H.; Kamatani, H.; Okada, S.; Oikawa, H.; Matsuda, H.; Nakanishi, H. Size-Dependent Colors and Luminescences of Organic Microcrystals. *Jpn. J. Appl. Phys. 2* **1996**, *35*, L221–L223.
169. Tachikawa, T.; Chung, H.-R.; Masuhara, A.; Kasai, H.; Oikawa, H.; Nakanishi, H.; Fujitsuka, M.; Majima, T. *In Situ* and *Ex Situ* Observations of the Growth Dynamics of Single Perylene Nanocrystals in Water. *J. Am. Chem. Soc.* **2006**, *128*, 15944–15945.
170. Oikawa, H.; Mitsui, T.; Onodera, T.; Kasai, H.; Nakanishi, H.; Sekiguchi, T. Crystal Size Dependence of Fluorescence Spectra from Perylene Nanocrystals Evaluated by Scanning Near-Field Optical Microspectroscopy. *Jpn. J. Appl. Phys. 2* **2003**, *42*, L111–L113.
171. Nakanishi, H.; Katagi, H. Microcrystals of Polydiacetylene Derivatives and Their Linear and Nonlinear Optical Properties. *Supramol. Sci.* **1998**, *5*, 289–295.
172. Matsune, H.; Asahi, T.; Masuhara, H.; Kasai, H.; Nakanishi, H. Size-Effect on Fluorescence Spectrum of Perylene Nanocrystal Studied by Single-Particle Microspectroscopy Coupled with Atomic Force Microscope Observation. In *Organic and Nanocomposite Optical Materials*; Cartwright, A., Cooper, T. M., Karna, S. P., Nakanishi, H., Eds.; Materials Research Society: Warrendale, PA, 2005; Vol. 846, pp 263–268.
173. Kasai, H.; Oikawa, H.; Okada, S.; Nakanishi, H. Crystal Growth of Perylene Microcrystals in the Reprecipitation Method. *Bull. Chem. Soc. Jpn.* **1998**, *71*, 2597–2601.
174. Sytnyk, M.; Głowacki, E. D.; Yakunin, S.; Voss, G.; Schöfberger, W.; Kriegner, D.; Stangl, J.; Trotta, R.; Gollner, C.; Tollabimazraehno, S.; Romanazzi, G.; Bozkurt, Z.; Havlicek, M.; Sariciftci, N. S.; Heiss, W. Hydrogen-Bonded Organic Semiconductor Micro- and Nanocrystals: From Colloidal Syntheses to (Opto-)Electronic Devices. *J. Am. Chem. Soc.* **2014**, *136*, 16522–16532.
175. Herbst, W.; Hunger, K. *Industrial Organic Pigments: Production, Properties, Applications*, 3rd ed.; Wiley: New York, 2004; pp 1–179.
176. Xia, Y.; Xiong, Y.; Lim, B.; Skrabalak, S. E. Shape-Controlled Synthesis of Metal Nanocrystals: Simple Chemistry Meets Complex Physics? *Angew. Chem., Int. Ed.* **2009**, *48*, 60–103.
177. de Jonge, N.; Ross, F. M. Electron Microscopy of Specimens in Liquid. *Nat. Nanotechnol.* **2011**, *6*, 695–704.
178. Yuk, J. M.; Park, J.; Ercius, P.; Kim, K.; Hellebusch, D. J.; Crommie, M. F.; Lee, J. Y.; Zettl, A.; Alivisatos, A. P. High-Resolution EM of Colloidal Nanocrystal Growth Using Graphene Liquid Cells. *Science* **2012**, *336*, 61–64.
179. Woehl, T. J.; Evans, J. E.; Arslan, I.; Ristenpart, W. D.; Browning, N. D. Direct *In Situ* Determination of the Mechanisms Controlling Nanoparticle Nucleation and Growth. *ACS Nano* **2012**, *6*, 8599–8610.
180. Peng, X. G.; Wickham, J.; Alivisatos, A. P. Kinetics of II–VI and III–V Colloidal Semiconductor Nanocrystal Growth: "Focusing" of Size Distributions. *J. Am. Chem. Soc.* **1998**, *120*, 5343–5344.
181. Qu, L.; Yu, W. W.; Peng, X. *In Situ* Observation of the Nucleation and Growth of CdSe Nanocrystals. *Nano Lett.* **2004**, *4*, 465–469.
182. Bullen, C. R.; Mulvaney, P. Nucleation and Growth Kinetics of CdSe Nanocrystals in Octadecene. *Nano Lett.* **2004**, *4*, 2303–2307.
183. Kudera, S.; Zanella, M.; Giannini, C.; Rizzo, A.; Li, Y.; Gigli, G.; Cingolani, R.; Ciccarella, G.; Spahl, W.; Parak, W. J.; Manna, L. Sequential Growth of Magic-Size CdSe Nanocrystals. *Adv. Mater.* **2007**, *19*, 548–552.
184. Owen, J. S.; Chan, E. M.; Liu, H.; Alivisatos, A. P. Precursor Conversion Kinetics and the Nucleation of Cadmium Selenide Nanocrystals. *J. Am. Chem. Soc.* **2010**, *132*, 18206–18213.
185. Yu, K.; Liu, X.; Zeng, Q.; Yang, M.; Ouyang, J.; Wang, X.; Tao, Y. The Formation Mechanism of Binary Semiconductor Nanomaterials: Shared by Single-Source and Dual-Source Precursor Approaches. *Angew. Chem., Int. Ed.* **2013**, *52*, 11034–11039.

186. Yu, K. CdSe Magic-Sized Nuclei, Magic-Sized Nanoclusters and Regular Nanocrystals: Monomer Effects on Nucleation and Growth. *Adv. Mater.* **2012**, *24*, 1123–1132.
187. Yu, K.; Liu, X.; Zeng, Q.; Leek, D. M.; Ouyang, J.; Whitmore, K. M.; Ripmeester, J. A.; Tao, Y.; Yang, M. Effect of Tertiary and Secondary Phosphines on Low-Temperature Formation of Quantum Dots. *Angew. Chem., Int. Ed.* **2013**, *52*, 4823–4828.
188. Yu, K.; Liu, X.; Chen, Q. Y.; Yang, H.; Yang, M.; Wang, X.; Wang, X.; Cao, H.; Whitfield, D. M.; Hu, C.; Tao, Y. Mechanistic Study of the Role of Primary Amines in Precursor Conversions to Semiconductor Nanocrystals at Low Temperature. *Angew. Chem., Int. Ed.* **2014**, *53*, 6898–6904.
189. Abecassis, B.; Testard, F.; Spalla, O.; Barboux, P. Probing *in Situ* the Nucleation and Growth of Gold Nanoparticles by Small-Angle X-ray Scattering. *Nano Lett.* **2007**, *7*, 1723–1727.
190. Yao, T.; Sun, Z.; Li, Y.; Pan, Z.; Wei, H.; Xie, Y.; Nomura, M.; Niwa, Y.; Yan, W.; Wu, Z. J.; *et al.* Insights into Initial Kinetic Nucleation of Gold Nanocrystals. *J. Am. Chem. Soc.* **2010**, *132*, 7696–7701.
191. Uehara, M.; Sun, Z. H.; Oyanagi, H.; Yamashita, K.; Fukano, A.; Nakamura, H.; Maeda, H. *In Situ* Extended X-ray Absorption Fine Structure Study of Initial Processes in CdSe Nanocrystals Formation Using a Microreactor. *Appl. Phys. Lett.* **2009**, *94*, 063104.
192. *Reiss et al.*, manuscript in preparation, results presented and discussed at NaNaX 6 conference.
193. Zhou, H.; Hsu, W.-C.; Duan, H.-S.; Bob, B.; Yang, W.; Song, T.-B.; Hsu, C.-J.; Yang, Y. CZTS Nanocrystals: A Promising Approach for Next Generation Thin Film Photovoltaics. *Energy Environ. Sci.* **2013**, *6*, 2822–2838.
194. van Huis, M. A.; Young, N. P.; Pandraud, G.; Creemer, J. F.; Vanmaekelbergh, D.; Kirkland, A. I.; Zandbergen, H. W. Atomic Imaging of Phase Transitions and Morphology Transformations in Nanocrystals. *Adv. Mater.* **2009**, *21*, 4992–4995.
195. Figuerola, A.; Huis, M. v.; Zanella, M.; Genovese, A.; Marras, S.; Falqui, A.; Zandbergen, H. W.; Cingolani, R.; Manna, L. Epitaxial CdSe-Au Nanocrystal Heterostructures by Thermal Annealing. *Nano Lett.* **2010**, *10*, 3028–3036.
196. van Huis, M. A.; Figuerola, A.; Fang, C.; Béché, A.; Zandbergen, H. W.; Manna, L. Chemical Transformation of Au-Tipped CdS Nanorods into AuS/Cd Core/Shell Particles by Electron Beam Irradiation. *Nano Lett.* **2011**, *11*, 4555–4561.
197. De Trizio, L.; De Donato, F.; Casu, A.; Genovese, A.; Falqui, A.; Povia, M.; Manna, L. Colloidal CdSe/Cu_3P/CdSe Nanocrystal Heterostructures and Their Evolution upon Thermal Annealing. *ACS Nano* **2013**, *7*, 3997–4005.
198. Zheng, H. M.; Rivest, J. B.; Miller, T. A.; Sadtler, B.; Lindenberg, A.; Toney, M. F.; Wang, L. W.; Kisielowski, C.; Alivisatos, A. P. Observation of Transient Structural-Transformation Dynamics in a Cu_2S Nanorod. *Science* **2011**, *333*, 206–209.
199. Yalcin, A. O.; Fan, Z.; Goris, B.; Li, W.-F.; Koster, R. S.; Fang, C.-M.; van Blaaderen, A.; Casavola, M.; Tichelaar, F. D.; Bals, S.; *et al.* Atomic Resolution Monitoring of Cation Exchange in CdSe−PbSe Heteronanocrystals during Epitaxial Solid−Solid−Vapor Growth. *Nano Lett.* **2014**, *14*, 3661–3667.
200. Voznyy, O.; Sargent, E. H. Atomistic Model of Fluorescence Intermittency of Colloidal Quantum Dots. *Phys. Rev. Lett.* **2014**, *112*, 157401.
201. Voznyy, O.; Thon, S. M.; Ip, A. H.; Sargent, E. H. Dynamic Trap Formation and Elimination in Colloidal Quantum Dots. *J. Phys. Chem. Lett.* **2013**, *4*, 987–992.
202. Hens, Z.; Martins, J. C. A Solution NMR Toolbox for Characterizing the Surface Chemistry of Colloidal Nanocrystals. *Chem. Mater.* **2013**, *25*, 1211–1221.
203. Jasieniak, J.; Bullen, C.; van Embden, J.; Mulvaney, P. Phosphine-Free Synthesis of CdSe Nanocrystals. *J. Phys. Chem. B* **2005**, *109*, 20665–20668.
204. Fritzinger, B.; Capek, R. K.; Lambert, K.; Martins, J. C.; Hens, Z. Utilizing Self-Exchange To Address the Binding of Carboxylic Acid Ligands to CdSe Quantum Dots. *J. Am. Chem. Soc.* **2010**, *132*, 10195–10201.
205. Anderson, N. C.; Owen, J. S. Soluble, Chloride-Terminated CdSe Nanocrystals: Ligand Exchange Monitored by H-1 and P-31 NMR Spectroscopy. *Chem. Mater.* **2013**, *25*, 69–76.
206. Owen, J. S.; Park, J.; Trudeau, P. E.; Alivisatos, A. P. Reaction Chemistry and Ligand Exchange at Cadmium-Selenide Nanocrystal Surfaces. *J. Am. Chem. Soc.* **2008**, *130*, 12279–12281.
207. Cros-Gagneux, A.; Delpech, F.; Nayral, C.; Cornejo, A.; Coppel, Y.; Chaudret, B. Surface Chemistry of InP Quantum Dots: A Comprehensive Study. *J. Am. Chem. Soc.* **2010**, *132*, 18147–18157.
208. Hassinen, A.; Gomes, R.; De Nolf, K.; Zhao, Q.; Vantomme, A.; Martins, J. C.; Hens, Z. Surface Chemistry of CdTe Quantum Dots Synthesized in Mixtures of Phosphonic Acids and Amines: Formation of a Mixed Ligand Shell. *J. Phys. Chem. C* **2013**, *117*, 13936–13943.
209. Moreels, I.; Justo, Y.; De Geyter, B.; Haustraete, K.; Martins, J. C.; Hens, Z. Size-Tunable, Bright, and Stable PbS Quantum Dots: A Surface Chemistry Study. *ACS Nano* **2011**, *5*, 2004–2012.
210. Gomes, R.; Hassinen, A.; Szczygiel, A.; Zhao, Q. A.; Vantomme, A.; Martins, J. C.; Hens, Z. Binding of Phosphonic Acids to CdSe Quantum Dots: A Solution NMR Study. *J. Phys. Chem. Lett.* **2011**, *2*, 145–152.
211. Moreels, I.; Fritzinger, B.; Martins, J. C.; Hens, Z. Surface Chemistry of Colloidal PbSe Nanocrystals. *J. Am. Chem. Soc.* **2008**, *130*, 15081–15086.
212. Morris-Cohen, A. J.; Frederick, M. T.; Lilly, G. D.; McArthur, E. A.; Weiss, E. A. Organic Surfactant-Controlled Composition of the Surfaces of CdSe Quantum Dots. *J. Phys. Chem. Lett.* **2010**, *1*, 1078–1081.
213. Hassinen, A.; Moreels, I.; Donega, C. D.; Martins, J. C.; Hens, Z. Nuclear Magnetic Resonance Spectroscopy Demonstrating Dynamic Stabilization of CdSe Quantum Dots by Alkylamines. *J. Phys. Chem. Lett.* **2010**, *1*, 2577–2581.
214. Fritzinger, B.; Moreels, I.; Koole, R.; Lommens, P.; Hens, Z.; Martins, J. C. *In Situ* Observation of Rapid Ligand Exchange in Colloidal Nanocrystal Suspensions Using Transfer NOE Nuclear Magnetic Resonance Spectroscopy. *J. Am. Chem. Soc.* **2009**, *131*, 3024–3032.
215. Morris-Cohen, A. J.; Donakowski, M. D.; Knowles, K. E.; Weiss, E. A. The Effect of a Common Purification Procedure on the Chemical Composition of the Surfaces of CdSe Quantum Dots Synthesized with Trioctylphosphine Oxide. *J. Phys. Chem. C* **2010**, *114*, 897–906.
216. De Roo, J.; Van den Broeck, F.; De Keukeleere, K.; Martins, J. C.; Van Driessche, I.; Hens, Z. Unravelling the Surface Chemistry of Metal Oxide Nanocrystals, the Role of Acids and Bases. *J. Am. Chem. Soc.* **2014**, *136*, 9650–9657.
217. Anderson, N. C.; Hendricks, M. P.; Choi, J. J.; Owen, J. S. Ligand Exchange and the Stoichiometry of Metal Chalcogenide Nanocrystals: Spectroscopic Observation of Facile Metal-Carboxylate Displacement and Binding. *J. Am. Chem. Soc.* **2013**, *135*, 18536–18548.
218. Gao, Y. N.; Aerts, M.; Sandeep, C. S. S.; Talgorn, E.; Savenije, T. J.; Kinge, S.; Siebbeles, L. D. A.; Houtepen, A. J. Photoconductivity of PbSe Quantum-Dot Solids: Dependence on Ligand Anchor Group and Length. *ACS Nano* **2012**, *6*, 9606–9614.
219. Wang, F. D.; Tang, R.; Buhro, W. E. The Trouble with TOPO; Identification of Adventitious Impurities Beneficial to the Growth of Cadmium Selenide Quantum Dots, Rods, and

Wires. *Nano Lett.* **2008**, *8*, 3521–3524.
220. Kopping, J. T.; Patten, T. E. Identification of Acidic Phosphorus-Containing Ligands Involved in the Surface Chemistry of CdSe Nanoparticles Prepared in Tri-*N*-octylphosphine Oxide Solvents. *J. Am. Chem. Soc.* **2008**, *130*, 5689–5698.
221. Hassinen, A.; Moreels, I.; De Nolf, K.; Smet, P. F.; Martins, J. C.; Hens, Z. Short-Chain Alcohols Strip X-Type Ligands and Quench the Luminescence of PbSe and CdSe Quantum Dots, Acetonitrile Does Not. *J. Am. Chem. Soc.* **2012**, *134*, 20705–20712.
222. Hartmann, L.; Kumar, A.; Welker, M.; Fiore, A.; Julien-Rabant, C.; Gromova, M.; Bardet, M.; Reiss, P.; Baxter, P. N.; Chandezon, F. Quenching Dynamics in CdSe Nanoparticles: Surface-Induced Defects upon Dilution. *ACS Nano* **2012**, *6*, 9033–9041.
223. Brust, M.; Walker, M.; Bethell, D.; Schiffrin, D. J.; Whyman, R. J. Synthesis of Thiol-Derivatised Gold Nanoparticles in a Two-Phase Liquid-Liquid System. *Chem. Commun.* **1994**, *7*, 801–802.
224. Nag, A.; Kovalenko, M. V.; Lee, J.-S.; Liu, W.; Spokoyny, B.; Talapin, D. V. Metal-Free Inorganic Ligands for Colloidal Nanocrystals: S^{2-}, HS^{-}, Se^{2-}, HSe^{-}, Te^{2-}, HTe^{-}, TeS_3^{2-}, OH^{-}, and NH_2^{-} as Surface Ligands. *J. Am. Chem. Soc.* **2011**, *133*, 10612–10620.
225. Norman, Z. M.; Anderson, N. C.; Owen, J. S. Electrical Transport and Grain Growth in Solution-Cast, Chloride-Terminated Cadmium Selenide Nanocrystal Thin Films. *ACS Nano* **2014**, *8*, 7513–7521.
226. Zhang, H.; Jang, J.; Liu, W.; Talapin, D. V. Colloidal Nanocrystals with Inorganic Halide, Pseudohalide, and Halometallate Ligands. *ACS Nano* **2014**, 7359–7369.
227. Fafarman, A. T.; Koh, W. K.; Diroll, B. T.; Kim, D. K.; Ko, D. K.; Oh, S. J.; Ye, X. C.; Doan-Nguyen, V.; Crump, M. R.; Reifsnyder, D. C.; *et al.* Thiocyanate-Capped Nanocrystal Colloids: Vibrational Reporter of Surface Chemistry and Solution-Based Route to Enhanced Coupling in Nanocrystal Solids. *J. Am. Chem. Soc.* **2011**, *133*, 15753–15761.
228. Kovalenko, M. V.; Scheele, M.; Talapin, D. V. Colloidal Nanocrystals with Molecular Metal Chalcogenide Surface Ligands. *Science* **2009**, *324*, 1417–1420.
229. Tangirala, R.; Baker, J. L.; Alivisatos, A. P.; Milliron, D. J. Modular Inorganic Nanocomposites by Conversion of Nanocrystal Superlattices. *Angew. Chem., Int. Ed.* **2010**, *49*, 2878–2882.
230. Dirin, D. N.; Dreyfuss, S.; Bodnarchuk, M. I.; Nedelcu, G.; Papagiorgis, P.; Itskos, G.; Kovalenko, M. V. Lead Halide Perovskites and Other Metal Halide Complexes as Inorganic Capping Ligands for Colloidal Nanocrystals. *J. Am. Chem. Soc.* **2014**, *136*, 6550–6553.
231. Wang, Y.; Neyman, A.; Arkhangelsky, E.; Gitis, V.; Meshi, L.; Weinstock, I. A. Self-Assembly and Structure of Directly Imaged Inorganic-Anion Monolayers on a Gold Nanoparticle. *J. Am. Chem. Soc.* **2009**, *131*, 17412–17422.
232. Keita, B.; Liu, T.; Nadjo, L. Synthesis of Remarkably Stabilized Metal Nanostructures Using Polyoxometalates. *J. Mater. Chem.* **2009**, *19*, 19–33.
233. Llordes, A.; Hammack, A. T.; Buonsanti, R.; Tangirala, R.; Aloni, S.; Helms, B. A.; Milliron, D. J. Polyoxometalates and Colloidal Nanocrystals as Building Blocks for Metal Oxide Nanocomposite Films. *J. Mater. Chem.* **2011**, *21*, 11631–11638.
234. Huang, J.; Liu, W.; Dolzhnikov, D. S.; Protesescu, L.; Kovalenko, M. V.; Koo, B.; Chattopadhyay, S.; Shenchenko, E. V.; Talapin, D. V. Surface Functionalization of Semiconductor and Oxide Nanocrystals with Small Inorganic Oxoanions (PO_4^{3-}, MoO_4^{2-}) and Polyoxometalate Ligands. *ACS Nano* **2014**, *8*, 9388–9402.
235. Llordes, A.; Garcia, G.; Gazquez, J.; Milliron, D. J. Tunable Near-Infrared and Visible-Light Transmittance in Nanocrystal-in-Glass Composites. *Nature* **2013**, *500*, 323–326.
236. Dong, A.; Ye, X.; Chen, J.; Kang, Y.; Gordon, T.; Kikkawa, J. M.; Murray, C. B. A Generalized Ligand-Exchange Strategy Enabling Sequential Surface Functionalization of Colloidal Nanocrystals. *J. Am. Chem. Soc.* **2010**, *133*, 998–1006.
237. Rosen, E. L.; Buonsanti, R.; Llordes, A.; Sawvel, A. M.; Milliron, D. J.; Helms, B. A. Exceptionally Mild Reactive Stripping of Native Ligands from Nanocrystal Surfaces By Using Meerwein's Salt. *Angew. Chem., Int. Ed.* **2012**, *51*, 684–689.
238. Lee, J. S.; Kovalenko, M. V.; Huang, J.; Chung, D. S.; Talapin, D. V. Band-like Transport, High Electron Mobility and High Photoconductivity in All-Inorganic Nanocrystal Arrays. *Nat. Nanotechnol.* **2011**, *6*, 348–352.
239. Liu, Y.; Tolentino, J.; Gibbs, M.; Ihly, R.; Perkins, C. L.; Liu, Y.; Crawford, N.; Hemminger, J. C.; Law, M. PbSe Quantum Dot Field-Effect Transistors with Air-Stable Electron Mobilities above 7 cm^2/Vs. *Nano Lett.* **2013**, *13*, 1578–1587.
240. Choi, J.-H.; Fafarman, A. T.; Oh, S. J.; Ko, D.-K.; Kim, D. K.; Diroll, B. T.; Muramoto, S.; Gillen, J. G.; Murray, C. B.; Kagan, C. R. Bandlike Transport in Strongly Coupled and Doped Quantum Dot Solids: A Route to High-Performance Thin-Film Electronics. *Nano Lett.* **2012**, *12*, 2631–2638.
241. Ip, A. H.; Thon, S. M.; Hoogland, S.; Voznyy, O.; Zhitomirsky, D.; Debnath, R.; Levina, L.; Rollny, L. R.; Carey, G. H.; Fischer, A.; *et al.* Hybrid Passivated Colloidal Quantum Dot Solids. *Nat. Nanotechnol.* **2012**, *7*, 577–582.
242. Ning, Z.; Voznyy, O.; Pan, J.; Hoogland, S.; Adinolfi, V.; Xu, J.; Li, M.; Kirmani, A. R.; Sun, J.-P.; Minor, J.; *et al.* Air-Stable n-Type Colloidal Quantum Dot Solids. *Nat. Mater.* **2014**, *13*, 822–828.
243. Wang, R. Y.; Tangirala, R.; Raoux, S.; Jordan-Sweet, J. L.; Milliron, D. J. Ionic and Electronic Transport in Ag_2S Nanocrystal–GeS_2 Matrix Composites with Size-Controlled Ag_2S Nanocrystals. *Adv. Mater.* **2012**, *24*, 99–103.
244. Kovalenko, M. V.; Schaller, R. D.; Jarzab, D.; Loi, M. A.; Talapin, D. V. Inorganically Functionalized PbS–CdS Colloidal Nanocrystals: Integration into Amorphous Chalcogenide Glass and Luminescent Properties. *J. Am. Chem. Soc.* **2012**, *134*, 2457–2460.
245. Jiang, C.; Lee, J.-S.; Talapin, D. V. Soluble Precursors for $CuInSe_2$, $CuIn_{1-x}Ga_xSe_2$, and $Cu_2ZnSn(S,Se)_4$ Based on Colloidal Nanocrystals and Molecular Metal Chalcogenide Surface Ligands. *J. Am. Chem. Soc.* **2012**, *134*, 5010–5013.
246. Damasceno, P. F.; Engel, M.; Glotzer, S. C. Predictive Self-Assembly of Polyhedra into Complex Structures. *Science* **2012**, *337*, 453–457.
247. de Graaf, J.; Manna, L. A Roadmap for the Assembly of Polyhedral Particles. *Science* **2012**, *337*, 417–418.
248. Deka, S.; Miszta, K.; Dorfs, D.; Genovese, A.; Bertoni, G.; Manna, L. Octapod-Shaped Colloidal Nanocrystals of Cadmium Chalcogenides *via* "One-Pot" Cation Exchange and Seeded Growth. *Nano Lett.* **2010**, *10*, 3770–3776.
249. Kim, M. R.; Miszta, K.; Povia, M.; Brescia, R.; Christodoulou, S.; Prato, M.; Marras, S.; Manna, L. Influence of Chloride Ions on the Synthesis of Colloidal Branched CdSe/CdS Nanocrystals by Seeded Growth. *ACS Nano* **2012**, *6*, 11088–11096.
250. Miszta, K.; de Graaf, J.; Bertoni, G.; Dorfs, D.; Brescia, R.; Marras, S.; Ceseracciu, L.; Cingolani, R.; van Roij, R.; Dijkstra, M.; *et al.* Hierarchical Self-Assembly Of Suspended Branched Colloidal Nanocrystals Into Superlattice Structures. *Nat. Mater.* **2011**, *10*, 872–876.
251. Qi, W.; de Graaf, J.; Qiao, F.; Marras, S.; Manna, L.; Dijkstra, M. Ordered Two-Dimensional Superstructures of Colloidal Octapod-Shaped Nanocrystals on Flat Substrates. *Nano Lett.* **2012**, *12*, 5299–5303.
252. Arciniegas, M. P.; Kim, M. R.; de Graaf, J.; Brescia, R.; Marras, S.; Miszta, K.; Dijkstra, M.; van Roij, R.; Manna, L. Self-Assembly of Octapod-Shaped Colloidal Nanocrystals into a

Hexagonal Ballerina Network Embedded in a Thin Polymer Film. *Nano Lett.* **2014**, *14*, 1056–1063.
253. Zhang, Y.; Miszta, K.; Manna, L.; Di Fabrizio, E.; Krahne, R. Cold Field Emission Dominated Photoconductivity in Ordered Three-Dimensional Assemblies of Octapod-Shaped CdSe/CdS Nanocrystals. *Nanoscale* **2013**, *5*, 7596–7600.
254. Qi, W.; de Graaf, J.; Qiao, F.; Marras, S.; Manna, L.; Dijkstra, M. Phase Diagram of Octapod-Shaped Nanocrystals in a Quasi-Two-Dimensional Planar Geometry. *J. Chem. Phys.* **2013**, *138*, 154504.
255. Paik, T.; Murray, C. B. Shape-Directed Binary Assembly of Anisotropic Nanoplates: A Nanocrystal Puzzle with Shape-Complementary Building Blocks. *Nano Lett.* **2013**, *13*, 2952–2956.
256. Boneschanscher, M. P.; Evers, W. H.; Geuchies, J. J.; Altantzis, T.; Goris, B.; Rabouw, F. T.; van Rossum, S. A. P.; van der Zant, H. S. J.; Siebbeles, L. D. A.; Van Tendeloo, G.; *et al.* Long-Range Orientation and Atomic Attachment of Nanocrystals in 2D Honeycomb Superlattices. *Science* **2014**, *344*, 1377–1380.
257. Zherebetskyy, D.; Scheele, M.; Zhang, Y.; Bronstein, N.; Thompson, C.; Britt, D.; Salmeron, M.; Alivisatos, P.; Wang, L.-W. Hydroxylation of the Surface of Pbs Nanocrystals Passivated with Oleic Acid. *Science* **2014**, *344*, 1380–1384.
258. Boles, M. A.; Talapin, D. V. Connecting the Dots. *Science* **2014**, *344*, 1340–1341.
259. Kalesaki, E.; Delerue, C.; Smith, C. M.; Beugeling, W.; Allan, G.; Vanmaekelbergh, D. Dirac Cones, Topological Edge States, and Nontrivial Flat Bands in Two-Dimensional Semiconductors with a Honeycomb Nanogeometry. *Phys. Rev. X* **2014**, *4*, 011010.
260. Snyder, G. J.; Toberer, E. S. Complex Thermoelectric Materials. *Nat. Mater.* **2008**, *7*, 105–114.
261. Vineis, C. J.; Shakouri, A.; Majumdar, A.; Kanatzidis, M. G. Nanostructured Thermoelectrics: Big Efficiency Gains from Small Features. *Adv. Mater.* **2010**, *22*, 3970–3980.
262. Dresselhaus, M. S.; Chen, G.; Tang, M. Y.; Yang, R. G.; Lee, H.; Wang, D. Z.; Ren, Z. F.; Fleurial, J. P.; Gogna, P. New Directions for Low-Dimensional Thermoelectric Materials. *Adv. Mater.* **2007**, *19*, 1043–1053.
263. Alam, H.; Ramakrishna, S. A Review on the Enhancement of Figure of Merit from Bulk to Nano-Thermoelectric Materials. *Nano Energy* **2013**, *2*, 190–212.
264. Li, J.-F.; Liu, W.-S.; Zhao, L.-D.; Zhou, M. High-Performance Nanostructured Thermoelectric Materials. *NPG Asia Mater.* **2010**, *2*, 152–158.
265. Pichanusakorn, P.; Bandaru, P. Nanostructured Thermoelectrics. *Mater. Sci. Eng., R* **2010**, *67*, 19–63.
266. Zhao, Y.; Dyck, J. S.; Burda, C. Toward High-Performance Nanostructured Thermoelectric Materials: The Progress of Bottom-Up Solution Chemistry Approaches. *J. Mater. Chem.* **2011**, *21*, 17049–17058.
267. Sootsman, J. R.; Chung, D. Y.; Kanatzidis, M. G. New and Old Concepts in Thermoelectric Materials. *Angew. Chem., Int. Ed.* **2009**, *48*, 8616–8639.
268. Zebarjadi, M.; Esfarjani, K.; Dresselhaus, M. S.; Ren, Z. F.; Chen, G. Perspectives on Thermoelectrics: From Fundamentals to Device Applications. *Energy Environ. Sci.* **2012**, *5*, 5147–5162.
269. Zhou, J.; Li, X.; Chen, G.; Yang, R. Semiclassical Model for Thermoelectric Transport in Nanocomposites. *Phys. Rev. B* **2010**, *82*, 115308.
270. Wang, R. Y.; Feser, J. P.; Lee, J.-S.; Talapin, D. V.; Segalman, R.; Majumdar, A. Enhanced Thermopower in PbSe Nanocrystal Quantum Dot Superlattices. *Nano Lett.* **2008**, *8*, 2283–2288.
271. Mahan, G. D.; Sofo, J. O. The Best Thermoelectric. *Proc. Natl. Acad. Sci. U.S.A.* **1996**, *93*, 7436–7439.
272. Humphrey, T. E.; Linke, H. Reversible Thermoelectric Nanomaterials. *Phys. Rev. Lett.* **2005**, *94*, 096601.
273. Venkatasubramanian, R.; Siivola, E.; Colpitts, T.; O'Quinn, B. Thin-Film Thermoelectric Devices with High Room-Temperature Figures of Merit. *Nature* **2001**, *413*, 597–602.
274. Harman, T. C.; Taylor, P. J.; Walsh, M. P.; LaForge, B. E. Quantum Dot Superlattice Thermoelectric Materials and Devices. *Science* **2002**, *297*, 2229–2232.
275. Minnich, A. J.; Dresselhaus, M. S.; Ren, Z. F.; Chen, G. Bulk Nanostructured Thermoelectric Materials: Current Research and Future Prospects. *Energy Environ. Sci.* **2009**, *2*, 466–479.
276. Quarez, E.; Hsu, K.-F.; Pcionek, R.; Frangis, N.; Polychroniadis, E. K.; Kanatzidis, M. G. Nanostructuring, Compositional Fluctuations, and Atomic Ordering in the Thermoelectric Materials $AgPb_mSbTe_{2+m}$. The Myth of Solid Solutions. *J. Am. Chem. Soc.* **2005**, *127*, 9177–9190.
277. Hsu, K. F.; Loo, S.; Guo, F.; Chen, W.; Dyck, J. S.; Uher, C.; Hogan, T.; Polychroniadis, E. K.; Kanatzidis, M. G. Cubic $AgPbmSbTe_{2+m}$: Bulk Thermoelectric Materials with High Figure of Merit. *Science* **2004**, *303*, 818–821.
278. Cao, Y. Q.; Zhao, X. B.; Zhu, T. J.; Zhang, X. B.; Tu, J. P. Syntheses and Thermoelectric Properties of Bi_2Te_3/Sb_2Te_3 Bulk Nanocomposites with Laminated Nanostructure. *Appl. Phys. Lett.* **2008**, *92*, 143106.
279. Poudel, B.; Hao, Q.; Ma, Y.; Lan, Y.; Minnich, A.; Yu, B.; Yan, X.; Wang, D.; Muto, A.; Vashaee, D.; *et al.* High-Thermoelectric Performance of Nanostructured Bismuth Antimony Telluride Bulk Alloys. *Science* **2008**, *320*, 634–638.
280. Cadavid, D.; Ibáñez, M.; Gorsse, S.; López, A. M.; Cirera, A.; Morante, J.; Cabot, A. Bottom-Up Processing of Thermoelectric Nanocomposites from Colloidal Nanocrystal Building Blocks: The Case of Ag_2Te–PbTe. *J. Nanopart. Res.* **2012**, *14*, 1–10.
281. Zhang, Y.; Stucky, G. D. Heterostructured Approaches to Efficient Thermoelectric Materials. *Chem. Mater.* **2013**, *26*, 837–848.
282. Ibáñez, M.; Zamani, R.; Gorsse, S.; Fan, J.; Ortega, S.; Cadavid, D.; Morante, J. R.; Arbiol, J.; Cabot, A. Core–Shell Nanoparticles as Building Blocks for the Bottom-Up Production of Functional Nanocomposites: PbTe–PbS Thermoelectric Properties. *ACS Nano* **2013**, *7*, 2573–2586.
283. Scheele, M.; Oeschler, N.; Veremchuk, I.; Peters, S.-O.; Littig, A.; Kornowski, A.; Klinke, C.; Weller, H. Thermoelectric Properties of Lead Chalcogenide Core–Shell Nanostructures. *ACS Nano* **2011**, *5*, 8541–8551.
284. Kovalenko, M. V.; Spokoyny, B.; Lee, J.-S.; Scheele, M.; Weber, A.; Perera, S.; Landry, D.; Talapin, D. V. Semiconductor Nanocrystals Functionalized with Antimony Telluride Zintl Ions for Nanostructured Thermoelectrics. *J. Am. Chem. Soc.* **2010**, *132*, 6686–6695.
285. Kovalenko, M. V.; Bodnarchuk, M. I.; Zaumseil, J.; Lee, J.-S.; Talapin, D. V. Expanding the Chemical Versatility of Colloidal Nanocrystals Capped with Molecular Metal Chalcogenide Ligands. *J. Am. Chem. Soc.* **2010**, *132*, 10085–10092.
286. Kovalenko, M. V.; Bodnarchuk, M. I.; Talapin, D. V. Nanocrystal Superlattices with Thermally Degradable Hybrid Inorganic-Organic Capping Ligands. *J. Am. Chem. Soc.* **2010**, *132*, 15124–15126.
287. Yakunin, S.; Dirin, D. N.; Protesescu, L.; Sytnyk, M.; Tollabimazraehno, S.; Humer, M.; Hackl, F.; Fromherz, T.; Bodnarchuk, M. I.; Kovalenko, M. V.; Heiss, W. High Infrared Photoconductivity in Films of Arsenic-Sulfide-Encapsulated Lead-Sulfide Nanocrystals. *ACS Nano* **2014**, *8*, 12883–12894.
288. Nag, A.; Kovalenko, M. V.; Lee, J.-S.; Liu, W.; Spokoyny, B.; Talapin, D. V. Metal-Free Inorganic Ligands for Colloidal Nanocrystals: S^{2-}, HS^{2-}, Se^{2-}, HSe^{-}, Te^{2-}, HTe^{-}, $TeS_3^{(2-)}$, OH^{-}, and NH_2^{-} as Surface Ligands. *J. Am. Chem. Soc.* **2011**, *133*, 10612–10620.
289. Nag, A.; Chung, D. S.; Dolzhnikov, D. S.; Dimitrijevic, N. M.; Chattopadhyay, S.; Shibata, T.; Talapin, D. V. Effect of Metal Ions on Photoluminescence, Charge Transport, Magnetic and Catalytic Properties of All-Inorganic Colloidal Nanocrystals and

Nanocrystal Solids. *J. Am. Chem. Soc.* **2012**, *134*, 13604–13615.
290. Kovalenko, M. V.; Scheele, M.; Talapin, D. V. Colloidal Nanocrystals with Molecular Metal Chalcogenide Surface Ligands. *Science* **2009**, *324*, 1417–1420.
291. Cadavid, D.; Ibáñez, M.; Shavel, A.; Dura, O. J.; Lopez de la Torre, M. A.; Cabot, A. Organic Ligand Displacement By Metal Salts To Enhance Nanoparticle Functionality: Thermoelectric Properties of Ag_2Te. *J. Mater. Chem. A* **2013**, *1*, 4864–4870.
292. Zhang, Y.; Snedaker, M. L.; Birkel, C. S.; Mubeen, S.; Ji, X.; Shi, Y.; Liu, D.; Liu, X.; Moskovits, M.; Stucky, G. D. Silver-Based Intermetallic Heterostructures in Sb_2Te_3 Thick Films with Enhanced Thermoelectric Power Factors. *Nano Lett.* **2012**, *12*, 1075–1080.
293. Buonsanti, R.; Milliron, D. J. Chemistry of Doped Colloidal Nanocrystals. *Chem. Mater.* **2013**, *25*, 1305–1317.
294. Sahu, A.; Kang, M. S.; Kompch, A.; Notthoff, C.; Wills, A. W.; Deng, D.; Winterer, M.; Frisbie, C. D.; Norris, D. J. Electronic Impurity Doping in CdSe Nanocrystals. *Nano Lett.* **2012**, *12*, 2587–2594.
295. Ibáñez, M.; Cadavid, D.; Anselmi Tamburini, U.; Zamani, R.; Gorsse, S.; Li, W.; Shavel, A.; López, A. M.; Morante, J. R.; Arbiol, J.; *et al.* Colloidal Synthesis and Thermoelectric Properties of Cu_2SnSe_3 Nanocrystals. *J. Mater. Chem. A* **2013**, *1*, 1421–1426.
296. Zhao, Y.; Dyck, J. S.; Hernandez, B. M.; Burda, C. Enhancing Thermoelectric Performance of Ternary Nanocrystals through Adjusting Carrier Concentration. *J. Am. Chem. Soc.* **2010**, *132*, 4982–4983.
297. Ko, D.-K.; Urban, J. J.; Murray, C. B. Carrier Distribution and Dynamics of Nanocrystal Solids Doped with Artificial Atoms. *Nano Lett.* **2010**, *10*, 1842–1847.
298. Urban, J. J.; Talapin, D. V.; Shevchenko, E. V.; Kagan, C. R.; Murray, C. B. Synergism in Binary Nanocrystal Superlattices Leads to Enhanced p-Type Conductivity in Self-Assembled PbTe/Ag_2Te Thin Films. *Nat. Mater.* **2007**, *6*, 115–121.
299. Scheele, M.; Oeschler, N.; Meier, K.; Kornowski, A.; Klinke, C.; Weller, H. Synthesis and Thermoelectric Characterization of Bi_2Te_3 Nanoparticles. *Adv. Funct. Mater.* **2009**, *19*, 3476–3483.
300. Son, J. S.; Park, K.; Han, M.-K.; Kang, C.; Park, S.-G.; Kim, J.-H.; Kim, W.; Kim, S.-J.; Hyeon, T. Large-Scale Synthesis and Characterization of the Size-Dependent Thermoelectric Properties of Uniformly Sized Bismuth Nanocrystals. *Angew. Chem., Int. Ed.* **2010**, *50*, 1363–1366.
301. Son, J. S.; Choi, M. K.; Han, M.-K.; Park, K.; Kim, J.-Y.; Lim, S. J.; Oh, M.; Kuk, Y.; Park, C.; Kim, S.-J.; *et al.* n-Type Nanostructured Thermoelectric Materials Prepared from Chemically Synthesized Ultrathin Bi_2Te_3 Nanoplates. *Nano Lett.* **2012**, *12*, 640–647.
302. Zhang, H.; Son, J. S.; Jang, J.; Lee, J.-S.; Ong, W.-L.; Malen, J. A.; Talapin, D. V. $Bi_{1-x}Sb_x$ Alloy Nanocrystals: Colloidal Synthesis, Charge Transport, Thermoelectric Properties. *ACS Nano* **2013**, *7*, 10296–10306.
303. Medlin, D. L.; Snyder, G. J. Interfaces in Bulk Thermoelectric Materials: A Review for Current Opinion in Colloid and Interface Science. *Adv. Colloid Interface Sci.* **2009**, *14*, 226–235.
304. Oszajca, M. F.; Bodnarchuk, M. I.; Kovalenko, M. V. Precisely Engineered Colloidal Nanoparticles and Nanocrystals for Li-Ion and Na-Ion Batteries: Model Systems or Practical Solutions? *Chem. Mater.* **2014**, *26*, 5422–5432.
305. Oh, M. H.; Yu, T.; Yu, S.-H.; Lim, B.; Ko, K.-T.; Willinger, M.-G.; Seo, D.-H.; Kim, B. H.; Cho, M. G.; Park, J.-H.; *et al.* Galvanic Replacement Reactions in Metal Oxide Nanocrystals. *Science* **2013**, *340*, 964–968.
306. Koo, B.; Xiong, H.; Slater, M. D.; Prakapenka, V. B.; Balasubramanian, M.; Podsiadlo, P.; Johnson, C. S.; Rajh, T.; Shevchenko, E. V. Hollow Iron Oxide Nanoparticles for Application in Lithium Ion Batteries. *Nano Lett.* **2012**, *12*, 2429–2435.
307. Koo, B.; Chattopadhyay, S.; Shibata, T.; Prakapenka, V. B.; Johnson, C. S.; Rajh, T.; Shevchenko, E. V. Intercalation of Sodium Ions into Hollow Iron Oxide Nanoparticles. *Chem. Mater.* **2013**, *25*, 245–252.
308. Wang, D.-S.; Xie, T.; Peng, Q.; Zhang, S.-Y.; Chen, J.; Li, Y.-D. Direct Thermal Decomposition of Metal Nitrates in Octadecylamine to Metal Oxide Nanocrystals. *Chem.—Eur. J.* **2008**, *14*, 2507–2513.
309. Ha, D.-H.; Islam, M. A.; Robinson, R. D. Binder-Free and Carbon-Free Nanoparticle Batteries: A Method for Nanoparticle Electrodes without Polymeric Binders or Carbon Black. *Nano Lett.* **2012**, *12*, 5122–5130.
310. Lee, S. H.; Yu, S.-H.; Lee, J. E.; Jin, A.; Lee, D. J.; Lee, N.; Jo, H.; Shin, K.; Ahn, T.-Y.; Kim, Y.-W.; *et al.* Self-Assembled Fe_3O_4 Nanoparticle Clusters as High-Performance Anodes for Lithium Ion Batteries *via* Geometric Confinement. *Nano Lett.* **2013**, *13*, 4249–4256.
311. Buonsanti, R.; Pick, T. E.; Krins, N.; Richardson, T. J.; Helms, B. A.; Milliron, D. J. Assembly of Ligand-Stripped Nanocrystals into Precisely Controlled Mesoporous Architectures. *Nano Lett.* **2012**, *12*, 3872–3877.
312. Wang, H.; Cui, L.-F.; Yang, Y.; Casalongue, H. S.; Robinson, J. T.; Liang, Y.; Cui, Y.; Dai, H. Mn_3O_4–Graphene Hybrid as a High-Capacity Anode Material for Lithium Ion Batteries. *J. Am. Chem. Soc.* **2010**, *132*, 13978–13980.
313. Ming, J.; Park, J.-B.; Sun, Y.-K. Encapsulation of Metal Oxide Nanocrystals into Porous Carbon with Ultrahigh Performances in Lithium-Ion Battery. *ACS Appl. Mater. Interfaces* **2013**, *5*, 2133–2136.
314. Bodnarchuk, M. I.; Kravchyk, K. V.; Krumeich, F.; Wang, S.; Kovalenko, M. V. Colloidal Tin–Germanium Nanorods and Their Li-Ion Storage Properties. *ACS Nano* **2014**, *8*, 2360–2368.
315. Kravchyk, K.; Protesescu, L.; Bodnarchuk, M. I.; Krumeich, F.; Yarema, M.; Walter, M.; Guntlin, C.; Kovalenko, M. V. Monodisperse and Inorganically Capped Sn and Sn/SnO_2 Nanocrystals for High-Performance Li-Ion Battery Anodes. *J. Am. Chem. Soc.* **2013**, *135*, 4199–4202.
316. He, M.; Kravchyk, K. V.; Walter, M.; Kovalenko, M. V. Monodisperse Antimony Nanocrystals for High-Rate Li-ion and Na-ion Battery Anodes: Nano *vs.* Bulk. *Nano Lett.* **2014**, *14*, 1255–1262.
317. Xu, L.; Kim, C.; Shukla, A. K.; Dong, A.; Mattox, T. M.; Milliron, D. J.; Cabana, J. Monodisperse Sn Nanocrystals as a Platform for the Study of Mechanical Damage during Electrochemical Reactions with Li. *Nano Lett.* **2013**, *13*, 1800–1805.
318. Park, C.-M.; Kim, J.-H.; Kim, H.; Sohn, H.-J. Li-Alloy Based Anode Materials for Li Secondary Batteries. *Chem. Soc. Rev.* **2010**, *39*, 3115–3141.
319. Darwiche, A.; Marino, C.; Sougrati, M. T.; Fraisse, B.; Stievano, L.; Monconduit, L. Better Cycling Performances of Bulk Sb in Na-Ion Batteries Compared to Li-Ion Systems: An Unexpected Electrochemical Mechanism. *J. Am. Chem. Soc.* **2012**, *134*, 20805–20811.
320. Heß, M.; Novák, P. Shrinking Annuli Mechanism and Stage-Dependent Rate Capability of Thin-Layer Graphite Electrodes for Lithium-Ion Batteries. *Electrochim. Acta* **2013**, *106*, 149–158.
321. Nakahara, K.; Nakajima, R.; Matsushima, T.; Majima, H. Preparation of Particulate $Li_4Ti_5O_{12}$ Having Excellent Characteristics as an Electrode Active Material for Power Storage Cells. *J. Power Sources* **2003**, *117*, 131–136.
322. Kanehara, M.; Koike, H.; Yoshinaga, T.; Teranishi, T. Indium Tin Oxide Nanoparticles with Compositionally Tunable Surface Plasmon Resonance Frequencies in the Near-IR Region. *J. Am. Chem. Soc.* **2009**, *131*, 17736–17737.
323. Buonsanti, R.; Milliron, D. J. Chemistry of Doped Colloidal Nanocrystals. *Chem. Mater.* **2013**, *25*, 1305–1317.
324. Lounis, S. D.; Runnerstrorm, E. L.; Llordes, A.; Milliron, D. J. Defect Chemistry and Plasmon Physics of

Colloidal Metal Oxide Nanocrystals. *J. Phys. Chem. Lett.* **2014**, *5*, 1564–1574.
325. Gordon, T. R.; Cargnello, M.; Paik, T.; Mangolini, F.; Weber, R. T.; Fornasiero, P.; Murray, C. B. Nonaqueous Synthesis of TiO_2 Nanocrystals Using TiF_4 To Engineer Morphology, Oxygen Vacancy Concentration, and Photocatalytic Activity. *J. Am. Chem. Soc.* **2012**, *134*, 6751–6761.
326. Manthiram, K.; Alivisatos, A. P. Tunable Localized Surface Plasmon Resonances in Tungsten Oxide Nanocrystals. *J. Am. Chem. Soc.* **2012**, *134*, 3995–3998.
327. Gordon, T. R.; Paik, T.; Klein, D. R.; Naik, G. V.; Caglayan, H.; Boltasseva, A.; Murray, C. B. Shape-Dependent Plasmonic Response and Directed Self-Assembly in a New Semiconductor Building Block, Indium-Doped Cadmium Oxide (ICO). *Nano Lett.* **2013**, *13*, 2857–2863.
328. Mattox, T. M.; Bergerud, A.; Agrawal, A.; Milliron, D. J. Influence of Shape on the Surface Plasmon Resonance of Tungsten Bronze Nanocrystals. *Chem. Mater.* **2014**, *26*, 1779–1784.
329. Lounis, S. D.; Runnerstrom, E. L.; Bergerud, A.; Nordlund, D.; Milliron, D. J. Influence of Dopant Distribution on the Plasmonic Properties of Indium Tin Oxide Nanocrystals. *J. Am. Chem. Soc.* **2014**, *136*, 7110–7116.
330. Garcia, G.; Buonsanti, R.; Runnerstrom, E. L.; Mendelsberg, R. J.; Llordes, A.; Anders, A.; Richardson, T. J.; Milliron, D. J. Dynamically Modulating the Surface Plasmon Resonance of Doped Semiconductor Nanocrystals. *Nano Lett.* **2011**, *11*, 4415–4420.
331. Garcia, G.; Buonsanti, R.; Llordes, A.; Runnerstrom, E. L.; Bergerud, A.; Milliron, D. J. Near-Infrared Spectrally Selective Plasmonic Electrochromic Thin Films. *Adv. Opt. Mater.* **2013**, *1*, 215–220.
332. Milliron, D. J.; Buonsanti, R.; Llordes, A.; Helms, B. A. Constructing Functional Mesostructured Materials from Colloidal Nanocrystal Building Blocks. *Acc. Chem. Res.* **2014**, *47*, 236–246.
333. Leatherdale, C. A.; Kagan, C. R.; Morgan, N. Y.; Empedocles, S. A.; Kastner, M. A.; Bawendi, M. G. Photoconductivity in CdSe Quantum Dot Solids. *Phys. Rev. B* **2001**, *63*, 039901.
334. Talapin, D. V.; Murray, C. B. PbSe Nanocrystal Solids for n- and p-Channel Thin Film Field-Effect Transistors. *Science* **2005**, *310*, 86–89.
335. Shim, M.; Guyot-Sionnest, P. n-Type Colloidal Semiconductor Nanocrystals. *Nature* **2000**, *407*, 981–983.
336. Yu, M. K.; Kim, D.; Lee, I. H.; So, J. S.; Jeong, Y. Y.; Jon, S. Image-Guided Prostate Cancer Therapy Using Aptamer-Functionalized Thermally Cross-Linked Superparamagnetic Iron Oxide Nanoparticles. *Small* **2011**, *7*, 2241–2249.
337. Liu, W.; Lee, J.-S.; Talapin, D. V. III–V Nanocrystals Capped with Molecular Metal Chalcogenide Ligands: High Electron Mobility and Ambipolar Photoresponse. *J. Am. Chem. Soc.* **2013**, *135*, 1349–1357.
338. Talgorn, E.; Gao, Y.; Aerts, M.; Kunneman, L. T.; Schins, J. M.; Savenije, T. J.; van Huis, M. A.; van der Zant, H. S. J.; Houtepen, A. J.; Siebbeles, L. D. A. Unity Quantum Yield of Photogenerated Charges and Band-like Transport in Quantum-Dot Solids. *Nat. Nanotechnol.* **2011**, *6*, 733–739.
339. Oh, S. J.; Berry, N. E.; Choi, J.-H.; Gaulding, E. A.; Paik, T.; Hong, S.-H.; Murray, C. B.; Kagan, C. R. Stoichiometric Control of Lead Chalcogenide Nanocrystal Solids To Enhance Their Electronic and Optoelectronic Device Performance. *ACS Nano* **2013**, *7*, 2413–2421.
340. Jang, J.; Liu, W.; Son, J. S.; Talapin, D. V. Temperature-Dependent Hall and Field-Effect Mobility in Strongly Coupled All-Inorganic Nanocrystal Arrays. *Nano Lett.* **2014**, *14*, 653–662.
341. Luther, J. M.; Pietryga, J. M. Stoichiometry Control in Quantum Dots: A Viable Analog to Impurity Doping of Bulk Materials. *ACS Nano* **2013**, *7*, 1845–1849.
342. Oh, S. J.; Berry, N. E.; Choi, J.-H.; Gaulding, E. A.; Lin, H.; Paik, T.; Diroll, B. T.; Muramoto, S.; Murray, C. B.; Kagan, C. R. Designing High-Performance PbS and PbSe Nanocrystal Electronic Devices through Stepwise, Post-Synthesis, Colloidal Atomic Layer Deposition. *Nano Lett.* **2014**, *14*, 1559–1566.
343. Kim, D. K.; Fafarman, A. T.; Diroll, B. T.; Chan, S. H.; Gordon, T. R.; Murray, C. B.; Kagan, C. R. Solution-Based Stoichiometric Control over Charge Transport in Nanocrystalline CdSe Devices. *ACS Nano* **2013**, *7*, 8760–8770.
344. Kim, D.; Kim, D.-H.; Lee, J.-H.; Grossman, J. C. Impact of Stoichiometry on the Electronic Structure of PbS Quantum Dots. *Phys. Rev. Lett.* **2013**, *110*, 196802.
345. Ning, Z.; Ren, Y.; Hoogland, S.; Voznyy, O.; Levina, L.; Stadler, P.; Lan, X.; Zhitomirsky, D.; Sargent, E. H. All-Inorganic Colloidal Quantum Dot Photovoltaics Employing Solution-Phase Halide Passivation. *Adv. Mater.* **2012**, *24*, 6295–6299.
346. Zhitomirsky, D.; Furukawa, M.; Tang, J.; Stadler, P.; Hoogland, S.; Voznyy, O.; Liu, H.; Sargent, E. H. n-Type Colloidal-Quantum-Dot Solids for Photovoltaics. *Adv. Mater.* **2012**, *24*, 6181–6185.
347. Pourret, A.; Guyot-Sionnest, P.; Elam, J. W. Atomic Layer Deposition of ZnO in Quantum Dot Thin Films. *Adv. Mater.* **2009**, *21*, 232–235.
348. Baumgardner, W. J.; Whitham, K.; Hanrath, T. Confined-but-Connected Quantum Solids *via* Controlled Ligand Displacement. *Nano Lett.* **2013**, *13*, 3225–3231.
349. Kim, D. K.; Lai, Y.; Vemulkar, T. R.; Kagan, C. R. Flexible, Low-Voltage, and Low-Hysteresis PbSe Nanowire Field-Effect Transistors. *ACS Nano* **2011**, *5*, 10074–10083.
350. Kim, D. K.; Lai, Y.; Diroll, B. T.; Murray, C. B.; Kagan, C. R. Flexible and Low-Voltage Integrated Circuits Constructed from High-Performance Nanocrystal Transistors. *Nat. Commun.* **2012**, *3*, 1216.
351. Choi, J.-H.; Oh, S. J.; Lai, Y.; Kim, D. K.; Zhao, T.; Fafarman, A. T.; Diroll, B. T.; Murray, C. B.; Kagan, C. R. *In Situ* Repair of High-Performance, Flexible Nanocrystal Electronics for Large-Area Fabrication and Operation in Air. *ACS Nano* **2013**, *7*, 8275–8283.
352. Miszta, K.; Greullet, F.; Marras, S.; Prato, M.; Toma, A.; Arciniegas, M.; Manna, L.; Krahne, R. Nanocrystal Film Patterning by Inhibiting Cation Exchange *via* Electron-Beam or X-ray Lithography. *Nano Lett.* **2014**, *14*, 2116–2122.
353. Rizzo, A.; Li, Y.; Kudera, S.; Della Sala, F.; Zanella, M.; Parak, W. J.; Cingolani, R.; Manna, L.; Gigli, G. Blue Light Emitting Diodes Based on Fluorescent CdSe/ZnS Nanocrystals. *Appl. Phys. Lett.* **2007**, *90*, 051106.
354. Colvin, V. L.; Schlamp, M. C.; Alivisatos, A. P. Light-Emitting-Diodes Made from Cadmium Selenide Nanocrystals and a Semiconducting Polymer. *Nature* **1994**, *370*, 354–357.
355. Coe, S.; Woo, W.-K.; Bawendi, M. G.; Bulovic, V. Electroluminescence from Single Monolayers of Nanocrystals in Molecular Organic Devices. *Nature* **2002**, *420*, 800–803.
356. Mueller, A. H.; Petruska, M. A.; Achermann, M.; Werder, D. J.; Akhadov, E. A.; Koleske, D. D.; Hoffbauer, M. A.; Klimov, V. I. Multicolor Light-Emitting Diodes Based on Semiconductor Nanocrystals Encapsulated in GaN Injection Layers. *Nano Lett.* **2005**, *5*, 1039–1044.
357. Kwak, J.; Bae, W. K.; Lee, D.; Park, I.; Lim, J.; Park, M.; Cho, H.; Woo, H.; Yoon, D. Y.; Char, K.; *et al.* Bright and Efficient Full-Color Colloidal Quantum Dot Light-Emitting Diodes Using an Inverted Device Structure. *Nano Lett.* **2012**, *12*, 2362–2366.
358. Shirasaki, Y.; Supran, G. J.; Bawendi, M. G.; Bulovic, V. Emergence of Colloidal Quantum-Dot Light-Emitting Technologies. *Nat. Photonics* **2013**, *7*, 13–23.
359. Mashford, B. S.; Stevenson, M.; Popovic, Z.; Hamilton, C.; Zhou, Z. Q.; Breen, C.; Steckel, J.; Bulovic, V.; Bawendi, M.; Coe-Sullivan, S.; *et al.* High-Efficiency Quantum-Dot Light-Emitting Devices with

Enhanced Charge Injection. *Nat. Photonics* **2013**, *7*, 407–412.
360. Anikeeva, P. O.; Madigan, C. F.; Halpert, J. E.; Bawendi, M. G.; Bulovic, V. Electronic and Excitonic Processes in Light-Emitting Devices Based on Organic Materials and Colloidal Quantum Dots. *Phys. Rev. B* **2008**, *78*, 085434.
361. Bae, W. K.; Park, Y. S.; Lim, J.; Lee, D.; Padilha, L. A.; McDaniel, H.; Robel, I.; Lee, C.; Pietryga, J. M.; Klimov, V. I. Controlling the Influence of Auger Recombination on the Performance of Quantum-Dot Light-Emitting Diodes. *Nat. Commun.* **2013**, *4*, 2661.
362. Cohn, A. W.; Rinehart, J. D.; Schimpf, A. M.; Weaver, A. L.; Gamelin, D. R. Size Dependence of Negative Trion Auger Recombination in Photodoped CdSe Nanocrystals. *Nano Lett.* **2014**, *14*, 353–358.
363. Park, Y.-S.; Bae, W. K.; Pietryga, J. M.; Klimov, V. I. Auger Recombination of Biexcitons and Negative and Positive Trions in Individual Quantum Dots. *ACS Nano* **2014**, 7288–7296.
364. Klimov, V. I. Multicarrier Interactions in Semiconductor Nanocrystals in Relation to the Phenomena of Auger Recombination and Carrier Multiplication. *Annu. Rev. Condens. Matter Phys.* **2014**, *5*, 13.1–13.32.
365. Bae, W. K.; Brovelli, S.; Klimov, V. I. Spectroscopic Insights into the Performance of Quantum Dot Light Emitting Diodes. *MRS Bull.* **2013**, *38*, 721–730.
366. Cragg, G. E.; Efros, A. L. Suppression of Auger Processes in Confined Structures. *Nano Lett.* **2010**, *10*, 313–317.
367. Garcia-Santamaria, F.; Brovelli, S.; Viswanatha, R.; Hollingsworth, J. A.; Htoon, H.; Crooker, S. A.; Klimov, V. I. Breakdown of Volume Scaling in Auger Recombination in CdSe/CdS Heteronanocrystals: The Role of the Core–Shell Interface. *Nano Lett.* **2011**, *11*, 687–693.
368. Klimov, V. I.; Mikhailovsky, A. A.; Xu, S.; Malko, A.; Hollingsworth, J. A.; Leatherdale, C. A.; Eisler, H. J.; Bawendi, M. G. Optical Gain and Stimulated Emission in Nanocrystal Quantum Dots. *Science* **2000**, *290*, 314–317.
369. Klimov, V. I.; Mikhailovsky, A. A.; McBranch, D. W.; Leatherdale, C. A.; Bawendi, M. G. Quantization of Multiparticle Auger Rates in Semiconductor Quantum Dots. *Science* **2000**, *287*, 1011–1013.
370. Robel, I.; Gresback, R.; Kortshagen, U.; Schaller, R. D.; Klimov, V. I. Universal Size-Dependent Trend in Auger Recombination in Direct-Gap and Indirect-Gap Semiconductor Nanocrystals. *Phys. Rev. Lett.* **2009**, *102*, 177404.
371. Kazes, M.; Lewis, D. Y.; Evenstein, Y.; Mokari, T.; Banin, U. Lasing from Semiconductor Quantum Rods in a Cylindrical Microcavity. *Adv. Mater.* **2002**, *14*, 317–321.
372. Htoon, H.; Hollingsworth, J. A.; Malko, A. V.; Dickerson, R.; Klimov, V. I. Light Amplification in Semiconductor Nanocrystals: Quantum Rods *vs*. Quantum Dots. *Appl. Phys. Lett.* **2003**, *82*, 4776–4778.
373. Garcia-Santamaria, F.; Chen, Y. F.; Vela, J.; Schaller, R. D.; Hollingsworth, J. A.; Klimov, V. I. Suppressed Auger Recombination in "Giant" Nanocrystals Boosts Optical Gain Performance. *Nano Lett.* **2009**, *9*, 3482–3488.
374. Moreels, I.; Rainò, G.; Gomes, R.; Hens, Z.; Stöferle, T.; Mahrt, R. F. Nearly Temperature-Independent Threshold for Amplified Spontaneous Emission in Colloidal CdSe/CdS Quantum Dot-in-Rods. *Adv. Mater.* **2012**, *24*, OP231–OP235.
375. Ivanov, S. A.; Nanda, J.; Piryatinski, A.; Achermann, M.; Balet, L. P.; Bezel, I. V.; Anikeeva, P. O.; Tretiak, S.; Klimov, V. I. Light Amplification Using Inverted Core/Shell Nanocrystals: Towards Lasing in the Single-Exciton Regime. *J. Phys. Chem. B* **2004**, *108*, 10625–10630.
376. Oron, D.; Kazes, M.; Banin, U. Multiexcitons in Type-II Colloidal Semiconductor Quantum Dots. *Phys. Rev. B* **2007**, *75*, 035330.
377. Piryatinski, A.; Ivanov, S. A.; Tretiak, S.; Klimov, V. I. Effect of Quantum and Dielectric Confinement on the Exciton–Exciton Interaction Energy in Type-II Core/Shell Semiconductor Nanocrystals. *Nano Lett.* **2007**, *7*, 108–115.
378. Klimov, V. I.; Ivanov, S. A.; Nanda, J.; Achermann, M.; Bezel, I.; McGuire, J. A.; Piryatinski, A. Single-Exciton Optical Gain in Semiconductor Nanocrystals. *Nature* **2007**, *447*, 441–446.
379. Kelestemur, Y.; Cihan, A. F.; Guzelturk, B.; Demir, H. V. Type-Tunable Amplified Spontaneous Emission from Core-Seeded CdSe/CdS Nanorods Controlled by Exciton–Exciton Interaction. *Nanoscale* **2014**, *6*, 8509–8514.
380. Grivas, C.; Li, C.; Andreakou, P.; Wang, P.; Ding, M.; Brambilla, G.; Manna, L.; Lagoudakis, P. Single-Mode Tunable Laser Emission in the Single-Exciton Regime from Colloidal Nanocrystals. *Nat. Commun.* **2013**, *4*, 2376.
381. Zavelani-Rossi, M.; Krahne, R.; Della Valle, G.; Longhi, S.; Franchini, I. R.; Girardo, S.; Scotognella, F.; Pisignano, D.; Manna, L.; Lanzani, G.; *et al.* Self-Assembled CdSe/CdS Nanorod Micro-Lasers Fabricated from Solution by Capillary Jet Deposition. *Laser Photonics Rev.* **2012**, *6*, 678–683.
382. Di Stasio, F.; Grim, J. Q.; Lesnyak, V.; Rastogi, P.; Manna, L.; Krahne, R. Single-Mode Lasing from Colloidal Water-Soluble CdSe/CdS Quantum Dot-in-Rods. *Small* **2014**, 10.1002/smll.201402527.
383. Wang, Y.; Leck, K. S.; Ta, V. D.; Chen, R.; Nalla, V.; Gao, Y.; He, T.; Demir, H. V.; Sun, H. Blue Liquid Lasers from Solution of CdZnS/ZnS Ternary Alloy Quantum Dots with Quasi-Continuous Pumping. *Adv. Mater.* **2015**, *27*, 169–175.
384. Li, Z.; Qin, H.; Guzun, D.; Benamara, M.; Salamo, G.; Peng, X. Uniform Thickness and Colloidal-Stable CdS Quantum Disks with Tunable Thickness: Synthesis and Properties. *Nano Res.* **2012**, *5*, 337–351.
385. Bouet, C.; Mahler, B.; Nadal, B.; Abecassis, B.; Tessier, M. D.; Ithurria, S.; Xu, X.; Dubertret, B. Two-Dimensional Growth of CdSe Nanocrystals, from Nanoplatelets to Nanosheets. *Chem. Mater.* **2013**, *25*, 639–645.
386. Mahler, B.; Nadal, B.; Bouet, C.; Patriarche, G.; Dubertret, B. Core/Shell Colloidal Semiconductor Nanoplatelets. *J. Am. Chem. Soc.* **2012**, *134*, 18591–18598.
387. Ithurria, S.; Talapin, D. V. Colloidal Atomic Layer Deposition (c-ALD) Using Self-Limiting Reactions at Nanocrystal Surface Coupled to Phase Transfer between Polar and Nonpolar Media. *J. Am. Chem. Soc.* **2012**, *134*, 18585–18590.
388. Achtstein, A. W.; Schliwa, A.; Prudnikau, A.; Hardzei, M.; Artemyev, M. V.; Thomsen, C.; Woggon, U. Electronic Structure and Exciton–Phonon Interaction in Two-Dimensional Colloidal CdSe Nanosheets. *Nano Lett.* **2012**, *12*, 3151–3157.
389. She, C.; Fedin, I.; Dolzhnikov, D. S.; Demortière, A.; Schaller, R. D.; Pelton, M.; Talapin, D. V. Low-Threshold Stimulated Emission Using Colloidal Quantum Wells. *Nano Lett.* **2014**, *14*, 2772–2777.
390. Guzelturk, B.; Kelestemur, Y.; Olutas, M.; Delikanli, S.; Demir, H. V. Amplified Spontaneous Emission and Lasing in Colloidal Nanoplatelets. *ACS Nano* **2014**, *8*, 6599–6605.
391. Grim, J. Q.; Christodoulou, S.; Di Stasio, F.; Krahne, R.; Cingolani, R.; Manna, L.; Moreels, I. Continuous-Wave Biexciton Lasing at Room Temperature Using Solution-Processed Quantum Wells. *Nat. Nanotechnol.* **2014**, *9*, 891–895.
392. Li, H.; Kang, Z.; Liu, Y.; Lee, S.-T. Carbon Nanodots: Synthesis, Properties and Applications. *J. Mater. Chem.* **2012**, *22*, 24230–24253.
393. Sun, Y. P.; Zhou, B.; Lin, Y.; Wang, W.; Fernando, K. A. S.; Pathak, P.; Meziani, M. J.; Harruff, B. A.; Wang, X.; Wang, H. F.; *et al.* Quantum-Sized Carbon Dots for Bright and Colorful Photoluminescence. *J. Am. Chem. Soc.* **2006**, *128*, 7756–7757.
394. Zhu, S.; Meng, Q.; Wang, L.; Zhang, J.; Song, Y.; Jin, H.; Zhang, K.; Sun, H.; Wang, H.; Yang, B. Highly Photoluminescent Carbon Dots for Multicolor Patterning, Sensors, and

Bioimaging. *Angew. Chem., Int. Ed.* **2013**, *52*, 3953–3957.
395. Dong, Y.; Pang, H.; Yang, H. B.; Guo, C.; Shao, J.; Chi, Y.; Li, C. M.; Yu, T. Carbon-Based Dots Co-doped with Nitrogen and Sulfur for High Quantum Yield and Excitation-Independent Emission. *Angew. Chem., Int. Ed.* **2013**, *52*, 7800–7804.
396. Wang, F.; Chen, Y.-h.; Liu, C.-y.; Ma, D.-g. White Light-Emitting Devices Based on Carbon Dots' Electroluminescence. *Chem. Commun.* **2011**, *47*, 3502–3504.
397. Guo, X.; Wang, C.-F.; Yu, Z.-Y.; Chen, L.; Chen, S. Facile Access to Versatile Fluorescent Carbon Dots toward Light-Emitting Diodes. *Chem. Commun.* **2012**, *48*, 2692–2694.
398. Wang, Y.; Kalytchuk, S.; Zhang, Y.; Shi, H.; Kershaw, S. V.; Rogach, A. L. Thickness-Dependent Full-Color Emission Tunability in a Flexible Carbon Dot Ionogel. *J. Phys. Chem. Lett.* **2014**, *5*, 1412–1420.
399. Zhang, X.; Zhang, Y.; Wang, Y.; Kalytchuk, S.; Kershaw, S. V.; Wang, Y.; Wang, P.; Zhang, T.; Zhao, Y.; Zhang, H.; Cui, T.; *et al.* Color-Switchable Electroluminescence of Carbon Dot Light-Emitting Diodes. *ACS Nano* **2013**, *7*, 11234–11241.
400. Sun, C.; Zhang, Y.; Wang, Y.; Liu, W.; Kalytchuk, S.; Kershaw, S. V.; Zhang, T.; Zhang, X.; Zhao, J.; Yu, W. W.; *et al.* High Color Rendering Index White Light Emitting Diodes Fabricated from a Combination of Carbon Dots and Zinc Copper Indium Sulfide Quantum Dots. *Appl. Phys. Lett.* **2014**, *104*, 261106.
401. Rogalski, A. Progress in Focal Plane Array Technologies. *Progr. Quant. Electron.* **2012**, *36*, 342–473.
402. Phillips, J. Evaluation of the Fundamental Properties of Quantum Dot Infrared Detectors. *J. Appl. Phys.* **2002**, *91*, 4590–4594.
403. Guyot-Sionnest, P.; Hines, M. A. Intraband Transitions in Semiconductor Nanocrystals. *Appl. Phys. Lett.* **1998**, *72*, 686–688.
404. Klimov, V. I.; McBranch, D. W. Femtosecond 1P-to-1S Electron Relaxation in Strongly Confined Semiconductor Nanocrystals. *Phys. Rev. Lett.* **1998**, *80*, 4028–4031.
405. Pandey, A.; Guyot-Sionnest, P. Slow Electron Cooling in Colloidal Quantum Dots. *Science* **2008**, *322*, 929–932.
406. Mocatta, D.; Cohen, G.; Schattner, J.; Millo, O.; Rabani, E.; Banin, U. Heavily Doped Semiconductor Nanocrystal Quantum Dots. *Science* **2011**, *332*, 77–81.
407. Wise, F. W. Lead Salt Quantum Dots: The Limit of Strong Quantum Confinement. *Acc. Chem. Res.* **2000**, *33*, 773–780.
408. Murray, C. B.; Sun, S. H.; Gaschler, W.; Doyle, H.; Betley, T. A.; Kagan, C. R. Colloidal Synthesis of Nanocrystals and Nanocrystal Superlattices. *IBM J. Res. Dev.* **2001**, *45*, 47–56.
409. Rogach, A.; Kershaw, S.; Burt, M.; Harrison, M.; Kornowski, A.; Eychmuller, A.; Weller, H. Colloidally Prepared Hgte Nanocrystals with Strong Room-Temperature Infrared Luminescence. *Adv. Mater.* **1999**, *11*, 552–555.
410. Kovalenko, M. V.; Kaufmann, E.; Pachinger, D.; Roither, J.; Huber, M.; Stangl, J.; Hesser, G.; Schaffler, F.; Heiss, W. Colloidal HgTe Nanocrystals with Widely Tunable Narrow Band Gap Energies: From Telecommunications to Molecular Vibrations. *J. Am. Chem. Soc.* **2006**, *128*, 3516–3517.
411. Guyot-Sionnest, P.; Wang, C. Fast Voltammetric and Electrochromic Response of Semiconductor Nanocrystal Thin Films. *J. Phys. Chem. B* **2003**, *107*, 7355–7359.
412. Yu, D.; Wang, C.; Guyot-Sionnest, P. n-Type Conducting CdSe Nanocrystal Solids. *Science* **2003**, *300*, 1277–1280.
413. Jarosz, M. V.; Porter, V. J.; Fisher, B. R.; Kastner, M. A.; Bawendi, M. G. Photoconductivity Studies of Treated CdSe Quantum Dot Films Exhibiting Increased Exciton Ionization Efficiency. *Phys. Rev. B* **2004**, *70*, 195327.
414. Konstantatos, G.; Howard, I.; Fischer, A.; Hoogland, S.; Clifford, J.; Klem, E.; Levina, L.; Sargent, E. H. Ultrasensitive Solution-Cast Quantum Dot Photodetectors. *Nature* **2006**, *442*, 180–183.
415. Rauch, T.; Boberl, M.; Tedde, S. F.; Furst, J.; Kovalenko, M. V.; Hesser, G. N.; Lemmer, U.; Heiss, W.; Hayden, O. Near-Infrared Imaging with Quantum-Dot-Sensitized Organic Photodiodes. *Nat. Photonics* **2009**, *3*, 332–336.
416. Boberl, M.; Kovalenko, M. V.; Gamerith, S.; List, E. J. W.; Heiss, W. Inkjet-Printed Nanocrystal Photodetectors Operating up to 3 Micron Wavelengths. *Adv. Mater.* **2007**, *19*, 3574–3578.
417. Lhuillier, E.; Keuleyan, S.; Liu, H.; Guyot-Sionnest, P. Mid-IR Colloidal Nanocrystals. *Chem. Mater.* **2013**, *25*, 1272–1282.
418. Keuleyan, S. E.; Guyot-Sionnest, P.; Delerue, C.; Allan, G. Mercury Telluride Colloidal Quantum Dots: Electronic Structure, Size-Dependent Spectra, and Photocurrent Detection up to 12 μm. *ACS Nano* **2014**, *8*, 8676–8682.
419. Deng, Z.; Jeong, K. S.; Guyot-Sionnest, P. Colloidal Quantum Dots Intraband Photodetectors. *ACS Nano* **2014**, 11707–11714.
420. Jeong, K. S.; Deng, Z. Y.; Keuleyan, S.; Liu, H.; Guyot-Sionnest, P. Air-Stable n-Doped Colloidal HgS Quantum Dots. *J. Phys. Chem. Lett.* **2014**, *5*, 1139–1143.
421. Konstantatos, G.; Clifford, J.; Levina, L.; Sargent, E. H. Sensitive Solution-Processed Visible-Wavelength Photodetectors. *Nat. Photonics* **2007**, *1*, 531–534.
422. Clifford, J. P.; Konstantatos, G.; Johnston, K. W.; Hoogland, S.; Levina, L.; Sargent, E. H. Fast, Sensitive and Spectrally Tuneable Colloidal Quantum-Dot Photodetectors. *Nat. Nanotechnol.* **2009**, *4*, 40–44.
423. Sukhovatkin, V.; Hinds, S.; Brzozowski, L.; Sargent, E. H. Colloidal Quantum-Dot Photodetectors Exploiting Multiexciton Generation. *Science* **2009**, *324*, 1542–1544.
424. Keuleyan, S.; Lhuillier, E.; Brajuskovic, V.; Guyot-Sionnest, P. Mid-Infrared HgTe Colloidal Quantum Dot Photodetectors. *Nat. Photonics* **2011**, *5*, 489–493.
425. Konstantatos, G.; Levina, L.; Fischer, A.; Sargent, E. H. Engineering the Temporal Response of Photoconductive Photodetectors *via* Selective Introduction of Surface Trap States. *Nano Lett.* **2008**, *8*, 1446–1450.
426. Novoselov, K. S.; Fal'ko, V. I.; Colombo, L.; Gellert, P. R.; Schwab, M. G.; Kim, K. A Roadmap for Graphene. *Nature* **2012**, *490*, 192–200.
427. Bonaccorso, F.; Sun, Z.; Hasan, T.; Ferrari, A. C. Graphene Photonics and Optoelectronics. *Nat. Photonics* **2010**, *4*, 611–622.
428. Konstantatos, G.; Badioli, M.; Gaudreau, L.; Osmond, J.; Bernechea, M.; Garcia de Arquer, F. P.; Gatti, F.; Koppens, F. H. L. Hybrid Graphene–Quantum Dot Phototransistors with Ultrahigh Gain. *Nat. Nanotechnol.* **2012**, *7*, 363–368.
429. Radisavljevic, B.; Kis, A. Mobility Engineering and a Metal-Insulator Transition in Monolayer MoS_2. *Nat. Mater.* **2013**, *12*, 815–820.
430. Kim, J. Y.; Voznyy, O.; Zhitomirsky, D.; Sargent, E. H. 25th Anniversary Article: Colloidal Quantum Dot Materials and Devices: A Quarter-Century of Advances. *Adv. Mater.* **2013**, *25*, 4986–5010.
431. Semonin, O. E.; Luther, J. M.; Choi, S.; Chen, H. Y.; Gao, J. B.; Nozik, A. J.; Beard, M. C. Peak External Photocurrent Quantum Efficiency Exceeding 100% *via* MEG in a Quantum Dot Solar Cell. *Science* **2011**, *334*, 1530–1533.
432. Wang, X.; Koleilat, G. I.; Tang, J.; Liu, H.; Kramer, I. J.; Debnath, R.; Brzozowski, L.; Barkhouse, D. A. R.; Levina, L.; Hoogland, S.; Sargent, E. H. Tandem Colloidal Quantum Dot Solar Cells Employing a Graded Recombination Layer. *Nat. Photonics* **2011**, *5*, 480–484.
433. Pattantyus-Abraham, A. G.; Kramer, I. J.; Barkhouse, A. R.; Wang, X.; Konstantatos, G.; Debnath, R.; Levina, L.; Raabe, I.; Nazeeruddin, M. K.; Graetzel, M.; *et al.* Depleted-Heterojunction Colloidal Quantum Dot Solar Cells. *ACS Nano* **2010**, *4*, 3374–3380.
434. Tang, J.; Kemp, K. W.; Hoogland, S.; Jeong, K. S.; Liu, H.; Levina, L.; Furukawa, M.; Wang, X.; Debnath,

R.; Cha, D.; *et al.* Colloidal-Quantum-Dot Photovoltaics Using Atomic-Ligand Passivation. *Nat. Mater.* **2011**, *10*, 765–771.
435. Ip, A. H.; Thon, S. M.; Hoogland, S.; Voznyy, O.; Zhitomirsky, D.; Debnath, R.; Levina, L.; Rollny, L. R.; Carey, G. H.; Fischer, A.; *et al.* Hybrid Passivated Colloidal Quantum Dot Solids. *Nat. Nanotechnol.* **2012**, *7*, 577–582.
436. Chuang, C.-H. M.; Brown, P. R.; Bulovic, V.; Bawendi, M. G. Improved Performance and Stability in Quantum Dot Solar Cells through Band Alignment Engineering. *Nat. Mater.* **2014**, *13*, 796–801.
437. Rath, A. K.; Bernechea, M.; Martinez, L.; Garcia de Arquer, F. P.; Osmond, J.; Konstantatos, G. Solution-Processed Inorganic Bulk Nano-Heterojunctions and Their Application to Solar Cells. *Nat. Photonics* **2012**, *6*, 529–534.
438. Rath, A. K.; Garcia de Arquer, F. P.; Stavrinadis, A.; Lasanta, T.; Bernechea, M.; Diedenhofen, S. L.; Konstantatos, G. Remote Trap Passivation in Colloidal Quantum Dot Bulk Nano-Heterojunctions and Its Effect in Solution-Processed Solar Cells. *Adv. Mater.* **2014**, *26*, 4741–4747.
439. Sargent, E. H. Colloidal Quantum Dot Solar Cells. *Nat. Photonics* **2012**, *6*, 133–135.
440. Luther, J. M.; Gao, J.; Lloyd, M. T.; Semonin, O. E.; Beard, M. C.; Nozik, A. J. Stability Assessment on a 3% Bilayer PbS/ZnO Quantum Dot Heterojunction Solar Cell. *Adv. Mater.* **2010**, *22*, 3704–3707.
441. Kamat, P. V. Quantum Dot Solar Cells. Semiconductor Nanocrystals as Light Harvesters. *J. Phys. Chem. C* **2008**, *112*, 18737–18753.
442. Wang, X.; Koleilat, G. I.; Tang, J.; Liu, H.; Kramer, I. J.; Debnath, R.; Brzozowski, L.; Barkhouse, D. A. R.; Levina, L.; Hoogland, S.; Sargent, E. H. Tandem Colloidal Quantum Dot Solar Cells Employing a Graded Recombination Layer. *Nat. Photonics* **2011**, *6*, 480–484.
443. Erickson, C. S.; Bradshaw, L. R.; McDowall, S.; Gilbertson, J. D.; Gamelin, D. R.; Patrick, D. L. Zero-Reabsorption Doped-Nanocrystal Luminescent Solar Concentrators. *ACS Nano* **2014**, *8*, 3461–3467.
444. Bronstein, N. D.; Li, L.; Xu, L.; Yao, Y.; Ferry, V. E.; Alivisatos, A. P.; Nuzzo, R. G. Luminescent Solar Concentration with Semiconductor Nanorods and Transfer-Printed Micro-Silicon Solar Cells. *ACS Nano* **2014**, *8*, 44–53.
445. Meinardi, F.; Colombo, A.; Velizhanin, K. A.; Simonutti, R.; Lorenzon, M.; Beverina, L.; Viswanatha, R.; Klimov, V. I.; Brovelli, S. Large-Area Luminescent Solar Concentrators Based on 'Stokes-Shift-Engineered' Nanocrystals in a Mass-Polymerized PMMA Matrix. *Nat. Photonics* **2014**, *8*, 392–399.
446. Nozik, A. J. Quantum Dot Solar Cells. *Physica E* **2002**, *14*, 115–120.
447. Beard, M. C.; Luther, J. M.; Semonin, O. E.; Nozik, A. J. Third Generation Photovoltaics Based on Multiple Exciton Generation in Quantum Confined Semiconductors. *Acc. Chem. Res.* **2013**, *46*, 1252–1260.
448. Padilha, L. A.; Stewart, J. T.; Sandberg, R. L.; Bae, W. K.; Koh, W. K.; Pietryga, J. M.; Klimov, V. I. Carrier Multiplication in Semiconductor Nanocrystals: Influence of Size, Shape, and Composition. *Acc. Chem. Res.* **2013**, *46*, 1261–1269.
449. Klimov, V. I. Detailed-Balance Power Conversion Limits of Nanocrystal-Quantum-Dot Solar Cells in the Presence of Carrier Multiplication. *Appl. Phys. Lett.* **2006**, *89*, 123118.
450. Hanna, M. C.; Nozik, A. J. Solar Conversion Efficiency of Photovoltaic and Photoelectrolysis Cells with Carrier Multiplication Absorbers. *J. Appl. Phys.* **2006**, *100*, 074510.
451. Schaller, R. D.; Klimov, V. I. High Efficiency Carrier Multiplication in PbSe Nanocrystals: Implications for Solar Energy Conversion. *Phys. Rev. Lett.* **2004**, *92*, 186601.
452. Ellingson, R. J.; Beard, M. C.; Johnson, J. C.; Yu, P.; Micic, O. I.; Nozik, A. J.; Shabaev, A.; Efros, A. L. Highly Efficient Multiple Exciton Generation in Colloidal PbSe and PbS Quantum Dots. *Nano Lett.* **2005**, *5*, 865–871.
453. Xiao, J.; Wang, Y.; Hua, Z.; Wang, X.; Zhang, C.; Xiao, M. Carrier Multiplication in Semiconductor Nanocrystals Detected by Energy Transfer to Organic Dye Molecules. *Nat. Commun.* **2012**, *3*, 1170.
454. Yang, Y.; Rodriguez-Cordoba, W.; Lian, T. Q. Multiple Exciton Generation and Dissociation in PbS Quantum Dot−Electron Acceptor Complexes. *Nano Lett.* **2012**, *12*, 4235–4241.
455. Gesuele, F.; Sfeir, M. Y.; Koh, W. K.; Murray, C. B.; Heinz, T. F.; Wong, C. W. Ultrafast Supercontinuum Spectroscopy of Carrier Multiplication and Biexcitonic Effects in Excited States of PbS Quantum Dots. *Nano Lett.* **2012**, *12*, 2658–2664.
456. Gachet, D.; Avidan, A.; Pinkas, I.; Oron, D. An Upper Bound to Carrier Multiplication Efficiency in Type II Colloidal Quantum Dots. *Nano Lett.* **2010**, *10*, 164–170.
457. Timmerman, D.; Valenta, J.; Dohnalova, K.; de Boer, W. D. A. M.; Gregorkiewicz, T. Step-like Enhancement of Luminescence Quantum Yield of Silicon Nanocrystals. *Nat. Nanotechnol.* **2011**, *6*, 710–713.
458. Sandberg, R. L.; Padilha, L. A.; Qazilbash, M. M.; Bae, W. K.; Schaller, R. D.; Pietryga, J. M.; Stevens, M. J.; Baek, B.; Nam, S. W.; Klimov, V. I. Multiexciton Dynamics in Infrared-Emitting Colloidal Nanostructures Probed by a Superconducting Nanowire Single-Photon Detector. *ACS Nano* **2012**, *6*, 9532–9540.
459. Padilha, L. A.; Stewart, J. T.; Sandberg, R. L.; Bae, W. K.; Koh, W.-K.; Pietryga, J. M.; Klimov, V. I. Aspect Ratio Dependence of Auger Recombination and Carrier Multiplication in PbSe Nanorods. *Nano Lett.* **2013**, *13*, 1092–1099.
460. Gabor, N. M.; Zhong, Z.; Bosnick, K.; Park, J.; McEuen, P. L. Extremely Efficient Multiple Electron−Hole Pair Generation in Carbon Nanotube Photodiodes. *Science* **2009**, *325*, 1367–1371.
461. Aerts, M.; Bielewicz, T.; Klinke, C.; Grozema, F. C.; Houtepen, A. J.; Schins, J. M.; Siebbeles, L. D. A. Highly Efficient Carrier Multiplication in PbS Nanosheets. *Nat. Commun.* **2014**, *5*, 3789.
462. Tielrooij, K. J.; Song, J. C. W.; Jensen, S. A.; Centeno, A.; Pesquera, A.; Zurutuza Elorza, A.; Bonn, M.; Levitov, L. S.; Koppens, F. H. L. Photoexcitation Cascade and Multiple Hot-Carrier Generation in Graphene. *Nat. Phys.* **2013**, *9*, 248–252.
463. Sambur, J. B.; Novet, T.; Parkinson, B. A. Multiple Exciton Collection in a Sensitized Photovoltaic System. *Science* **2010**, *330*, 63–66.
464. Cirloganu, C. M.; Padilha, L. A.; Lin, Q.; Makarov, N. S.; Velizhanin, K. A.; Luo, H.; Robel, I.; Pietryga, J. M.; Klimov, V. I. Enhanced Carrier Multiplication in Engineered Quasi-Type-II Quantum Dots. *Nat. Commun.* **2014**, *5*, 4148.
465. Stewart, J. T.; Padilha, L. A.; Bae, W. K.; Koh, W.-K.; Pietryga, J. M.; Klimov, V. I. Carrier Multiplication in Quantum Dots within the Framework of Two Competing Energy Relaxation Mechanisms. *J. Phys. Chem. Lett.* **2013**, *4*, 2061–2068.
466. Rivera Gil, P.; Jimenez de Aberasturi, D.; Wulf, V.; Pelaz, B.; del Pino, P.; Zhao, Y.; de la Fuente, J.; Ruiz de Larramendi, I.; Rojo, T.; Liang, X.-J.; *et al.* The Challenge To Relate the Physicochemical Properties of Colloidal Nanoparticles to Their Cytotoxicity. *Acc. Chem. Res.* **2013**, *46*, 743–749.
467. Jing, L.; Ding, K.; Kershaw, S. V.; Kempson, I. M.; Rogach, A. L.; Gao, M. Magnetically Engineered Semiconductor Quantum Dots as Multimodal Imaging Probes. *Adv. Mater.* **2014**, *26*, 6367–6386.
468. Ali, Z.; Abbasi, A. Z.; Zhang, F.; Arosio, P.; Lascialfari, A.; Casula, M. F.; Wenk, A.; Kreyling, W.; Plapper, R.; Seidel, M.; Niessner, R.; Knoll, J.; Seubert, A.; Parak, W. J. Multifunctional Nanoparticles for Dual Imaging. *Anal. Chem.* **2011**, *83*, 2877–2882.
469. Stasiuk, G. J.; Tamang, S.; Imbert, D.; Poillot, C.; Giardiello, M.; Tisseyre, C.; Barbier, E. L.; Fries, P. H.; De Waard, M.; Reiss, P. Cell-Permeable Ln(III)

Chelate-Functionalized InP Quantum Dots as Multimodal Imaging Agents. *ACS Nano* **2011**, *5*, 8193–8201.
470. Stasiuk, G. J.; Tamang, S.; Imbert, D.; Gateau, C.; Reiss, P.; Fries, P.; Mazzanti, M. Optimizing the Relaxivity of Gd(III) Complexes Appended to InP/ZnS Quantum Dots by Linker Tuning. *Dalton Trans.* **2013**, *42*, 8197–8200.
471. Lartigue, L.; Hugounenq, P.; Alloyeau, D.; Clarke, S. P.; Levy, M.; Bacri, J. C.; Bazzi, R.; Brougham, D. F.; Wilhelm, C.; Gazeau, F. Cooperative Organization in Iron Oxide Multi-Core Nanoparticles Potentiates Their Efficiency as Heating Mediators and MRI Contrast Agents. *ACS Nano* **2012**, *6*, 10935–10949.
472. Lee, J.-H.; Jang, J.-t.; Choi, J.-s.; Moon, S. H.; Noh, S.-h.; Kim, J.-w.; Kim, J.-G.; Kim, I.-S.; Park, K. I.; Cheon, J. Exchange-Coupled Magnetic Nanoparticles for Efficient Heat Induction. *Nat. Nanotechnol.* **2011**, *6*, 418–422.
473. Alphandéry, E.; Faure, S.; Seksek, O.; Guyot, F.; Chebbi, I. Chains of Magnetosomes Extracted from AMB-1 Magnetotactic Bacteria for Application in Alternative Magnetic Field Cancer Therapy. *ACS Nano* **2011**, *5*, 6279–6296.
474. Guardia, P.; Di Corato, R.; Lartigue, L.; Wilhelm, C.; Espinosa, A.; Garcia-Hernandez, M.; Gazeau, F.; Manna, L.; Pellegrino, T. Water-Soluble Iron Oxide Nanocubes with High Values of Specific Absorption Rate for Cancer Cell Hyperthermia Treatment. *ACS Nano* **2012**, *6*, 3080–3091.
475. Ashraf, S.; Carrillo-Carrion, C.; Zhang, Q.; Soliman, M. G.; Hartmann, R.; Pelaz, B.; del Pino, P.; Parak, W. J. Fluorescence-Based Ion-Sensing with Colloidal Particles. *Curr. Opin. Pharmacol.* **2014**, *18*, 98–103.
476. Huang, H.; Delikanli, S.; Zeng, H.; Ferkey, D. M.; Pralle, A. Remote Control of Ion Channels and Neurons through Magnetic-Field Heating of Nanoparticles. *Nat. Nanotechnol.* **2010**, *5*, 602–606.
477. Niazov, A.; Freeman, R.; Girsh, J.; Willner, I. Following Glucose Oxidase Activity by Chemiluminescence and Chemiluminescence Resonance Energy Transfer (CRET) Processes Involving Enzyme–DNAzyme Conjugates. *Sensors* **2011**, *11*, 10388–10397.
478. Stanley, S. A.; Gagner, J. E.; Damanpour, S.; Yoshida, M.; Dordick, J. S.; Friedman, J. M. Radio-Wave Heating of Iron Oxide Nanoparticles Can Regulate Plasma Glucose in Mice. *Science* **2012**, *336*, 604–608.
479. Ling, D.; Park, W.; Park, S. J.; Lu, Y.; Kim, K. S.; Hackett, M. J.; Kim, B. H.; Yim, H.; Jeon, Y. S.; Na, K.; Hyeon, T. Multifunctional Tumor pH-Sensitive Self-Assembled Nanoparticles for Bimodal Imaging and Treatment of Resistant Heterogeneous Tumors. *J. Am. Chem. Soc.* **2014**, *136*, 5647–5655.
480. Ling, D.; Xia, H.; Park, W.; Hackett, M. J.; Song, C.; Na, K.; Hui, K. M.; Hyeon, T. pH-Sensitive Nanoformulated Triptolide as a Targeted Therapeutic Strategy for Hepatocellular Carcinoma. *ACS Nano* **2014**, *8*, 8027–8039.
481. Peteiro-Cartelle, J.; Rodríguez-Pedreira, M.; Zhang, F.; Rivera-Gil, P.; Mercato, L. L. d.; Parak, W. J. One Example on How Colloidal Nano- and Microparticles Could Contribute to Medicine. *Nanomedicine* **2009**, *4*, 967–979.
482. Sykes, E. A.; Chen, J.; Zheng, G.; Chan, W. C. W. Investigating the Impact of Nanoparticle Size on Active and Passive Tumor Targeting Efficiency. *ACS Nano* **2014**, *8*, 5696–5706.
483. Tay, C. Y.; Setyawati, M. I.; Xie, J.; Parak, W. J.; Leong, D. T. Back to Basics: Exploiting the Innate Physico-Chemical Characteristics of Nanomaterials for Biomedical Applications. *Adv. Funct. Mater.* **2014**, *24*, 5936–5955.
484. Yarema, M.; Caputo, R.; Kovalenko, M. V. Precision Synthesis of Colloidal Inorganic Nanocrystals Using Metal and Metalloid Amides. *Nanoscale* **2013**, *5*, 8398–8410.
485. Hui, Z.; Mingshang, J.; Younan, X. Noble-Metal Nanocrystals with Concave Surfaces: Synthesis and Applications. *Angew. Chem., Int. Ed.* **2012**, *51*, 7656–7673.
486. Samokhvalov, P.; Artemyev, M.; Nabiev, I. Basic Principles and Current Trends in Colloidal Synthesis of Highly Luminescent Semiconductor Nanocrystals. *Chem.—Eur. J.* **2013**, *19*, 1534–1546.
487. Xia, Y. N.; Xia, X. H.; Wang, Y.; Xie, S. F. Shape-Controlled Synthesis of Metal Nanocrystals. *MRS Bull.* **2013**, *38*, 335–344.
488. Li, H. B.; Kanaras, A. G.; Manna, L. Colloidal Branched Semiconductor Nanocrystals: State of the Art and Perspectives. *Acc. Chem. Res.* **2013**, *46*, 1387–1396.
489. Wu, Y.; Wang, D.; Li, Y. Nanocrystals from Solutions: Catalysts. *Chem. Soc. Rev.* **2014**, *43*, 2112–2124.
490. Hens, Z.; Čapek, R. K. Size Tuning at Full Yield in the Synthesis of Colloidal Semiconductor Nanocrystals, Reaction Simulations and Experimental Verification. *Coord. Chem. Rev.* **2014**, *263–264*, 217–228.
491. Lan, X.; Masala, S.; Sargent, E. H. Charge-Extraction Strategies for Colloidal Quantum Dot Photovoltaics. *Nat. Mater.* **2014**, *13*, 233–240.
492. Hetsch, F.; Zhao, N.; Kershaw, S. V.; Rogach, A. L. Quantum Dot Field Effect Transistors. *Mater. Today* **2013**, *16*, 312–325.
493. Shirasaki, Y.; Supran, G. J.; Bawendi, M. G.; Bulovic, V. Emergence of Colloidal Quantum-Dot Light-Emitting Technologies. *Nat. Photonics* **2013**, *7*, 13–23.
494. Kershaw, S. V.; Susha, A. S.; Rogach, A. L. Narrow Bandgap Colloidal Metal Chalcogenide Quantum Dots: Synthetic Methods, Heterostructures, Assemblies, Electronic and Infrared Optical Properties. *Chem. Soc. Rev.* **2013**, *42*, 3033–3087.
495. Pichaandi, J.; van Veggel, F. Near-Infrared Emitting Quantum Dots: Recent Progress on Their Synthesis and Characterization. *Coord. Chem. Rev.* **2014**, *263*, 138–150.
496. Wheeler, D. A.; Zhang, J. Z. Exciton Dynamics in Semiconductor Nanocrystals. *Adv. Mater.* **2013**, *25*, 2878–2896.
497. Padilha, L. A.; Stewart, J. T.; Sandberg, R. L.; Bae, W. K.; Koh, W. K.; Pietryga, J. M.; Klimov, V. I. Carrier Multiplication in Semiconductor Nanocrystals: Influence of Size, Shape, and Composition. *Acc. Chem. Res.* **2013**, *46*, 1261–1269.
498. Jain, P. K. Plasmon-in-a-Box: On the Physical Nature of Few-Carrier Plasmon Resonances. *J. Phys. Chem. Lett.* **2014**, *5*, 3112–3119.
499. Liu, J.; Erogbogbo, F.; Yong, K.-T.; Ye, L.; Liu, J.; Hu, R.; Chen, H.; Hu, Y.; Yang, Y.; Yang, J.; Roy, I.; Karker, N. A.; Swihart, M. T.; Prasad, P. N. Assessing Clinical Prospects of Silicon Quantum Dots: Studies in Mice and Monkeys. *ACS Nano* **2013**, *7*, 7303–7310.
500. Runnerstrom, E. L.; Llordes, A.; Lounis, S. D.; Milliron, D. J. Nanostructured Electrochromic Smart Windows: Traditional Materials and NIR-Selective Plasmonic Nanocrystals. *Chem. Commun.* **2014**, *50*, 10555–10572.
501. Loiudice, A.; Rizzo, A.; Grancini, G.; Biasiucci, M.; Belviso, M. R.; Corricelli, M.; Curri, M. L.; Striccoli, M.; Agostiano, A.; Cozzoli, P. D.; *et al.* Fabrication of Flexible All-Inorganic Nanocrystal Solar Cells by Room-Temperature Processing. *Energy Environ. Sci.* **2013**, *6*, 1565–1572.
502. Protesescu, L.; Rossini, A. J.; Kriegner, D.; Valla, M.; de Kergommeaux, A.; Walter, M.; Kravchyk, K. V.; Nachtegaal, M.; Stangl, J.; Malaman, B.; *et al.* Unraveling the Core–Shell Structure of Ligand-Capped Sn/SnOx Nanoparticles by Surface-Enhanced Nuclear Magnetic Resonance, Mössbauer, and X-ray Absorption Spectroscopies. *ACS Nano* **2014**, *8*, 2639–2648.
503. Lignos, I.; Protesescu, L.; Stavrakis, S.; Piveteau, L.; Speirs, M. J.; Loi, M. A.; Kovalenko, M. V.; deMello, A. J. Facile Droplet-Based Microfluidic Synthesis of Monodisperse IV–VI Semiconductor Nanocrystals with Coupled In-Line NIR Fluorescence Detection. *Chem. Mater.* **2014**, *26*, 2975–2982.
504. Agresti, J. J.; Antipov, E.; Abate, A. R.; Ahn, K.; Rowat, A. C.; Baret, J.-C.;

Marquez, M.; Klibanov, A. M.; Griffiths, A. D.; Weitz, D. A. Ultra-high-Throughput Screening in Drop-Based Microfluidics for Directed Evolution. *Proc. Natl. Acad. Sci. U.S.A.* **2010**, *107*, 4004–4009.
505. Phillips, T. W.; Lignos, I. G.; Maceiczyk, R. M.; deMello, A. J.; deMello, J. C. Nanocrystal Synthesis in Microfluidic Reactors: Where Next? *Lab Chip* **2014**, *14*, 3172–3180.
506. Zhang, L.; Xia, Y. Scaling up the Production of Colloidal Nanocrystals: Should We Increase or Decrease the Reaction Volume? *Adv. Mater.* **2014**, *26*, 2600–2606.
507. Narita, A.; Feng, X.; Hernandez, Y.; Jensen, S. A.; Bonn, M.; Yang, H.; Verzhbitskiy, I. A.; Casiraghi, C.; Hansen, M. R.; Koch, A. H. R.; *et al.* Synthesis of Structurally Well-Defined and Liquid-Phase-Processable Graphene Nanoribbons. *Nat. Chem.* **2014**, *6*, 126–132.
508. Baalousha, M.; Lead, J. R. Nanoparticle Dispersity in Toxicology. *Nat. Nanotechnol.* **2013**, *8*, 308–309.
509. Galindo, T. P.; Pereira, R.; Freitas, A. C.; Santos-Rocha, T. A.; Rasteiro, M. G.; Antunes, F.; Rodrigues, D.; Soares, A. M.; Goncalves, F.; Duarte, A. C.; *et al.* Toxicity of Organic and Inorganic Nanoparticles to Four Species of White-Rot Fungi. *Sci. Total Environ.* **2013**, *458−460*, 290–297.
510. Hansen, S. F. The European Union's Chemical Legislation Needs Revision. *Nat. Nanotechnol.* **2013**, *8*, 305–306.
511. Tajani, A. Substance Identification of Nanomaterials Not Key To Ensuring Their Safe Use. *Nat. Nanotechnol.* **2013**, *8*, 306–307.
512. Alkilany, A. M.; Murphy, C. J. Toxicity and Cellular Uptake of Gold Nanoparticles: What We Have Learned so Far? *J. Nanopart. Res.* **2010**, *12*, 2313–2333.
513. Crisp, R. W.; Panthani, M. G.; Rance, W. L.; Duenow, J. N.; Parilla, P. A.; Callahan, R.; Dabney, M. S.; Berry, J. J.; Talapin, D. V.; Luther, J. M. Nanocrystal Grain Growth and Device Architectures for High-Efficiency CdTe Ink-Based Photovoltaics. *ACS Nano* **2014**, *8*, 9063–9072.
514. Fan, J.; Chu, P. K. Group Iv Nanoparticles: Synthesis, Properties, and Biological Applications. *Small* **2010**, *6*, 2080–2098.
515. Hola, K.; Zhang, Y.; Wang, Y.; Giannelis, E. P.; Zboril, R.; Rogach, A. L. Carbon Dots—Emerging Light Emitters for Bioimaging, Cancer Therapy and Optoelectronics. *Nano Today* **2014**, 10.1016/j.nantod.2014.09.004.
516. Nie, H.; Li, M. J.; Li, Q. S.; Liang, S. J.; Tan, Y. Y.; Sheng, L.; Shi, W.; Zhang, S. X. A. Carbon Dots with Continuously Tunable Full-Color Emission and Their Application in Ratiometric pH Sensing. *Chem. Mater.* **2014**, *26*, 3104–3112.
517. Zhitomirsky, D.; Voznyy, O.; Levina, L.; Hoogland, S.; Kemp, K. W.; Ip, A. H.; Thon, S. M.; Sargent, E. H. Engineering Colloidal Quantum Dot Solids within and beyond the Mobility-Invariant Regime. *Nat. Commun.* **2014**, *5*, 3803.
518. Piliego, C.; Protesescu, L.; Bisri, S. Z.; Kovalenko, M. V.; Loi, M. A. 5.2% Efficient PbS Nanocrystal Schottky Solar Cells. *Energy Environ. Sci.* **2013**, *6*, 3054–3059.
519. Green, M. A.; Ho-Baillie, A.; Snaith, H. J. The Emergence of Perovskite Solar Cells. *Nat. Photonics* **2014**, *8*, 506–514.
520. Klem, E.; Lewis, J.; Gregory, C.; Cunningham, G.; Temple, D.; D'Souza, A.; Robinson, E.; Wijewarnasuriya, P. S.; Dhar, N. High-Performance SWIR Sensing From Colloidal Quantum Dot Photodiode Arrays. *SPIE* **2013**, 886806.
521. Supran, G. J.; Shirasaki, Y.; Song, K. W.; Caruge, J.-M.; Kazlas, P. T.; Coe-Sullivan, S.; Andrew, T. L.; Bawendi, M. G.; Bulović, V. QLEDs for Displays and Solid-State Lighting. *MRS Bull.* **2013**, *38*, 703–711.
522. Lukianova-Hleb, E. Y.; Ren, X.; Sawant, R. R.; Wu, X.; Torchilin, V. P.; Lapotko, D. O. On-Demand Intracellular Amplification of Chemoradiation with Cancer-Specific Plasmonic Nanobubbles. *Nat. Med.* **2014**, *20*, 778–784.
523. Kang, J. H.; Super, M.; Yung, C. W.; Cooper, R. M.; Domansky, K.; Graveline, A. R.; Mammoto, T.; Berthet, J. B.; Tobin, H.; Cartwright, M. J.; *et al.* An Extracorporeal Blood-Cleansing Device for Sepsis Therapy. *Nat. Med.* **2014**, *20*, 1211–1216.
524. Simon, T.; Bouchonville, N.; Berr, M. J.; Vaneski, A.; Adrovic, A.; Volbers, D.; Wyrwich, R.; Doblinger, M.; Susha, A. S.; Rogach, A. L.; *et al.* Redox Shuttle Mechanism Enhances Photocatalytic H Generation on Ni-Decorated CdS Nanorods. *Nat. Mater.* **2014**, *13*, 1013–1018.
525. de Nijs, B.; Dussi, S.; Smallenburg, F.; Meeldijk, J. D.; Groenendijk, D. J.; Filion, L.; Imhof, A.; van Blaaderen, A.; Dijkstra, M. Entropy-Driven Formation Of Large Icosahedral Colloidal Clusters By Spherical Confinement. *Nat. Mater.* **2014**, *14*, 56–60.
526. Jia, G.; Sitt, A.; Hitin, G. B.; Hadar, I.; Bekenstein, Y.; Amit, Y.; Popov, I.; Banin, U. Couples of Colloidal Semiconductor Nanorods Formed by Self-Limited Assembly. *Nat. Mater.* **2014**, *13*, 301–307.
527. Bodnarchuk, M. I.; Erni, R.; Krumeich, F.; Kovalenko, M. V. Binary Superlattices from Colloidal Nanocrystals and Giant Polyoxometalate Clusters. *Nano Lett.* **2013**, *13*, 1699–1705.
528. Bhadrachalam, P.; Subramanian, R.; Ray, V.; Ma, L. C.; Wang, W.; Kim, J.; Cho, K.; Koh, S. J. Energy-Filtered Cold Electron Transport at Room Temperature. *Nat. Commun.* **2014**, *5*, 4745.